REMOTE SENSING OF WETLANDS IN YELLOWSTONE NATIONAL PARK

by

Christopher Kevin Wright

A dissertation submitted in partial fulfillment
of the requirements for the degree

of

Doctor of Philosophy

in

Biological Sciences

MONTANA STATE UNIVERSITY
Bozeman, Montana

August 2004

UMI Number: 3143873

ProQuest Information and Learning Company
300 North Zeeb Road
PO Box 1346
Ann Arbor, MI 48106-1346

APPROVAL

of a dissertation submitted by

Christopher Kevin Wright

This dissertation has been read by each member of the dissertation committee and has been found to be satisfactory regarding content, English usage, format, citations, bibliographic style, and consistency, and is ready for submission to the College of Graduate Studies.

Dr. Daniel Goodman

Approved for the Department of Ecology

Dr. David Roberts

Approved for the College of Graduate Studies

Dr. Bruce R. McLeod

STATEMENT OF PERMISSION TO USE

Christopher Kevin Wright

9 August, 2004

Acknowledgements

This research was funded by the U.S. Department of the Interior Amphibian Research and Monitoring Initiative through a cooperative agreement between Montana State University and the U.S. Geological Survey EROS Data Center in Sioux Falls, SD. At the EROS Data Center, Alisa Gallant made an invaluable contribution. I am profoundly grateful for her help and encouragement. Many thanks go to Robert Klaver, my data contact at EROS, and to Paul Bartelt for demonstrating the usefulness of wetland likelihood mapping. Chuck Peterson, from Idaho State University, was an early advocate of the importance of this work to amphibian research in Yellowstone National Park and an invaluable committee member. Thanks to Daniel Goodman, my major advisor, for bringing me into the fold. Dan Gustafson provided a steady supply of Mountain Dew, technical assistance, and endless amusement. I never would have made it through graduate school without the love of my parents, Kevin and Trude Wright. Most of all, I thank my wife, Gretchen Meier, for all her support and sacrifice, and Liam Wright-Meier for the inspiration only a one year old can provide.

TABLE OF CONTENTS

TABLE OF CONTENTS - CONTINUED

LIST OF TABLES

LIST OF TABLES - CONTINUED

Table Page

LIST OF FIGURES

Figure Page

LIST OF FIGURES - CONTINUED

Figure Page

LIST OF FIGURES - CONTINUED

Figure Page

ABSTRACT

As part of the Amphibian Research and Monitoring Initiative, satellite remote sensing was used to identify potential wetland amphibian habitat in Yellowstone National Park. Landsat Thematic Mapper imagery was combined with ancillary predictors of wetland occurrence including habitat type, cover type, landform type, bedrock geology, soil attributes, terrain measures, and climate data. Classification trees were used to predict the likelihood of palustrine wetland occurrence across the Yellowstone landscape. Wetland maps generated by this study are intended to address shortcomings of the National Wetland Inventory in Yellowstone; namely, errors-of-omission and the temporally invariant nature of the inventory. Relative importance of Thematic Mapper imagery, image texture information, terrain measures, and thematic spatial data were assessed by comparing the accuracy of classification trees trained with different subsets of predictors. In general, classification trees using all available predictors exhibited the greatest accuracy. Classification tree structure was similar in models generated with satellite imagery from different years. Also, similar accuracy rates were found across years. The results indicate that the method could be applied to annual wetland monitoring. Average producer's accuracy for the palustrine wetland class was approximately 0.92. Five palustrine wetland classes were discriminated with an average overall accuracy of approximately 0.83. A wetland map derived from a 1 August, 2003 Thematic Mapper image was field-verified in late-summer and early-autumn of 2003. The classification tree methodology appears to be sensitive to within-season wetland condition and yearly wetland variability. Satellite remote sensing located wetlands not mapped by the National Wetland Inventory and also identified upland sites erroneously classified as wetland. Methods developed by this study are general enough to be applied in other physiographic settings and should prove to be useful to amphibian conservation efforts over large geographic extents.

CHAPTER 1

INTRODUCTION AND LITERATURE REVIEW

Introduction

Evidence of a global pattern of amphibian population declines and losses has generated a great deal of interest in the status of amphibians at a variety of scales. Across both Western Europe and North America, multiple studies reveal negative population trends (Houlahan et al. 2000). In southern California, ranid frogs have largely disappeared (Wake 1991). In 1987, a multi-species population crash occurred within the amphibian assemblage of the Monteverde Cloud Forest Preserve in Costa Rica, with 25 species of frogs and toads suspected to have gone locally extinct (Pounds et al. 1997). In the southern Rocky Mountains, boreal toad (*Bufo boreas*) declines have been observed in Colorado, southeast Wyoming, and northern New Mexico (Carey 1993; Corn 1998).

A number of factors have been advanced as potential causes of amphibian declines, including ultraviolet radiation (Blaustein et al. 1994; Starnes et al. 2000; Middleton et al. 2001), predatory fish introductions (Fisher and Shaffer 1996; Adams 1999), acid deposition and anthropogenic toxics (Alford and Richards 1999), disease (Kiesecker and Blaustein 1997; Kiesecker et al. 2001), and climate change (Pounds and Crump 1994, Beebee 1995). However, habitat loss is likely the most important cause of amphibian declines (Blaustein et al. 1994). More than half of U.S. wetlands have been drained since European settlement (Dahl 1990). From the mid 1970's to the mid 1980's, approximately 2.6 million acres of U.S. wetlands were lost (Wilen and Bates 1995).

Amphibian extirpations have been attributed to wetland drainage and agricultural conversion in Ontario, Canada (Hecnar and M'Closkey 1996). Landscape scale attributes including the area of forested wetland, area of permanent wetland, and patch habitat diversity were positively associated with amphibian richness in Wisconsin (Knutson et al. 1999). Given evidence that some amphibian species are prone to metapopulation dynamics where local extinction and colonization events are common (Sjogren Gulve 1994; Hecnar and M'Closkey 1997; Skelly et al. 1999), amphibians may be sensitive to habitat fragmentation (Halley et al. 1996; Dodd and Cade 1998; Semlitsch and Bodie 1998). Gibbs (1998) found that amphibian species with higher dispersal tendencies and lower relative densities tended to occupy a smaller proportion of suitable habitat as forest fragmentation increased. Lehtinen et al. (1999) found a negative relationship between amphibian species richness and site isolation in fragmented agricultural and urban landscapes in Minnesota. Several studies show that the amount of upland forest adjacent to wetlands is positively associated with amphibian richness, (Findlay and Houlahan 1997; Kolosvary and Swihart 1999; Knutson et al. 1999), suggesting the importance of suitable linkages between wetland habitats.

In 2000 the Department of the Interior was directed by executive order to develop a plan to monitor amphibians on lands managed by the department and to research causes of amphibian declines. Under the resulting Amphibian Research and Monitoring Initiative (ARMI), monitoring programs were instituted nationwide, including amphibian surveys in Yellowstone National Park.

As part of the ARMI effort in Yellowstone, this study was initiated to map potential wetland habitat using a combination of satellite remote sensing and ancillary spatial information. Classification trees were used to predict the likelihood of wetland presence across the Yellowstone landscape. Results are presented below in two journal article manuscripts. The first paper, "Improved Wetland Detection in Yellowstone National Park by Combination of Landsat Thematic Mapper Imagery, Image Texture, and Ancillary GIS Information", examines the role of image texture and ancillary information in improving wetland detection. The second manuscript, "Remote Sensing of Wetlands in Yellowstone National Park as Part of the Amphibian Research and Monitoring Initiative", discusses field verification of wetland maps generated from an August 1, 2003 TM image and application of wetland likelihood modeling to amphibian research.

Results of this study are intended for use in other contexts. Wetland maps are being used to guide and interpret continuing amphibian surveys in Yellowstone National Park and represent an improvement on the existing National Wetland Inventory. Model predictions are currently being used as inputs to a landscape amphibian habitat model (Bartelt and Gallant, in preparation) and in a study of tiger salamander (*Ambystoma tigrinum*) population genetics (Spear 2004). The developed methodology represents a decision support tool for future monitoring of wetland habitat and amphibian conservation planning, both in Yellowstone National Park and in the Greater Yellowstone Region. Finally, Yellowstone National Park presents an ideal location for prototyping

improved methods of wetland remote sensing that might be applied in other physiographic settings or over even greater geographic extents.

Literature Review

National Wetland Inventory

Given the physical inaccessibility of wetlands in general, synoptic inventories of wetlands have typically required some degree of remote sensing, whether by aerial photography or from satellite imagery. Yellowstone wetlands are currently mapped by the National Wetland Inventory (NWI). They were delineated primarily by stereoscopic interpretation of 1:58,000-scale color infrared aerial photography acquired in August and September of 1982-84 (Elliott and Hektner 2000), though some subsets of the Yellowstone NWI were interpreted from 1970s-era 1:80,000 scale black-and-white aerial photographs (Yellowstone NP Spatial Analysis Center, unpublished metadata).

The National Wetland Inventory classifies wetlands by the Cowardin system (Cowardin et al. 1979) where a location must satisfy at least one of three conditions to be considered a wetland: (1) at least periodically, the site supports predominantly hydrophytic vegetation (2) the substrate is predominantly undrained hydric soil (3) the substrate is not soil and is saturated or covered by shallow water at some time during the growing season of each year (Cowardin and Golet 1995).

The Cowardin scheme divides freshwater wetlands into lacustrine, riverine, and palustrine systems. Lacustrine systems include lakes and ponds larger than eight hectares (ha) or deeper than two meters at low water (Cowardin et al. 1979). In Yellowstone,

lacustrine systems encompass nearly 41,000 ha (dominated by Yellowstone Lake) or approximately 44% of the park's wetlands (Elliott and Hectner 2000).

Given difficulties associated with accurate delineation of river floodplain boundaries from aerial photographs, Cowardin et al. (1979) define riverine wetland systems in a limited way, including only stream or river channels containing nonpersistent vegetation or no vegetation (Cowardin and Golet 1995). The Yellowstone NWI identifies 3,784 ha of riverine wetlands, approximately 4% of the wetland total (Elliott and Hectner 2000).

The palustrine system includes vegetated wetlands dominated by trees, shrubs, persistent emergents, mosses or lichens and encompasses wetland types more traditionally identified as swamp, bog, marsh, or fen. Small, shallow, permanent or intermittent open water bodies are also included within the palustrine system (Cowardin et al. 1979). Palustrine wetland is the predominant wetland type in the Yellowstone NWI, covering approximately 48,000 ha (Elliott and Hectner 2000), and includes the vast majority of potential amphibian wetland habitat within the park.

Evaluation of the National Wetland Inventory has revealed varying degrees of accuracy. In Massachusetts, Swarthout et al. (1981) found that the NWI was 98-100% accurate discriminating wetlands 0.6 ha or larger from upland at nine study sites across the state. In southeast Nebraska, Kuzila et al. (1991) overlayed a 1981 NWI map on a 1981 soil survey map within a single 7.5 minute quadrangle, finding that hydric soils generally coincided with NWI wetland delineations. Approximately 70% of pixels identified as wetland by the NWI were also mapped as hydric soil and, overall, there was

a 94% rate of agreement between the two maps in terms of discriminating wetland from upland. However, only 53% of pixels identified as hydric soil were also mapped as wetland by the NWI, suggesting that the NWI tends to err by omission (Kuzila et al. 1991). Field verification in the Upper Peninsula of Michigan showed that 95% of wetlands delineated by the NWI were correctly identified while misclassification of true wetland sites as non-wetland was less than 4% (Kudray and Gale 2000). In the Blue Ridge Mountains of Virginia, Stolt and Baker (1995) found that all palustrine wetlands delineated on two 2.5 minute NWI maps were correctly identified, but with substantial errors of omission; 2.5 and 18.9 ha of wetland were identified by the NWI on the two maps, but field verification indicated 93.3 and 127.7 ha of wetland, respectively. Wetlands not identified included forested wetlands and seeps at the head of drainages and along floodplains. Generally, the size of these seeps was between 0.2 and 0.6 ha (Stolt and Baker 1995).

The minimal mapping unit for 1:58,000 scale color infrared photography is 0.5-1.2 ha for forested wetlands and less than 0.5 ha for non-forested ponds and pothole marshes (Tiner 1990). The minimal mapping unit for 1:80,000 scale black-and-white aerial photography is 7.5-12.5 ha (Kudray and Gale 2000). Apparently, portions of the Yellowstone NWI interpreted from 1:80,000 scale black-and-white photographs tend to omit drier emergent wetlands (Yellowstone NP Spatial Analysis Center, unpublished metadata). Saturated soils in forested wetlands tend to be obscured by the forest canopy, making infrared photo interpretation difficult, especially in coniferous forested wetlands (Tiner 1990).

In general, it appears that the National Wetland Inventory may be biased toward errors of omission. Tiner (1997) claims; "Despite some shortcomings, NWI maps…tend to err more by omission than commission. Consequently, if an area is designated on an NWI map as wetland, it is usually a wetland."

Nationwide, large gaps exist in the completion status and digital availability of the National Wetland Inventory (Figure 1.1), including most of Montana and Northern Idaho (U.S. Fish and Wildlife Service 2003). In the Greater Yellowstone region outside of

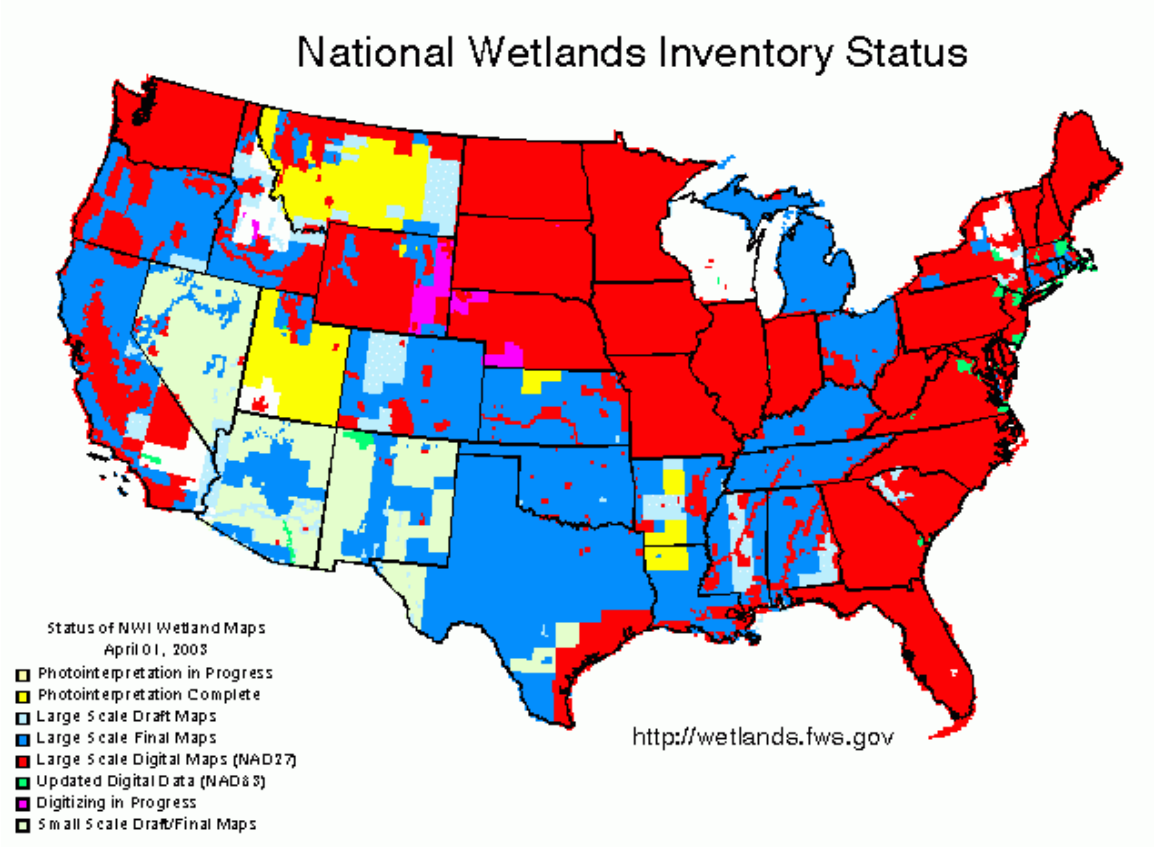

Figure 1.1. National Wetland Inventory completion status as of April 1, 2003.

Wyoming, few digitized NWI maps are available, and no other final maps (in paper format) have been completed. By demonstrating the feasibility of satellite remote sensing of wetlands in Yellowstone NP, this project should result in a methodology for producing timely digital maps to identify potential amphibian habitat and guide amphibian surveys where NWI data is unavailable.

Satellite Remote Sensing of Wetlands

Remote sensing of wetlands by satellite dates back to Landsat-1, launched in 1972. Work and Gilmer (1976) used Landsat-1 Multispectral Scanner (MSS) imagery to inventory ponds and lakes across the prairie pothole region of North Dakota. Thresholding of the near infrared band identified open water and detected a seasonal decline in pond numbers as seasonally flooded potholes dried between May and July. The nominal resolution of MSS imagery given a 79 m by 56 m pixel size is 0.4 ha, and almost all ponds larger than 1.6 ha were detected. Using a mixture model where proportions of open water, bare soil, and green vegetation within individual pixels were estimated from the red and near infrared bands, an approximately 3-fold increase in spatial resolution was achieved, with all ponds larger than 0.5 ha detected and many smaller ponds identified to a minimum of 0.13 ha.

Butera (1983) compared medium resolution Landsat-1 MSS imagery with high resolution airborne MSS (7.6 m resolution). The Landsat-1 MSS appeared to over-predict the total area of Roseau cane (*Phragmites communis*) in the Mississippi River delta. In mangrove wetlands of southwest Florida, Landsat-1 achieved a higher overall classification accuracy, though airborne MSS was able to distinguish three types of

grassland marsh where Landsat-1 could only identify a more general mixed wetland grasses cover type. This result suggests a tradeoff between discrimination detail and classification accuracy.

Jensen et al. (1986) used 1977 Landsat MSS imagery to develop a regional map of wetlands in the Savannah River watershed. Similarly, large-scale Landsat MSS wetland mapping efforts were conducted in the Great Dismal Swamp of Virginia and North Carolina (Gammon and Carter 1976) and in northwestern Tennessee (Jones and Shahrokki 1977).

The U.S. Fish and Wildlife Service actually considered using Landsat imagery as its sole source of remotely sensed data when the National Wetland Inventory began in 1979, but the service concluded that the Landsat MSS could not provide the needed classification detail and accuracy requirements, and mid- and high-altitude color infrared aerial photography were adopted instead (Wilen and Bates 1995). For example, Ernst-Dottavio et al. (1981) found that hardwood swamp, shrub swamp, and shallow marsh were spectrally similar over the four MSS bands. Maximum likelihood classification accuracies for shrub swamp and shallow marsh were less than 35% and it was impossible to separate hardwood swamp from upland hardwoods. Mixtures of vegetation and open water found in deep marshes spectrally resembled other classes. Mixtures containing less than 30% vegetation were spectrally similar to open water, mixtures containing 30-60% vegetation resembled tamarack bog, and mixtures containing more than 60% vegetation were spectrally similar to hardwood swamp, shallow water, and shrub swamp.

The Thematic Mapper (TM) multispectral intrument, first launched on Landsat-5 in 1984, brings increased spatial resolution (30 m) and increased spectral resolution (6 bands) to bear on the problem of wetland remote sensing. Evaluating TM performance in Cheasapeake Bay wetlands, Dotavio and Dotavio (1984) found that TM bands 4 (near infrared), 5 (mid-infrared), and 3 (red) were optimal for discriminating between low marsh and high marsh communities. While the classification accuracies for these two wetland types were modest, (47% and 50%), wetland was distinguished from upland at a 70% accuracy rate. In southeast Australia, Johnston and Barston (1993) found that TM imagery was useful for mapping the location and extent of wetlands down to 1 ha in size, largely making use of absorption in the middle infrared band (band 5) by water and saturated soil. Multi-temporal images were easily classified on the basis of water regime (ephemeral wetland vs. permanent wetland), but classification of wetlands by dominant vegetation type was unsuccessful. Wang et al. (1998) classified cattail marsh, *Phragmites* marsh, and forested swamp in southern Ontario, Canada and found a higher accuracy rate (90%) using a late spring (June) TM image then when using a late summer (August) TM image (80%). In the prairie pothole region of North Dakota, TM imagery was shown to correctly identify 91% of wetland basins 2-4 ha in size and 70% of wetland basins between 0.8 and 2 ha (Federal Geographic Data Committee 1992). The accuracy rate for wetlands smaller than 0.8 ha fell to 20%. 0.8 ha corresponds roughly to nine pixels and may represent a lower limit on the resolution of the TM sensor when applied to wetland remote sensing.

Other satellites used for wetland remote sensing include the French *System Pour l'Observation de la Terre* or SPOT satellite (20 m resolution), the Indian Remote Sensing (IRS-1) platform (36.5 m resolution), and the high resolution IKONOS (1 m panchromatic, 4 m multispectral resolution) satellite. SPOT imagery was used to map wetlands in the Florida Everglades with 81% overall accuracy, documenting spatial expansion of cattail wetland types and spatial contraction of sawgrass types between 1973 and 1991 (Rutchey and Vilcheck 1994; Jensen et al. 1995). Jensen et al. (1993) used multidate SPOT imagery to map seasonal changes in the spatial distribution of waterlilly beds in a 1,000 ha manmade wetland at the Savannah River Department of Energy site, and monitored successional changes in that wetland during a four year reduction in water levels (Jensen et al. 1997). Using high resolution Ikonos imagery in southern Saskatchewan, Dechka et al. (2002) were able to resolve different vegetation types, e.g. *Carex* spp., *Calamagrostis* spp., or *Scolochloa festucacea*, within individual prairie pothole wetlands.

In the only known wetland remote sensing study in the Greater Yellowstone Region, Kindscher et al. (1998) used IRS-1 multispectral imagery to identify wet meadows in Grand Teton NP. Cluster analysis identified six meadow types representing a distinct hydric-to-xeric gradient. Field sampling showed that two of the meadow types were dominated by obligate and facultative wetland vegetation, leading to identification of nearly 3,000 ha of wetland meadows in Grand Teton NP

To achieve better classification accuracy and improved detection of small wetlands, the Federal Geographic Data Committee (1992) recommends augmentation of

satellite imagery with ancillary spatial information. However, a review of the remote sensing literature reveals little use of ancillary data in wetland remote sensing. Forest wetland classification in Maine was improved using a GIS rule-based method based on the premise that ancillary variables are informative in indicating where the probability of wetland occurrence is greater (Sader et al. 1995). Pixels identified as forest by their TM spectral signature were assigned additional evidential weights depending on whether they satisfied a number of other conditions associated with forested wetland, i.e. if they fell inside an NWI polygon, if they were co-located with hydric soils, if their slope was less than 5%, and if they fell within a buffer around permanent water bodies. Bolstad and Lillesand (1992) used a similar rule-based classification model to increase the accuracy of wetland land cover classification in northeastern Wisconsin. Huang and Jensen (1997) improved wetland classification at the Savannah River Site using a classification tree methodology to combine ancillary GIS layers with spectral data.

An extensive body of ancillary GIS data is available for Yellowstone National Park, including vegetation, soils, terrain, landform, and climate data. These resources provide a unique opportunity for researching potential improvements in wetland remote sensing.

As noted above, satellite remote sensing has been used to assess wetland temporal variability, both within and between growing seasons. By contrast, the National Wetland Inventory provides only a static assessment of wetland extent. In Yellowstone, this picture is confounded by the fact that the NWI is actually a mixture of temporal snapshots, mostly over a period of three years (1982-1984), but in some cases including

aerial photography from as early as 1972 and as late as 1992 (Yellowstone NP Spatial Analysis Center, unpublished metadata).

In mountainous landscapes like Yellowstone, upland wetlands are nearly entirely dependent on precipitation as their source of water, and their presence and extent can be expected to vary as the amount of precipitation varies (Winter 2000). Lowland wetlands receive their water primarily from groundwater discharge and streams and are typically located near headwater streams or headwater ground-water flow systems where the upgradient watershed is relatively small. As a result, lowland wetlands in mountainous landscapes are also vulnerable to climatic variability (Winter 2000).

This study used Landsat TM imagery from 1988 to 2003, a span of years where precipitation inputs in Yellowstone ranged widely, e.g. approximately 28 cm precipitation at Mammoth Hot Springs in 1988 to over 43 cm precipitation at Mammoth in 1997. Demonstration of yearly variation in the extent and spatial pattern of Yellowstone wetlands would contribute a significant improvement to wetland mapping in the park. Finally, climate driven wetland variability should have important implications with respect to persistence of amphibian metapopulations.

Multi-Source Data Integration

Integration of spatial data available from multiple sources is an active area of research in the field of remote sensing (Ricchetti 2000; Treitz and Howarth 2000; Ma et al. 2001; Peddle and Ferguson 2002). One of the more difficult challenges in this area is combination of data recorded on different measurement scales, i.e. nominal, ordinal, interval, and ratio scales (Gong 1994). For example, soil maps represent information on

a nominal scale while multispectral images record surface radiance on a ratio scale. Data reported in different spatial formats, e.g. vector vs. raster data, or at different spatial scales may not be compatible (Wang and Howarth 1994). Rates of spatial, or positional error, and non-spatial, or "attribute" error, are typically not available for multi-source data (Gong 1994).

Early techniques developed to increase classification accuracy through the use of ancillary information include pre-classification stratification of image data using ancillary data, "logical channel" addition where ancillary data is simply stacked on top of multispectral data in a maximum likelihood classifier, and post-classification sorting by merging or splitting of spectral classes based on ancillary data (Hutchinson 1982). The "logical channel" approach tends to break down when ancillary data does not conform to the multivariate normality assumption of Gaussian maximum likelihood classification, a common example being elevation data (Lee et al. 1987). Maximum likelihood classifiers are also limited to analysis of lower dimensional, ratio scale data (Peddle and Ferguson 2002). Linear discriminant analysis makes no assumption of multivariate normality, accommodates high dimensional data, and has been used to combine spectral, texture, and terrain variables in forest and alpine land cover classifications (Peddle 1993; Treitz and Howarth 2000). However, linear discriminant analysis is also restricted to ratio scale data (Peddle 1993).

Neural network classifiers have been used to combine multispectral imagery with ratio scale and interval scale ancillary data. Neural networks make no distributional assumptions and are capable of defining highly nonlinear decision boundaries in a feature

space (Chen et al. 1995). As land cover classifiers, they have been shown in practice to outperform maximum likelihood classification (Bischof et al. 1992, Bruzzone et al. 1997) and linear discriminant analysis (Foody et al. 1995). However, neural network models can be very complex computationally, require a large number of training samples, are usually slow to converge during training, and can have difficulty classifying patterns that are not identical to one or more of the patterns they are trained on (Benediktsson et al. 1990).

Expert systems have been used to combine satellite imagery with GIS information (McKeown 1987) and have been successfully applied to wetland classification (Bolstad and Lillesand 1992; Huang and Jensen 1997). However, specification of rules forming an expert system's knowledge base can be problematic, especially when experts are not able to formulate their knowledge in a way that is sufficiently systematic, accurate, and complete to build a software application (Huang and Jensen 1997).

Two machine-learning techniques used to incorporate ancillary data from all measurement scales are naïve Bayes classifiers and classification trees. Both of these approaches apply inductive inference to the problem of classification. Huang and Jensen (1997) describe the process of inductive learning as a "heuristic search through a space of symbolic descriptions for plausible general descriptions, or concepts, that explain the given input training data and are useful for predicting new data." Rather than fitting data to a statistical model, inductive learning relies on using data to guide model specification, a process more akin to learning by experience.

Naïve Bayes classification has been used to combine satellite imagery, land cover information, and environmental variables to map wildlife habitat suitability (Aspinall 1991, Aspinall and Veitch 1993). In the naïve Bayes classifier, training data are used to estimate conditional probabilities of predictor variables given known class assignments. While the naïve Bayes classifier makes an assumption of conditional independence between predictor variables, an assumption that is surely almost never true (hence the name naïve Bayes), the method appears to be remarkably robust in practice (Hand and Yu 2001) and has been shown to outperform more sophisticated classifiers in a number of applications (Langley and Sage 1994).

Classification trees make no distributional assumptions, easily accommodate data from any measurement scale, and are insensitive to outliers. The hierarchical structure of classification trees allows them to detect nonadditive interactions between independent variables without explicit specification (Clark and Pregibon 1992). Classification trees divide a complicated decision regarding class assignment into a union of several simpler decisions (Pal and Mather 2001). Automatic variable selection and complexity minimization are important attributes of classification trees. Variables that contribute to the accuracy of a tree are used those that do not are ignored. The tree structure is complicated (deep) only where class separation requires it (German et al. 1999).

Given their explicit specification, classification trees are easily interpreted (Freidl and Brodley 1997). As an inductive learning method, they can be useful in an exploratory role (Hansen et al. 1996). Classification trees have been used to classify land cover in a number of studies (Moore et al. 1991; Hansen et al. 1996; Friedl and Brodley

1997; Lawrence and Wright 2001, Pal and Mather 2001; Wylie et al. 2001; Miller and Franklin 2002). Rather than associating a land cover class with a mean vector estimated from a collection of predictors, classification trees partition a feature space in a manner that identifies thresholds above or below which a class can be found. Moore et al. (1991) argue that, "…in many cases the specification of threshold values associated with community boundaries has greater ecological validity than descriptions based on statistical parameters such as means, standard deviations and cross-products." Given the many desireable properties of classification trees, a classification tree methodology was used in this study to merge numeric and categorical ancillary data with TM spectral data.

CHAPTER 2

DATA AND METHODS

Spatial datasets used in this study are discussed below. Methods used to compute derivative measures from raw data are summarized as the datasets are presented. Theoretical underpinning of the classification tree approach is discussed in detail.

Data

Landsat Imagery

Cloud-free and terrain-corrected Landsat TM images of Yellowstone NP were obtained from the U.S. Geological Survey EROS Data Center (table 2.1).

Table 2.1. Landsat images, 1988-2003.

Year	**Date(s)**	**Sensor Type**
1988	22 July	TM 5
1997	15 July	TM 5
1999	14 August, 15 September	TM 7
2000	15 July, 16 August	TM 7
2001	2 July, 20 September	TM 7
2002	5 July, 23 September	TM 7
2003	1 August	TM 5

Tasseled Cap Transformation

TM digital numbers were converted to at-satellite reflectance and transformed by the tasseled cap method (Crist and Cicone 1984; Huang et al. 2002). The tasseled cap transformation is motivated by the observation that most TM values from the six reflectance bands (bands 1-5 and 7) occupy three dimensions that can be biophysically

interpreted as brightness, greenness, and wetness (Crist and Cicone 1984). Two-dimensional scatterplots of pairs of these variables resemble a tasseled cap, hence the name of the transformation. Tasseled cap brightness is a weighted sum of the six TM bands and responds primarily to features that reflect strongly or weakly in all six bands, e.g. clear, open water with a low brightness; bare, dry soil with a high brightness. Greenness represents a contrast of high absorption by vegetation in the visible spectrum (TM bands 1-3) with high reflectance in the near-infrared (TM band 4) and is an indicator of the amount of green vegetation (Crist and Cicone 1984). Wetness is determined by a contrast of the mid-infrared bands (TM bands 5 and 7), where reflectance is inversely related to vegetation and soil moisture content, with the visible and near-infrared spectra (TM bands 1-4) which are less sensitive to moisture (Crist and Cicone 1984).

Tasseled cap wetness has been shown to be an effective estimator of coniferous forest structure (Cohen and Spies 1992; Hansen et al. 2001) and has been used to discriminate between different forest harvest methods (Franklin et al. 2000, Franklin et al. 2001a). Importantly, the wetness measure does not appear to be influenced by topography (solar incidence angle), in contrast to the sensitivity of greenness and brightness measures to increasing topographic complexity (Cohen and Spies 1992). In a two dimensional feature space defined by wetness and greenness, Hodgson et al. (1987) found that deep water, shallow water, and marsh clustered at similar wetness values with increasing values of greenness, respectively.

Image Texture Analysis

While tone is the relative brightness of an object in an image, i.e. the gray level of a pixel, image texture can be defined as the local spatial variability of tone (Ferro and Warner 2002). A common way to measure image texture is to consider the spatial co-occurrence of gray level values at defined inter-pixel distances and orientations as quantified by a gray level co-occurrence matricx (GLCM). A number of texture measures derived from GLCM's have been developed (Haralick 1973) and combination of GLCM-derived texture measures with spectral data has been shown to increase land cover classification accuracy (Franklin and Peddle 1989; Peddle and Franklin 1991; Franklin et al. 2001b), including RADARSAT classification of wetlands (Arzandeh and Wang 2002). However, GLCM-based methods require specification of three parameters (window size, inter-pixel distance, and inter-pixel orientation) in addition to choices regarding which GLCM texture measure(s) to compute. Choosing the optimal set of parameters/measures can present a substantial feature-selection problem (Chan et al. 2000). For example, Peddle and Franklin (1991) used an 11 pixel by 11 pixel window, three different orientations, and three different texture measures to classify three multispectral bands.

A more parisimonious way to quantify texture across a digital image is to compute the variance of pixel values within a moving window of arbitrary size. Quantifying image texture by the simpler variance measure requires specification of only the window size, and in some cases the variance measure has been shown to be as accurate a classifier as GLCM-based or similar texture measures (Weszka et al. 1976;

Connors and Harlow 1980; Marceau et al. 1990). Smaller window sizes may enhance class separability by reducing edge effects (Ferro and Warner 2002). Wilson (1997) found that a 5 pixel-by-5 pixel window was an effective compromise between the noise-sensitivity of 3-by-3 windows and the edge-smoothing tendency of 7-by-7 windows. Image texture was calculated in 3-by-3, 5-by-5, and 7-by-7 pixel moving windows in the three tasseled cap bands and in TM bands 4 and 5 using ERDAS IMAGINE V8.6 software (Leica Geosystems GIS & Mapping, Atlanta, GA). Variances computed for individual moving windows were assigned to the center pixel.

Pixel-Differencing

Early to mid-July TM images were available from 2000-2002. In 2000, a mid-August image was also available. Similarly, two late-September images were acquired from 2001 and 2002. Seasonal differences were calculated for each of these three years by subtracting August or September tasseled cap values or TM reflectance from July values on a per-pixel basis. It was expected that non-wetland grasses and forbs would tend to senesce by mid-August through September, while wetland vegetation remained green. Upland pixels were expected to exhibit a drop in tasseled cap greenness or reflectance in the near infrared (TM band 4) over this period while wetland greenness values and TM band 4 reflectance remained relatively constant. Senescing vegetation may also exhibit increased brightness between mid and late summer (Crist and Cicone 1984), resulting in a pixel difference signal in the brightness band. Pixel differences were also anticipated to detect ephemeral wetlands that were wet in mid-July, but dry by late summer.

Landform Classification

A landform is defined as "any physical, recognizable form or feature of the Earth's surface having a characteristic shape, and produced by natural causes; it includes major forms such as a plain, plateau, or mountain, and minor forms such as a hill, valley, slope, esker, or dune. Taken together, landforms make up the surface configuration of the earth (Gary et al. 1974)." Yellowstone landforms have been classified as "meso" level elements on the order of 1-100 ha in size (Shovic 1996). The classification is based on both visible and inferred characteristics including; genetic origin, type and degree of stream drainage dissection, slope gradient distribution, slope curvature, relief, proportion and shape of bedrock exposure, and type of surficial materials (Shovic 1996).

The landform classification is likely to include factors associated with wetland formation. As such, it seems reasonable to anticipate that the landform classfication might integrate factors influencing wetland presence at a scale of 1-100 ha. The Yellowstone landform classification is defined hierarchically, allowing a degree of flexibility in choosing the required level of aggregation or differentiation. At the "group" level, twelve landform types are defined (Shovic 1996):

1. Alluvial landforms
2. Breaklands and colluvial slopes
3. Fluvial plateaus
4. Fluvial rolling uplands
5. Glacial troughs and cirques
6. Glaciated plateaus
7. Glaciated rolling uplands
8. Glaciofluvial terraces and plains
9. Hydrothermal landforms
10. Landslides
11. Other glaciofluvial landforms
12. Water

Soil Classification

The primary parent materials of Yellowstone soils are Quatenary rhyolite ash-flow tuffs, Quatenary rhyolite flows and Tertiary andesitic lava, ash, mud, and debris flows (Rodman et al. 1996). Weathering of these two rock types has resulted in soils with distinctly different textures and mineral nutrient contents. Soils formed from andesite tend to be medium- to fine-textured while soils formed from rhyolite are typically coarse- to medium-textured (Rodman et al. 1996). Extensive glaciation is another dominant factor in Yellowstone soil genesis; glaciofluvial sediments and till are common (Despain 1990).

The Yellowstone soil classification was completed in 1996. Describing the precision of the classification, Rodman et al. (1996) note that "…soils are classified and mapped at a scale suitable for broad resource planning" but not at a resolution fine enough for site-specific application. Eighty soil complexes are delineated across the Yellowstone landscape. Each soil complex is described as a mixture of individual soil families and exposed bedrock with mixtures quantified by the proportion of the complex covered by each soil family and bedrock.

In the description of each soil family, five attributes are summarized: average percent rock fragments, average percent clay content, average depth to a root-limiting layer, average percent base saturation, and average depth of the mollic horizon (Rodman et al. 1996). Since the soil polygons identified in the Yellowstone soil classification are mixtures of soil families whose boundaries are not delineated within those units, associating specific soil properties with individual pixels within those polygons is

ambiguous. In this study, a weighted average was calculated for each soil property within individual soil polygons. Weights were proportional to the percent cover of each soil family. All pixels within individual soil polygons were then assigned the weighted average for each soil property.

Habitat Types

The habitat type coverage for Yellowstone indicates potential climax vegetation. Habitat types are classified by a set of environmental factors, including temperature and moisture regime, light availability, mineral nutrient availability, and disturbance frequency (Despain 1990). Habitat types are named by two defining species. The first species is broadly adapted and dominates the climax community while the second species indicates an environmental subtype, e.g. subalpine fir/grouse whortleberry.

Yellowstone habitat types were delineated using a combination of ground surveys and aerial photo interpretation (Despain 1990) with 67 classes identified. At a more coarse level, 18 general habitat types have been defined through consolidation (Yellowstone NP Spatial Analysis Center, unpublished metadata). These generalized habitat types appear to retain information germane to wetland presence, and thus will be used for reasons of simplification. They include Douglas fir (*Pseudotsuga menzieseii*), lodgepole pine (*Pinus contorta*), subalpine fir (*Abies lasiocarpa*), whitebark pine (*Pinus albicaulis*), and nonforeseted climax communities. Nonforest classes are modified by their moisture regime (dry, moist, wet) or by the dominance of willows (*Salix spp.*) or sagebrush (*Artemesia spp.*). Subalpine fir types are classified as either moist or wet, or

by the presence of lodgepole pine or whitebark pine as sub-dominant species. Additional general habitat types include thermal area vegetation, wet forest, water, and talus.

Cover Types

Cover types are defined by the successional stage of the plant community following the most recent major disturbance, typically fire in Yellowstone (Despain 1990). Yellowstone cover types are delineated for forested vegetation circa 1991, i.e. following the large scale fires of 1988.

Burned forest stands were identified by 1988 satellite imagery while unburned forest was classified using pre-1988 aerial photographs. Post-fire changes were incorporated using 1991 aerial photography (Yellowstone NP Spatial Analysis Center, unpublished metadata). 38 forested cover types were identified by seral stage in addition to an undifferentiated nonforest class and water.

A more general classification was defined by merging classes into 15 cover types. These general cover types were used in this study and include post-disturbance, successional, and climax stands of Douglas fir, lodgepole pine, and whitebark pine. The remaining cover types are aspen (*Populus tremuloides*), krummholz, water, and nonforest.

Bedrock Geology

The bedrock geology layer is derived from the 1972 USGS Geologic Map of Yellowstone National Park (Yellowstone NP Spatial Analysis Center, unpublished metadata). 14 classes are delineated, including Quatenary rhyolites, basalts, and

sediments, Tertiary andesites, basalts, and sediments, and a number of marine sediments. Yellowstone experienced extensive glaciation from 2 million to 14,000 years ago. The resulting glacial tills constitute the parent material of most present-day Yellowstone soils. Given that the Yellowstone ice cap was largely stationary, these glacial tills were generally not moved, and most soils formed from the underlying bedrock (Despain 1990). This may have important implications with respect to wetland formation - coarse textured rhyolitic soils have higher hydraulic conductivites and lower water holding capacities than andesitic soils. More water tends to percolate through the root zone of rhyolitic soils and may subsequently be available to form seeps and springs. Despain (1990) notes that wet forests tend to form on the margins of Quatenary rhyolitic flows. Wet vegetation types also appear to be associated with Quatenary sediments, a bedrock class where deep glacial till and glacial landforms (potholes) are found (Despain 1990).

Precipitation

Average annual precipitation across Yellowstone is calculated over a 30-year period from 1961-1990 using snow course, snow survey telemetry, and climate station data (Yellowstone NP Spatial Analysis Center, unpublished metadata). Lines of equal precipitation were drawn connecting known points. Polygons in the precipitation map report average annual precipitation as intervals, e.g. 45.72 cm - 50.80 cm.

Snowfall

Average annual snowfall is calculated over the 15-year interval from 1958-1972 from snow course data (Yellowstone NP Spatial Analysis Center, unpublished metadata). Elevation versus average annual snowfall curves were used to estimate elevations at which equal increments of snowfall are expected. Polygons in the snowfall coverage report average annual snowfall as intervals.

Digital Elevation Model

A 30 meter digital elevation models (DEM) is available for Yellowstone (Yellowstone NP Spatial Analysis Center, unpublished metadata). The 30 meter DEM was used to compute a number of terrain attributes; slope, aspect, plan curvature, and plane curvature using TAPES-G terrain analysis software (Wilson and Gallant 2000a). Undrained depressions in the DEM were filled using the algorithm of Planchon and Darboux (2002) in preparation for overland water flow analysis (Wilson and Gallant 2000a). Fill depths in meters were retained as a separate raster layer and upstream contributing areas were computed using TAPES-G.

A topographic wetness index assuming steady-state subsurface flow, $\log_e$(upstream contributing area / tan slope), was calculated across the Yellowstone landscape, potentially indicating where saturated soils are likely to occur (Jenson and Domingue 1988; O'Loughlin 1986; Wilson and Gallant 2000a).

Training Data

The Yellowstone NWI was used to identify wetland training pixels. To reduce the likelihood of misspecifications from spatial errors and pixel mixing, i.e. pixels reflecting light from a combination of wetland and upland land covers, and given the spatial resolution of the Thematic Mapper, random sampling was limited to wetland pixels falling inside palustrine polygons larger than one ha (approximately 11 TM pixels). Riverine wetland was not sampled given that linear and typically narrow riparian features (often < 90 m wide) are difficult to classify by satellite imagery (Federal Geographic Data Committee 1992). Riverine wetlands, as defined in the Cowardin system, also encompass only a small percentage of the total wetland cover in Yellowstone. Persistent wetland vegetation along rivers and streams is defined as palustrine wetland in the Cowardin system and thus was included in sampling. Lacustrine wetlands are already accurately identified as lakes and permanent ponds in a number of park GIS coverages, and also were not sampled.

The sampling frame for upland training pixels was determined relative to NWI polygons. One stratum of upland random sampling was limited to pixels located more than 60 meters and less than 120 meters distance from any lacustrine, riverine, or palustrine NWI polygon. The nominal separation distance of 2 pixels from all NWI polygons should limit misspecifications due to spatial errors and pixel mixing, while capturing the wetland to upland transition. To ensure adequate coverage of upland sites across the Yellowstone landscape, a second stratum was randomly sampled from all

pixels greater than 120 meters distance from any NWI polygon. The number of pixels sampled from each of the upland strata was proportional to the total area of each stratum.

Under the Cowardin system, palustrine wetlands are subdivided into emergent, forested, scrub-shrub, aquatic bed, and unconsolidated shore classes (Cowardin et al. 1979). These classes are further subdivided by hydrologic regime; e.g. temporary flooded, saturated, seasonally flooded, permanently flooded, etc. Wetland classification trees were developed hierarchically. At the most general level, the likelihood of palustrine wetland occurrence was modeled. At the next level, classification trees were developed to distinguish between the five palustrine classes. At the finest level, emergent, forested, and aquatic-bed palustrine wetlands were classified by hydrologic regime, with separate classification trees built for each class

Palustrine wetlands are relatively rare on the Yellowstone landscape. From the Yellowstone NWI, the proportion of land area occupied by palustrine wetland is approximately 0.0555 of the total Yellowstone land area minus lacustrine and riverine wetlands. This rarity poses a problem for discrimination between upland and wetland pixels. Sampling a reasonably large number of wetland training pixels, say 10,000 pixels, requires sampling 170,180 upland pixels to achieve a proportional sample reflecting a best prior estimate of the relative cover of wetland and upland. Classification trees trained on unbalanced data tend to produce models that are highly accurate classifying dominant classes and much less accurate classifying rare classes (Breiman et al. 1984). This discrepancy results from the fact that greater increases in overall accuracy can be achieved by focusing predictive power on the dominant class. If classification

trees are trained with equal amounts of data from each class, prediction accuracies tend to be similar (Breiman et al. 1984). However, these models no longer accurately predict the probability of occurrence of the rare class since the probability of the rare class is much larger in the training sample than it is in the actual population. Additionally, even if the classification accuracies for the common and rare classes are both relatively high, say 90%, a high rate of errors of commission will occur for the rare class when predictions are applied to the entire population. A 10% misclassification rate for the common class results in a large number of false-positives relative to the total number of correctly classified instances of the rare class. In general, one can anticipate that classification trees trained with proportionally sampled data will tend to under-predict the true extent of palustrine wetland while models produced from equal sized training samples will tend to over-predict the extent of palustrine wetland.

Use of the Yellowstone NWI for training data relies on an assumption that pixels identified as wetland by the NWI truly are wetland. Given that the NWI appears to err more by omission than by commission, this is likely a defensible assumption. If the NWI is biased toward errors of omission, than some proportion of non-wetland training pixels will be misidentified. However, given the *a priori* rarity of wetland, the number of misidentified non-wetland training pixels would be expected to be small relative to the total size of the non-wetland training sample. Given an argument that the number of misidentified wetland training pixels and the number of misidentified non-wetland training pixels will be small relative to the entire training sample, it seems appropriate to use the NWI to develop models for discriminating palustrine wetland from upland.

The accuracy at which the Yellowstone NWI classifies palustrine wetlands as emergent, forested, scrub-shrub, aquatic bed, and unconsolidated shore classes is unknown. Since the Yellowstone NWI is derived from single photographs, classification of wetland hydrologic regimes would appear to be highly dependent on the experience and interpretation of individual photo-interpreters. In both cases, the Yellowstone NWI was accepted as nominally true for training purposes.

Classification Trees

The classification tree methodology used in this study was developed by Breiman et al. (1984) and is summarized below.

In general, classification problems involve assignment of a feature vector, $\mathbf{x} = (x_1, x_2, \ldots, x_n)$ to some class in the set $C = \{1, 2, \ldots, J\}$. Given a measurement space X containing all possible feature vectors of dimension n, define a classifier as a partition of X into J disjoint subsets, $A_1, A_2, \ldots, A_j$ where $X = A_1 \cup A_2 \cup \ldots A_j$ such that for every $\mathbf{x} \in A_j$, $\mathbf{x}$ is assigned to class j. Let the space $X \times C$ be the set of all couples $(\mathbf{x}, j)$ where $\mathbf{x} \in X$ and j is a class label, $j \in C$. Define P(A, j) to be a probability distribution defined on $X \times C$, $A \subset X$, $j \in C$ where P(A, j) is the probability that a randomly selected case is a member of class j with a measurement vector found in A_j. A binary classification tree is constructed using a training sample where N cases $(\mathbf{x}_1, \mathbf{x}_2, \ldots \mathbf{x}_N)$ are randomly drawn from the distribution P(A, j). The measurement space X is partitioned into disjoint subsets by repeated splitting of X into descendant subsets. Splitting continues until a stopping rule is satisfied. The subsets of X that remain unsplit are called terminal nodes.

All feature vectors within a terminal node are assigned the same class label. Each A_j in the final partition of X is the union of terminal nodes assigned class label j.

Though classification trees can be helpful for describing/interpreting multivariate data, they are typically used to make predictions for new measurement vectors whose class is unknown. The first step in building a classification tree is to specify the prior probability for each class $\pi(j)$, j = 1, 2, … J. These probabilities can be estimated from the training data as the proportions N_j/N where N_j is the number of training data cases from class j and N is the total size of the training sample, or the $\pi(j)$ can be determined from some other source of information. Let the nodes in a tree be indexed by the variable t. Define N(t) to be the number of training cases falling into node t and let $N_j(t)$ be the number of cases from class j found in node t. The joint probability of a case being from class j and falling into node t, p(j, t), is estimated from the training data as $p(j, t) = \pi(j)N_j(t)/N_j$. By extension, the probability of any case falling into node t, p(t), is computed,

$$p(t) = \sum_j \frac{\pi_j N_j(t)}{N_j}. \qquad [2.1]$$

The conditional probability that a training case is from class j given that it falls in node t,

$$p(j \mid t) = \frac{p(j,t)}{p(t)} \text{ with } \sum_j p(j \mid t) = 1. \qquad [2.2]$$

P(j | t) is estimated from the training data as,

$$p(j \mid t) = \frac{\pi(j)N_j(t)/N_j}{\sum_j \pi(j)N_j(t)/N_j}. \qquad [2.3]$$

When the $\pi(j)$ are estimated from the training data as N_j/N, $p(j \mid t)$ can be simplified to

$$p(j \mid t) = \frac{N_j(t)}{\sum_j N_j(t)} = \frac{N_j(t)}{N_t}, \qquad [2.4]$$

which is simply the proportion of class j training cases assigned to node t.

The critical issue in building a classification tree is choosing the splits of the measurement space X. Each split is determined by a rule applied to one variable in X. Given numeric data, rules are composed of statements of the form " is $x_i < \alpha$?" where α is some critical value. For categorical data, rules are of the form, "is $x_i \in S$?" where S is some subset of the set of all categories represented by x_i. In developing a methodology to evaluate and compare potential splits, Breiman et al. (1984) first define an impurity function:

DEFINITION 1: An impurity function ϕ is defined on the set of all J-tuples ($p_1, p_2, \ldots, p_J$) such that $p_j \geq 0$, $\sum_j p_j = 1$, and

(i) ϕ attains a single maximum at the point (1/J, 1/J,…, 1/J)

(ii) ϕ attains a minimum at the points (1, 0, …,0), (0, 1, 0,…,0),…, (0,…, 0, 1)

(iii) ϕ is a symmetric function of $p_1,\ldots, p_J$.

Given an impurity function and the conditional probabilities for the J classes at any node t, an impurity measure i(t) can be defined,

$$i(t) = \phi(p(1 \mid t), p(2 \mid t),\ldots, p(J \mid t). \qquad [2.5]$$

Two different impurity functions are typically used in building classification trees. The first, an information criterion, is computed as,

$$i(t) = -\sum_{j} p(j \mid t)\log\{p(j \mid t)\}. \qquad [2.6]$$

The second impurity function, the Gini index, is defined,

$$i(t) = \sum_{j \neq i} p(j \mid t)p(i \mid t). \qquad [2.7]$$

Splitting a node sends a proportion of the training data residing in that node to a left child node, t_L, with the remaining cases assigned to a right child node, t_R. Call these proportions p_L and p_R, respectively. The decrease in impurity resulting from a split s(t), is quantified as,

$$\Delta i(s, t) = i(t) - p_L i(t_L) - p_R i(t_R). \qquad [2.8]$$

Candidate splits are evaluated by applying all possible splitting rules to the training data at node t. The split which maximizes the decrease in impurity, $s^*(t)$, is determined to be optimal and thus defines elaboration of the classification tree at that node.

A stop-splitting rule can be defined as follows. Given a threshold β, a node t is declared a terminal node if $s^*(t) < \beta$. Another stop-splitting rule is to declare a node terminal if the number of cases assigned to the node is less than some value. Measurement vectors in a terminal node are typically assigned to the class with the largest conditional probability, p(j | t). Note that if the class priors are determined from the training data, i.e. N_J/N, this rule assigns a terminal node to the class with the largest number of measurement vectors falling into the node.

Classification trees generated by splitting the measurement space as described above typically overfit their training data, i.e. too many splits are made. When used to make predictions from additional data they usually do not achieve classification accuracies comparable to those found during model training. A solution proposed by Breiman et al. (1984) is to selectively prune terminal nodes back to their parent branches, resulting in more general trees. Pruning is based on resubstitution estimates of the probability of misclassification, i.e. estimates obtained by passing an independent test sample through a tree. If test cases falling into some node t are classified according to the largest class conditional probability, the resubstitution estimate r(t) of the probability of misclassification given that a case falls into node t is defined as

$$r(t) = 1 - \max p(j \mid t). \qquad [2.9]$$

Similarly, the joint probability R(t) that a case falls into node t and is misclassified is,

$$R(t) = p(t)r(t). \qquad [2.10]$$

By extension, the resubstitution estimate R(T) of the overall misclassification rate for an entire tree classifier T is,

$$R(T) = \sum_{t \in \tilde{T}} R(t) \text{ where } \tilde{T} \text{ is the set of all teriminal nodes of T.} \qquad [2.11]$$

The pruning process begins with the original unpruned classification tree T_{max} and generates a sequence of subtrees by pruning upward toward the root node. Define a branch, T_t, of tree T as including node t and all descendants of t. Pruning T_t from T involves retaining node t while eliminating all of its descendants. The remaining tree is denoted $T - T_t$. Where $T' = T - T_t$, the nested subset relationship between T′ and T is denoted $T' \prec T$.

The pruning algorithm of Breiman et al. (1984) is called "minimal cost-complexity pruning." The cost-complexity measure is defined,

DEFINITION 2: Given a subtree $T \preceq T_{max}$, let the number of terminal nodes $|\tilde{T}|$ be a measure of the complexity of T. Given a complexity parameter, $\alpha \geq 0$, define a cost-complexity measure $R_\alpha(T)$ as

$$R_\alpha(T) = R(T) + \alpha|\tilde{T}|. \qquad [2.12]$$

The cost-complexity measure adds a penalty for tree complexity to the overall resubstitution error. For increasing values of α, the objective of cost-complexity pruning becomes one of finding the subtree $T(\alpha) \preceq T_{max}$ such that $R_\alpha(T)$ is minimized. More formally, Breiman et al. (1984) require that the minimizing subtree $T(\alpha)$ satisfy the following conditions,

DEFINITION 3: The smallest minimizing subtree $T(\alpha)$ for a given value of $\alpha \geq 0$ is defined by the conditions

(i) $R_\alpha(T(\alpha)) = \min_{T \preceq T_{max}} R_\alpha(T)$ [2.13]

(ii) If $R_\alpha(T) = R_\alpha(T(\alpha))$, then $T(\alpha) \preceq T$. [2.14]

The second condition guarantees that when two subtrees have the same cost-complexity, the minimizing subtree is the smaller of the two. Qualitatively, when α is small the penalty for tree complexity is also small, and the minimizing subtree $T(\alpha)$ is large. As α

increases, the minimizing subtree will have fewer terminal nodes. At some sufficiently large value of α, $T(\alpha)$ consists of only the root node $\{t_1\}$ and the pruning process is complete. Note that while α is continuous, there are obviously only a finite number of subtrees of T_{max}. Thus, a finite sequence of subtrees $T_1, T_2, T_3, \ldots, \{t_1\}$ will be created by the pruning process. Given this finiteness, if $T(\alpha)$ is the minimizing subtree for some value of α, then $T(\alpha)$ will continue to be the minimizing tree until some breakpoint α' is reached. At α' a new tree $T(\alpha')$ will become the minimizing tree until the next breakpoint α'' is reached, etc. Two important results follow from Defintion 3 (Breiman et al. 1984).

THEOREM 1: For any value of $\alpha \geq 0$, there exists a unique, smallest minimizing subtree as defined by Definition 3.

THEOREM 2: Given a tree T_{max} with root node $\{t_1\}$ and given increasing values of $\alpha \geq 0$, the finite sequence of minimizing subtrees $T_1, T_2, \ldots, T_k, \{t_1\}$ is a nested sequence such that,

$$T_1 \succ T_2 \ldots \succ T_k \succ \{t_1\}. \qquad [2.15]$$

Proofs of Theorems 1 and 2 are found in Breiman et al. (1984). These results indicate it is not necessary to search all possible subtrees to find the unique minimizer of $R_\alpha(T)$. Instead, the sequence of minimizing subtrees can be found by sequentially pruning a classification tree upward toward the root node. The minimal cost-complexity pruning algorithm (Breiman et al. 1984) is summarized below:

Minimal Cost-Complexity Pruning

1. Given a tree T_{max}, first find the smallest subtree T_1 such that $R(T_1) = R(T_{max})$. This is accomplished by finding some pair of terminal nodes that are descendants of a single node t, t_L and t_R, such that $R(t) = R(t_L) + R(t_R)$. Repeat until there are no pairs of terminal nodes satisfying this condition. Given T_1, let $\alpha_1 = 0$.

2. Beginning with T_1, for any node $t \in T_1$, denote by {t} a subbranch of T_1 containing only the node t. T_t, as defined above, is a subbranch beginning at node t and containing all of its descendants. The cost-complexity of T_t is,

$$R_\alpha(T_t) = R(T_t) + \alpha\left|\tilde{T}_t\right|, \text{ where } \left|\tilde{T}_t\right| \text{ is the number of terminal nodes in } T_t. \qquad [2.16]$$

Since {t} consists of only a single node, it can be treated as a terminal node with a cost-complexity, $R_\alpha(\{t\}) = R(t) + \alpha$. Now, if $R_\alpha(T_t) < R_\alpha(\{t\})$, T_t is considered a better classifier than {t} since T_t has a smaller cost-complexity. But as α increases there will be a critical value, α_2, where the cost-complexity of T_t equals the cost-complexity of {t}. At this critical value, the single node {t} is considered a better classifier and its descendants in T_t are pruned away. The specific node at which pruning occurs is determined by rearranging the equality $R(T_t) = R(\{t\})$ as,

$$\alpha_2 = \frac{R(t) - R(T_t)}{\left|\tilde{T}_t\right| - 1}, \qquad [2.17]$$

and solving for α_2 at all non-terminal nodes in T_1. Pruning occurs at the node t* where α_2 is smallest. In the case of ties, prune all of the nodes where α_2 equals the minimum. Denote the pruned tree, $T_1 - t^*$, as T_2.

3. Repeat step 2 until only the root node remains.

Modeling Implementation

Classification trees were built for each year that TM imagery was available. Trees were developed using S-Plus V6.1 software (Insightful Corp., Seattle, WA) and its native classification tree functions. Training data was randomly sampled from spatial datasets using ArcInfo V8 software (Environmental Systems Research Institute, Redlands, CA). Training datasets were split into three subsets used for classification tree specification, pruning, and model verification.

In Chapter 3, classification trees were pruned using the cost-complexity parameter associated with the lowest overall classification accuracy of the pruning dataset. In Chapter 4, optimally pruned sub-trees were selected based on *a priori* accuracy goals for specific classes.

Predictions from palustrine wetland/upland classification trees were generated across the Yellowstone landscape on a 30 meter grid coinciding with the TM raster and pixels with predicted likelihood values greater than 0.5 were classified as palustrine wetland. Wetland pixels were then reclassified as emergent, forested, scrub-shrub, aquatic bed, and unconsolidated shore palustrine types according to the class with the largest likelihood. Hydrologic regimes were predicted for pixels classified as emergent, forested, or aquatic bed and pixels were assigned to the hydrologic regime with the greatest likelihood.

CHAPTER 3

IMPROVED WETLAND DETECTION IN YELLOWSTONE NATIONAL PARK BY COMBINATION OF LANDSAT THEMATIC MAPPER IMAGERY, IMAGE TEXTURE, AND ANCILLARY GIS INFORMATION

Introduction

Given the physical inaccessibility of wetlands in general, synoptic inventories of wetlands have typically required some method of remote sensing, whether by aerial photography or from satellite imagery. Wetlands in Yellowstone National Park are currently mapped by the National Wetland Inventory (NWI) from late summer 1:58,000 scale color infrared aerial photography, with some map units interpreted from 1:80,000 scale black-and-white aerial photographs (Elliott and Hectner 2000). The NWI classifies wetlands using the Cowardin classification system developed by the U.S. Fish and Wildlife Service (Cowardin et al. 1979). Under the Cowardin scheme, freshwater wetlands are divided into lacustrine, riverine, and palustrine systems. Palustrine wetland includes small, shallow open-water bodies and vegetated wetlands dominated by trees, shrubs, or emergent grasses, sedges, and forbs, and is the predominant wetland type in the Yellowstone NWI (Elliott and Hectner 2000).

National Wetland Inventory maps appear to err more by omission than by commission (Kuzila et al. 1991; Stolt and Baker 1995; Tiner 1997). Failures to identify wetland typically occur in coniferous forested wetlands, grazed wetlands, drier emergent wetlands on level terrain, small wetlands, and narrow, linear wetlands (Tiner 1997).

Minimal mapping units for the NWI interpreted from 1:58,000 scale infrared photographs are 0.5-1.2 ha for forested wetlands and less than 0.5 ha for ponds and pothole marshes (Tiner 1990). Importantly, single-date aerial photographs are not informative with respect to wetland dynamics; wetland water levels and soil moisture status can vary widely within a given year or between years, and the composition of dominant wetland vegetation may vary both within and between years (Cowardin and Golet 1995). Across the United States, large gaps exist in the completion status and digital availability of the NWI, including most of the state of Montana and the northern portion of the state of Idaho. Outside of northwest Wyoming, few digitized NWI maps are available for the Greater Yellowstone Region (U.S. Fish and Wildlife Service 2003).

Satellite remote sensing may offer a timely method for generating digital wetland maps where they are currently unavailable under the NWI. Landsat imagery is available from multiple years in Yellowstone National Park, encompassing a range of environmental conditions. Methods developed in this study should lead to detection of wetlands missed by the Yellowstone NWI, as well as providing a means for assessing the spatial and temporal variability of Yellowstone wetlands.

An extensive body of ancillary information is available from Yellowstone National Park including terrain, vegetation, geologic, soil, and climate data. These resources present a unique opportunity for researching potential improvements in satellite remote sensing of wetlands through combination of multi-source spatial data within a classification tree framework.

Satellite Remote Sensing of Wetlands

Satellite remote sensing of wetlands dates back to early efforts using the Landsat Multispectral Scanner (MSS) on Landsat-1 (Gammon and Carter 1976; Work and Gilmer 1976; Carter et al. 1977). Key conclusions were that MSS imagery was effective identifying wetlands larger than 1.5 ha in non-forested environments (Work and Gilmer 1976), but the limited spatial and spectral characteristics of the sensor were less effective distinguishing between different wetland types (Butera 1983, Ernst-Dottavio et al. 1981). The U.S. Fish and Wildlife Service actually considered using Landsat imagery for the National Wetland Inventory but concluded that the MSS could not achieve classification detail and accuracy requirements (Wilen and Bates 1995).

The Landsat Thematic Mapper (TM) brings increased spatial and spectral resolution to bear on the problem of wetland remote sensing. In the prairie pothole region of North Dakota, TM imagery was shown to detect over 90% of wetland basins 2-4 ha in size and 70% of wetland basins between 0.8 and 2 ha, while the detection rate for wetlands smaller than 0.8 ha fell to 20% (Federal Geographic Data Committee 1992). 0.8 ha corresponds roughly to nine TM pixels and may represent a lower limit on the resolution of the TM sensor when applied to wetland remote sensing.

To achieve better classification accuracy and improved detection of small wetlands, the Federal Geographic Data Committee (1992) recommended augmentation of satellite imagery with ancillary spatial information. However, only a small number of wetland mapping studies have actually done so. Forest wetland classification in Maine was improved using a Geographic Information System (GIS) rule-based method (Sader et

al. 1995). Pixels identified as forest by their TM spectral signature were assigned additional evidential weights depending on whether they satisfied a number of other conditions associated with forested wetland. Bolstad and Lillesand (1992) used a similar rule-based classification model to increase the accuracy of wetland land cover classification in northeastern Wisconsin. Huang and Jensen (1997) used a classification tree methodology to combine ancillary GIS layers with spectral data to improve wetland classification at the U.S. Department of Energy Savannah River Site.

Classification Trees

Integration of spatial information from multiple sources is an active area of research in the field of remote sensing (Ricchetti 2000; Treitz and Howarth 2000; Ma et al. 2001; Peddle and Ferguson 2002). One of the more difficult challenges in this area is combination of data recorded on different measurement scales, i.e. nominal, ordinal, interval, and ratio scales (Gong 1994).

Classification trees easily accommodate data from all measurement scales and make no distributional assumptions (Breiman et al. 1984). The hierarchical structure of classification trees allows them to detect non-additive interactions between independent variables without explicit specification (Clark and Pregibon 1992). Classification trees divide a complicated decision regarding class assignment into a union of several simpler decisions (Pal and Mather 2001). Automatic variable selection and complexity minimization are important attributes of classification trees. Variables that contribute to the predictive accuracy of a tree are utilized; those that do not are ignored. The tree structure is complicated only where class separation requires it (German et al. 1999).

Given their explicit specification, classification trees are easily interpreted (Freidl and Brodley 1997) and have been used to classify land cover in a number of studies (Moore et al. 1991; Hansen et al. 1996; Friedl and Brodley 1997; Lawrence and Wright 2001, Pal and Mather 2001; Wylie et al. 2001; Miller and Franklin 2002).

Methods

Single date, cloudless, and terrain-corrected Landsat-5 images of Yellowstone National Park from 1988, 1997, and 2003 were acquired from the U.S. Geological Survey EROS Data Center. From 1999-2002, cloudless, terrain-corrected Landsat 7 TM images were available from two dates (mid-summer and late-summer) from each year (table 3.1).

Table 3.1. Acquisition dates of Thematic Mapper imagery, 1988-2003.

Year	**Date(s)**	**Landsat-**
1988	22 July	5
1997	15 July	5
1999	14 August, 15 September	7
2000	15 July, 16 August	7
2001	2 July, 20 September	7
2002	5 July, 23 September	7
2003	1 August	5

TM digital numbers were converted to at-satellite reflectance and tasseled cap transformed using coefficients derived by Huang et al. (2002). While the tasseled cap transformation rotates six-dimensional TM data in a way that concentrates most of the measured variability into three dimensions corresponding to biophysically interpretable brightness, greenness, and wetness variables, other linear transformations might rotate TM data in a fashion that is more efficient in terms of class separation. For example,

canonical discriminant analysis rotates multidimensional data in a way that emphasizes differences in group means. In developing wetland/upland models, a canonical discriminant analysis was first conducted on at-satellite reflectance. Since there were only two classes in the analysis, the linear transformation that emphasized the difference between the wetland and upland class means was summarized by assigning a single canonical discriminant score to each training pixel.

Image texture was measured by computing variances in 3-by-3, 5-by-5, and 7-by-7 pixel moving windows in the brightness, greenness, and wetness tasseled cap bands and in the near-infrared and mid-infrared TM bands (4 and 5) using ERDAS IMAGINE V8.6 software (Leica Geosystems GIS & Mapping, Atlanta, GA).

In the years where two TM scenes were available, i.e. 1999-2002, per pixel differences were computed in the six TM bands and the three tasseled cap bands by subtracting late summer values from mid-summer season values.

Undrained depressions in a 30 m DEM of Yellowstone were filled using the algorithm of Planchon and Darboux (2002). Depression fill depth was retained as an ancillary terrain variable while percent slope and a steady state topographic wetness index, $\log_e$(upstream contributing area/tan slope), were computed using TAPES-G terrain analysis software (Wilson and Gallant 2000).

Ancillary GIS information was obtained from the Yellowstone Spatial Analysis Center (Mammoth Hot Springs, WY). Available vegetation information included habitat types (potential climax vegetation) and cover types (existing vegetation following the 1988 Yellowstone fires). Yellowstone landforms have been classified based on slope

gradient distribution, type and degree of stream drainage dissection, slope curvature, relief, proportion and shape of bedrock exposure, and type of surficial materials (Shovic 1996). The bedrock geology classification for Yellowstone is derived from the 1972 USGS Geologic Map of Yellowstone National Park (Yellowstone NP Spatial Analysis Center, unpublished metadata). Habitat type, cover type, landform type, and bedrock geology class names and their abbreviations are summarized in table 3.2.

The Yellowstone soil classification consists of eighty soil complexes (Rodman et al. 1996), and as such contains too many classes to be used in a classification tree analysis. Complicating generalization of the Yellowstone soil classification is the fact that individual soil polygons are reported as mixtures of component soil families identified by the percent cover of each component. For each soil family in the mixture, a number of soil properties are summarized. Given these summaries, weighted averages based on the percent cover of each family were calculated for two soil properties thought to be important with respect to wetland hydrology; average percent clay content and average percent rock fragments. All pixels within individual soil polygons were then assigned these weighted averages.

Climate information for Yellowstone includes average annual precipitation calculated over a 30-year period from 1961-1990 and average annual snowfall calculated from 1958-1972 using snow course, snow survey telemetry, and climate station data (Yellowstone NP Spatial Analysis Center, unpublished metadata). Polygons in the precipitation coverage and snowfall coverage report precipitation and snowfall as isopleths.

Table 3.2. Habitat type, cover type, and landform type classes with corresponding abbreviations.

Habitat type		**Cover type**		**Landform type**	
Douglas fir	doug_fir	Aspen	aspen	Alluvial landforms	al
Lodgepole pine	lodgepole	Douglas fir, climax	dougfir_clim	Breaklands and colluvial slopes	bcs
Nonforested, alpine	nonforest_alp	Douglas fir, post disturbance	dougfir_post	Fluvial plateaus	fp
Nonforested, dry	nonforest_dry	Douglas fir, successional	dougfir_succ	Fluvial rolling uplands	fru
Nonforested, moist	nonforest_moist	Engelmann spruce and subalpine fir, climax	engel_subfir	Glacial troughs and cirques	gtc
Nonforested, sagebrush	nonforest_sage	Krummholz	krummholz	Glaciated plateaus	gp
Nonforested, wet	nonforest_wet	Lodgepole pine, climax	lodgepole_clim	Glaciated rolling uplands	gru
Nonforested, willow	nonforest_willow	Lodgepole pine, post disturbance	lodgepole_post	Glaciofluvial terraces and plains	gtp
Pitchstone plateau complex	pitchstone	Lodgepole pine, successional	lodgepole_succ	Hydrothermal landforms	hl
Subalpine fir, lodgepole pine	subfir_lodgepole	Nonforest	nonforest	Landslides	ls
Subalpine fir, moist	subfir_moist	Pygmy lodgepole pine	lodgepole_pyg	Other glaciofluvial landforms	ogl
Subalpine fir, wet	subfir_wet	Water	water	Water	w
Subalpine fir, whitebark pine	subfir_whitebark	Whitebark pine, climax	whitebark_clim		
Talus	talus	Whitebark pine, post disturbance	whitebark_post		
Thermal area vegetation	thermal_veg	Whitebark pine, successional	whitebark_succ		
Water	water				
Wet forest	wet_forest				
Whitebark pine	whitebark				

The 30 m DEM and derived terrain elements were re-sampled to coincide with TM pixels using ArcInfo V8 software (Environmental Systems Research Institute, Redlands, CA). Similarly, polygon coverages were converted to grid coverages using the 30 m TM grid.

Training pixels were identified using the Yellowstone National Wetland Inventory. To reduce the likelihood of misspecifications from spatial errors and pixel mixing, random sampling of wetland sites was limited to wetland pixels falling inside palustrine polygons larger than one ha (approximately 11 TM pixels). Riverine wetlands were not sampled given that linear and typically narrow riparian features (often < 90 m wide) are difficult to classify by satellite imagery (Federal Geographic Data Committee 1992), and also given the fact that riverine wetlands encompass only a small percentage of the total wetland cover in Yellowstone. Note that persistent wetland vegetation along rivers and streams is defined as palustrine wetland in the Cowardin system and thus was included in training samples. Lacustrine wetlands are already accurately identified as lakes and permanent ponds in a number of Yellowstone GIS coverages and also were not sampled.

Stratified sampling of upland training pixels was determined relative to NWI polygons. One stratum was limited to pixels located more than 60 meters and less than 120 meters distance from any lacustrine, riverine, or palustrine NWI polygon. The nominal separation distance of 2 pixels from all NWI polygons was intended to limit misspecifications due to spatial errors and pixel mixing while capturing the wetland to upland transition. To ensure adequate coverage of upland sites across the entire park, a

second stratum was randomly sampled from all pixels greater than 120 meters distance from any NWI polygon.

Under the Cowardin system, palustrine wetlands are divided into emergent, forested, scrub-shrub, aquatic bed, and unconsolidated shore classes (Cowardin et al. 1979). Following this scheme, wetland classification trees were developed hierarchically. At the most general level, the likelihood of palustrine wetland occurrence was modeled. At the next level, classification trees were developed to distinguish between the five palustrine classes.

Palustrine wetlands are relatively rare on the Yellowstone landscape. From the Yellowstone NWI, the proportion of land area occupied by palustrine wetland is approximately 5.6% of the total land area (minus lacustrine and riverine wetlands). This rarity poses a problem for discrimination between upland and wetland pixels. Sampling a reasonably large number of wetland training pixels, say 10,000 pixels, while ensuring that the stratified sample is proportionally equivalent to the true number of wetland and upland pixels, would require approximately 170,000 upland pixels. However, classification trees trained on unbalanced data tend to produce models that are highly accurate classifying dominant classes and much less accurate classifying rare classes (Breiman et al. 1984). This discrepancy results from the fact that greater increases in overall accuracy can be achieved by focusing predictive power on the dominant class, in this case the upland class. If classification trees are trained with equal amounts of data from each class, prediction accuracies tend to be similar (Breiman et al. 1984). However, these models no longer accurately predict the probability of occurrence of the rare class

since the probability of the rare class is much larger in the training sample than it is in the actual population. Additionally, even if the classification accuracies for the common and rare classes are both relatively high, say 90%, a 10% misclassification rate for the common class results in a large number of false-positives relative to the total number of correctly classified instances of the rare class. In general, one would anticipate that classification trees trained with proportionally sampled data would tend to under-predict the true extent of palustrine wetland while models produced from equal sized training samples would tend to over-predict the extent of palustrine wetland.

In this study, the objective was to identify true wetland pixels at a high rate. Thus equal numbers of wetland and upland pixels were used as training data, in this case 50,000 pixels from each class. Training data for discriminating the five palustrine wetland classes were randomly sampled from palustrine wetland polygons larger than 1 ha, and in proportion to their occurrence in the Yellowstone NWI, including 1,156 palustrine aquatic bed (PAB) pixels, 68,774 palustrine emergent (PEM) pixels, 22,242 palustrine forested (PFO) pixels, 5,232 palustrine scrub-shrub (PSS) pixels, and 2,596 palustrine unconsolidated shore (PUS) pixels for a total of 100,000 training locations.

The same training data locations were used for each year of TM imagery. This allowed a comparison of classification trees created using different combinations of ancillary data and an assessment of the consistency with which models made use of ancillary information given TM imagery from different years.

Use of the Yellowstone NWI for training data relies on an assumption that pixels identified as wetland by the NWI truly are wetland. This is likely a defensible

assumption if the Yellowstone NWI tends to err more by omission than by commission. If the NWI is biased toward errors of omission, then some proportion of upland training pixels would be expected to truly be wetland. However, given the *a priori* rarity of wetland, the number of misidentified upland training pixels would be expected to be small relative to the total size of the upland training sample. Similarly, if errors of commission are rare in the NWI, one could assume that the proportion of wetland training pixels that actually are upland would be small relative to the proportion of correctly labeled wetland training pixels.

The accuracy at which the Yellowstone NWI classifies palustrine wetlands as emergent, forested, scrub-shrub, aquatic bed, and unconsolidated shore classes is unknown. In this case, the Yellowstone NWI was accepted as nominally true for training purposes.

Classification tree analysis was conducted using S-Plus V6.1 software (Insightful Corporation, Seattle, WA). Cost-complexity pruning of classification trees (Breiman et al. 1984) was automated by using set-aside pruning data sampled identically to training data. Cost-complexity parameters associated with minimum overall classification accuracies of pruning data were used to identify optimally pruned trees. Error rates of optimally pruned trees were then assessed using a third set of data set aside for model verification.

Classification trees were constructed for the seven years of satellite imagery using four different combinations of predictors. 1.) TM imagery alone, including at-satellite reflectance in the six TM reflectance bands and the three tasseled cap bands; and in

wetland/upland trees only, canonical discriminant analysis scores. 2.) TM imagery plus texture measures (TM+TXT), where image texture was computed for tasseled cap brightness, greenness, and wetness, and TM bands 4 and 5. 3.) TM imagery plus texture and terrain information derived from the Yellowstone DEM (TM+TXT+DEM), including elevation, depression fill depth, slope and topographic wetness index. 4.) All predictors, including TM imagery, texture measures, terrain information, and all thematic ancillary GIS information (TM+TXT+DEM+GIS).

Classification tree predictions were made in the form of probabilities of occurrence for each class. In wetland/upland trees these values cannot be treated as unbiased estimates of the probability of wetland occurrence since training data contained proportionally more wetland pixels than found on the Yellowstone landscape. In this case, classification tree predictions are better considered as relative likelihoods of wetland occurrence. Pixels were classified as palustrine wetland for all likelihood values greater than 0.5. Palustrine wetland types were sampled in proportion to their presence in the NWI and thus classification tree output can be interpreted as unbiased probabilities. But in addition to being conditional on predictor variables, these probabilities are conditional on the fact that a given pixel is truly palustrine wetland. Individual pixels were assigned to the palustrine wetland class with the largest probability of occurrence.

Results

The effect of window size on the efficiency of variance texture measures was assessed by building wetland/upland and palustrine wetland type classification trees for

the seven years of TM imagery, three window sizes, and three combinations of predictors. Among wetland/upland classification trees for the seven years of TM imagery, the smallest average overall misclassification error rates were observed for the 5 pixel by 5 pixel window size in TM+TXT+DEM+GIS and TM+TXT+DEM models (table 3.3), though differences were small. For TM+TXT models, the lowest average misclassification error rate was observed for the 3 pixel by 3 pixel window size, 11.91%, though the 5 pixel by 5 pixel error rate was similar, 12.03%. Given these results, 5 pixel by 5 pixel textures were used in all subsequent wetland/upland classification trees.

Table 3.3. Overall misclassification error rate (%) for wetland and upland classes as a function of texture window size and model.

	TM + TXT + DEM + GIS			**TM + TXT + DEM**			**TM + TXT**		
Year	**3x3**	**5x5**	**7x7**	**3x3**	**5x5**	**7x7**	**3x3**	**5x5**	**7x7**
1988	7.73	7.48	7.67	9.48	9.38	9.52	11.74	11.57	11.61
1997	9.32	8.93	9.14	12.26	12.00	12.26	15.52	15.38	15.59
1999	7.57	7.56	7.77	9.16	9.02	9.30	11.09	10.65	11.13
2000	7.39	7.36	7.29	9.06	8.70	8.91	9.90	9.96	10.00
2001	7.96	7.93	8.15	10.09	11.05	10.22	11.68	13.64	12.06
2002	8.28	8.37	8.22	10.20	10.23	10.37	12.32	12.23	12.42
2003	7.68	7.23	7.45	9.39	8.81	9.16	11.10	10.81	11.13
Mean	**7.99**	**7.84**	**7.96**	**9.95**	**9.88**	**9.96**	**11.91**	**12.03**	**11.99**
Std. Error	**0.25**	**0.23**	**0.24**	**0.42**	**0.48**	**0.43**	**0.67**	**0.72**	**0.67**

Among classification trees for the five palustrine wetland types, 3 pixel by 3 pixel windows exhibited the lowest average overall misclassification error rates across the three models (table 3.4). As a result, the 3 pixel by 3 pixel window size was determined to be optimal and used in all subsequent palustrine wetland type classification trees.

However, once again note that differences in error rates varied little across the three window sizes.

Table 3.4. Overall misclassification error rate (%) for palustrine wetland types as a function of texture window size and model.

	TM + TXT + DEM + GIS			TM + TXT + DEM			TM + TXT		
Year	**3x3**	**5x5**	**7x7**	**3x3**	**5x5**	**7x7**	**3x3**	**5x5**	**7x7**
1988	14.32	14.76	14.90	16.24	16.38	16.72	17.24	17.56	18.42
1997	17.19	17.44	17.51	21.43	21.16	21.22	22.89	22.61	22.65
1999	16.63	16.46	16.66	19.23	19.52	19.52	20.41	20.56	23.18
2000	16.68	16.72	17.08	19.29	19.49	19.67	20.55	20.81	21.18
2001	15.69	15.72	16.15	17.57	17.45	17.80	18.51	18.84	18.95
2002	15.42	15.57	15.93	17.40	17.55	17.79	18.56	18.89	19.12
2003	17.50	17.36	17.72	21.06	21.12	21.29	22.05	22.17	22.57
Mean	**16.20**	**16.29**	**16.56**	**18.89**	**18.95**	**19.14**	**20.03**	**20.21**	**20.87**
Std. Error	**0.42**	**0.37**	**0.37**	**0.73**	**0.71**	**0.67**	**0.77**	**0.70**	**0.76**

Model verification error rates were calculated after each wetland/upland classification tree was optimally pruned. In general, model verification errors-of-omission (or producer's error rate) declined for wetland and upland classes as more predictors were added to classification trees (table 3.5). Average overall error rates for the TM and TM+TXT models were 14.19% and 12.51%, respectively. Average overall error rates for TM+TXT+DEM and TM+TXT+DEM+GIS classification trees were 10.09% and 8.18%, respectively. No significant increase in overall accuracy was found for classification trees using both a mid-summer and late-summer image; the average overall error rate for single date Landsat-5 imagery was 8.20% while the average overall error rate for two-date Landsat-7 imagery was 8.16%.

Table 3.5. Producer's and overall error rate (%) for wetland/upland classification trees given four predictive models; 1988, 1997, 1999-2003.

Model	**TM**			**TM+TXT**			**TM+TXT+DEM**			**TM+TXT+DEM+GIS**		
Year	**WET**	**UPL**	**Overall**	**WET**	**UPL**	**Overall**	**WET**	**UPL**	**Overall**	**WET**	**UPL**	**Overall**
1988	14.43	15.30	14.87	9.77	14.10	11.94	10.34	8.79	9.57	8.85	6.71	7.78
1997	15.35	20.53	17.94	13.80	17.92	15.86	11.09	13.41	12.25	9.97	8.65	9.31
1999	12.48	13.89	13.19	9.54	12.95	11.25	9.61	8.82	9.22	7.59	8.17	7.88
2000	12.20	11.73	11.97	10.24	10.58	10.41	7.71	9.94	8.83	7.57	8.00	7.79
2001	13.69	13.39	13.54	12.77	15.93	14.35	10.22	12.33	11.28	9.80	6.82	8.31
2002	13.45	14.41	13.93	12.97	12.48	12.73	11.08	9.76	10.42	8.68	8.68	8.68
2003	14.31	13.47	13.89	10.82	11.29	11.06	8.78	9.33	9.06	8.06	6.96	7.51
Mean	**13.70**	**14.67**	**14.19**	**11.42**	**13.61**	**12.51**	**9.83**	**10.34**	**10.09**	**8.65**	**7.71**	**8.18**
Std. Error	**0.42**	**1.06**	**0.71**	**0.65**	**0.98**	**0.75**	**0.47**	**0.68**	**0.49**	**0.37**	**0.33**	**0.24**

For the wetland class, the average error rate decreased 2.28 percentage points when image texture was added to TM information (table 3.5). Further adding terrain information and GIS layers decreased the average error rate for the wetland class by 1.59 and 1.18 percentage points, respectively. However, addition of image texture to TM information had a smaller effect on the average error rate of the upland class, reducing it by 1.06 percentage points. By contrast, adding ancillary information in the form of terrain measures and thematic GIS data appeared to benefit upland classification more than wetland classification, decreasing the average upland error rate by 3.27 and 2.63 percentage points, respectively.

Predictors retained by 1999-2002 optimal TM+TXT+DEM+GIS classification trees (table 3.6) are ordered by the level at which they first appear in each tree, a rough

Table 3.6. Predictors retained by wetland/upland classification trees, 1999-2002.

Level	**1999**	**2000**	**2001**	**2002**
1	U1	U1	U1	U1
2	Habitat type	Habitat type	Habitat type	Habitat type
2	Landform Type	Landform type		
3	AUG TM4 texture	AUG TM4 texture	Landform type	JULY TM4 texture
3			JULY TM4 texture	Landform type
4	SEPT greenness texture	Slope	Bedrock geology	Slope
4			Slope	Bedrock geology
4			SEPT TM4 texture	SEPT TM4 texture
5	AUG greenness texture	JULY TM4 texture	% Rock fragments	Greenness difference
5	Slope	% Clay	% Clay	Snow
5	% Rock fragments	Bedrock geology		SEPT greenness
5	Bedrock geology			
6	% Clay	Cover type	SEPT greenness	% Clay
6	SEPT TM4 texture		Greenness difference	Cover type
6				
7	AUG TM3	AUG greenness	Cover type	
7			JULY greenness	
8	AUG greenness		Precipitation	% Rock fragments
9	AUG TM7		Snow	JULY greenness texture

measure of the importance of each variable to the classification tree algorithm. The first four variables used are canonical discriminant analysis scores (U1), habitat type, landform type, and TM band 4 texture. Slope and bedrock geology are first used at intermediate depths (levels four or five) while percent clay content is first used at level five or six. Percent rock fragments was first used at level five in 1999 and 2001 trees. However, the 2000 classification tree did not retain percent rock fragments as a predictor and the 2002 tree did not use percent rock fragments until level 8. All classification trees made use of TM band 4 textures from a second month at intermediate positions (levels four through six) while tasseled cap greenness was used at intermediate to lower positions (levels five through eight). While the 1999 tree makes use of greenness texture from both August and September, only the 2002 tree also used greenness texture, and in this case, not until level nine. Per-pixel differences (in the greenness band) were used only in 2001 and 2002.

Single-date TM+TXT+DEM+GIS classification trees for 1988, 1997, and 2003 also use U1, habitat type, landform type, and TM band 4 texture at upper levels (table 3.7), though the 1988 and 2003 trees also make of greenness texture at level three. Slope, bedrock geology, percent clay content, percent rock fragments, and tasseled cap greenness are, again, typically first used at intermediate depths. The 1997 tree retained more predictors, including reflectance in TM bands 1,5, and 7. Note that 1997 was an unusually wet year in Yellowstone National Park and that the 1997 classification tree had the highest overall error rate among years (table 3.4). The 1997 tree appears to use more predictors in response to greater classification difficulty.

Table 3.7. Predictors retained by wetland/upland classification trees, 1988, 1997, and 2003.

Level	1988	1997	2003
1	U1	U1	U1
2	Habitat type	Habitat type	Landform type
3	Landform type	Landform type	Habitat type
3	JULY greenness texture		AUG greenness texture
3	JULY TM4 texture		AUG TM4 texture
4		JULY TM4 texture	% Clay
4		% Clay	Slope
4	Slope	Slope	
4	July greenness	% Rock fragments	
5	Bedrock geology	Cover type	AUG greenness
5		Snow	Bedrock geology
5		Bedrock geology	
5		JULY brightness texture	
5		JULY greenness	
6	% Rock fragments	Elevation	
6	Topographic wetness index	JULY TM1	
7	% Clay	JULY greenness texture	Precipitation
7		JULY TM7	Depression fill depth
8		JULY TM5	
9	JULY TM5 texture	Precipitation	% Rock fragments
10		JULY wetness	

Training models over multiple years at the same training locations given identical ancillary information and different TM data allows an assessment of the consistency at which classification trees make use of spectral and ancillary information in different years. Given the likely instability of classification trees at deeper levels between years, comparisons are limited to higher levels of tree structure. In figure 3.1, unlabeled optimal wetland/upland classification trees for 1988 and 1999 are drawn next to simplified, higher level trees. In each tree, branch lengths are proportional to the reduction in total deviance accounted for by the split they arise from. Simple trees account for a substantial proportion of the total deviance resolved by full trees.

1988 Palustrine Wetland/Upland Optimal Tree

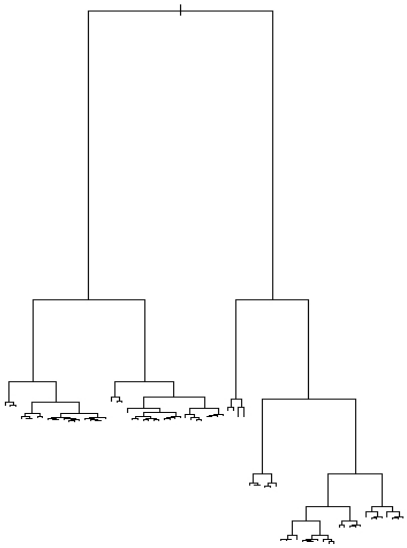

1988 Palustrine Wetland/Upland Simple Tree

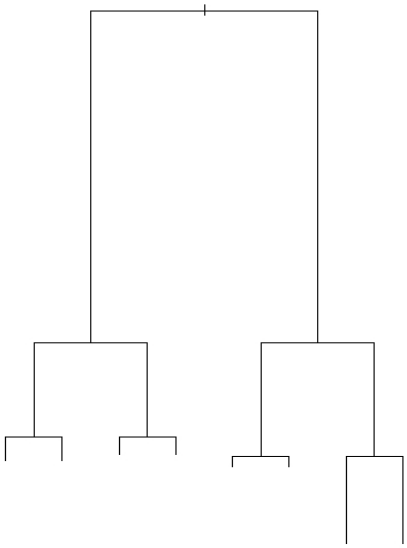

1999 Palustrine Wetland/Upland Optimal Tree

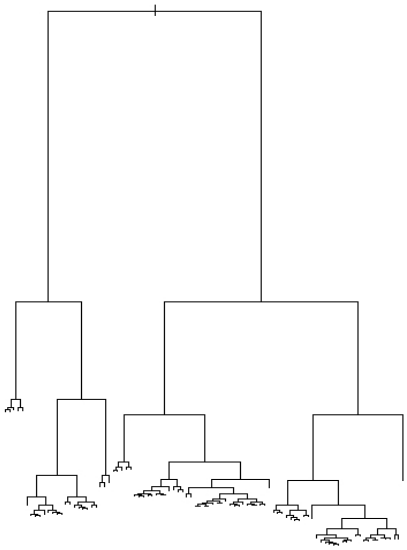

1999 Palustrine Wetland/Upland Simple Tree

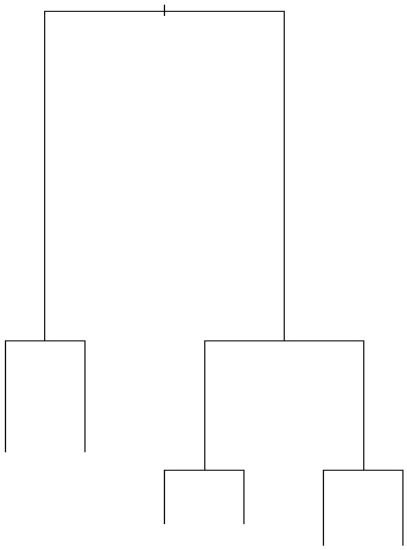

Figure 3.1. Optimal and simple wetland/upland classification trees, 1988 and 1999.

Simple wetland/upland classification trees for the seven years have similar high-level structures (figures 3.2-3.8) with no evidence that two-date imagery is used differently than single-date imagery. The first split in all trees is on canonical discriminant analysis scores, U1. Smaller U1 values are associated with upland, and in each year approximately 40,000 upland training pixels are sent down the left main branch of each tree. Larger canonical discriminant scores are associated with wetland, and approximately 40,000 wetland pixels are sent down the right main branch of each tree. Thus we have a wetland main branch and an upland main branch for each tree.

Moving down the upland main branch, all wetland/upland trees make a split on habitat type at node (4) (figures 3.2-3.8). Wetter habitat types (nonforest wet, nonforest willow, subalpine fir wet, thermal vegetation, water, and wet forest) are split to the left. Within these wetter habitat types, the 1999-2003 trees make a split on TM band 4 image texture at node (8). Smaller texture values are sent to an upland terminal node while larger texture values are sent to a wetland terminal node. In each year, earlier TM band 4 textures were used, i.e. August in 1999 and July in 2000-2002. The 1988 tree makes an equivalent split on tasseled cap greenness at node (8). By contrast, the 1997 tree uses a split on landform type at node (8). In this case wetland is associated with alluvial (al) and (hl) landforms.

Returning to the split on habitat type at node (4), pixels associated with drier habitat types are subjected to a subsequent split on TM band 4 texture at node (10) over all years but 1997 (figures 3.2, 3.4-3.8), with smaller TM band 4 textures sent to an upland terminal node. The 1997 classification tree relies on landform type at node (10)

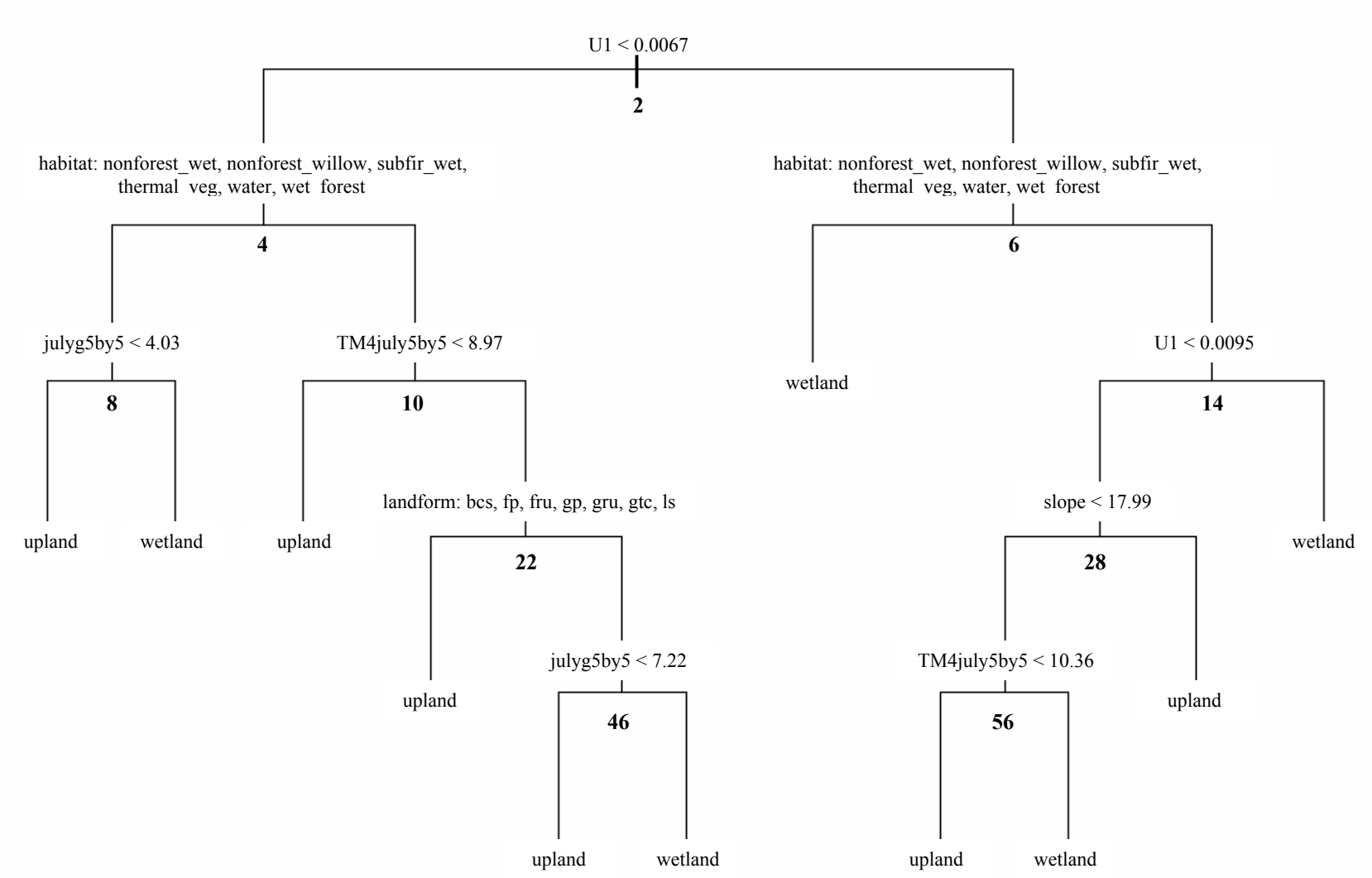

Figure 3.2. 1988 palustrine wetland/upland simple classification tree.

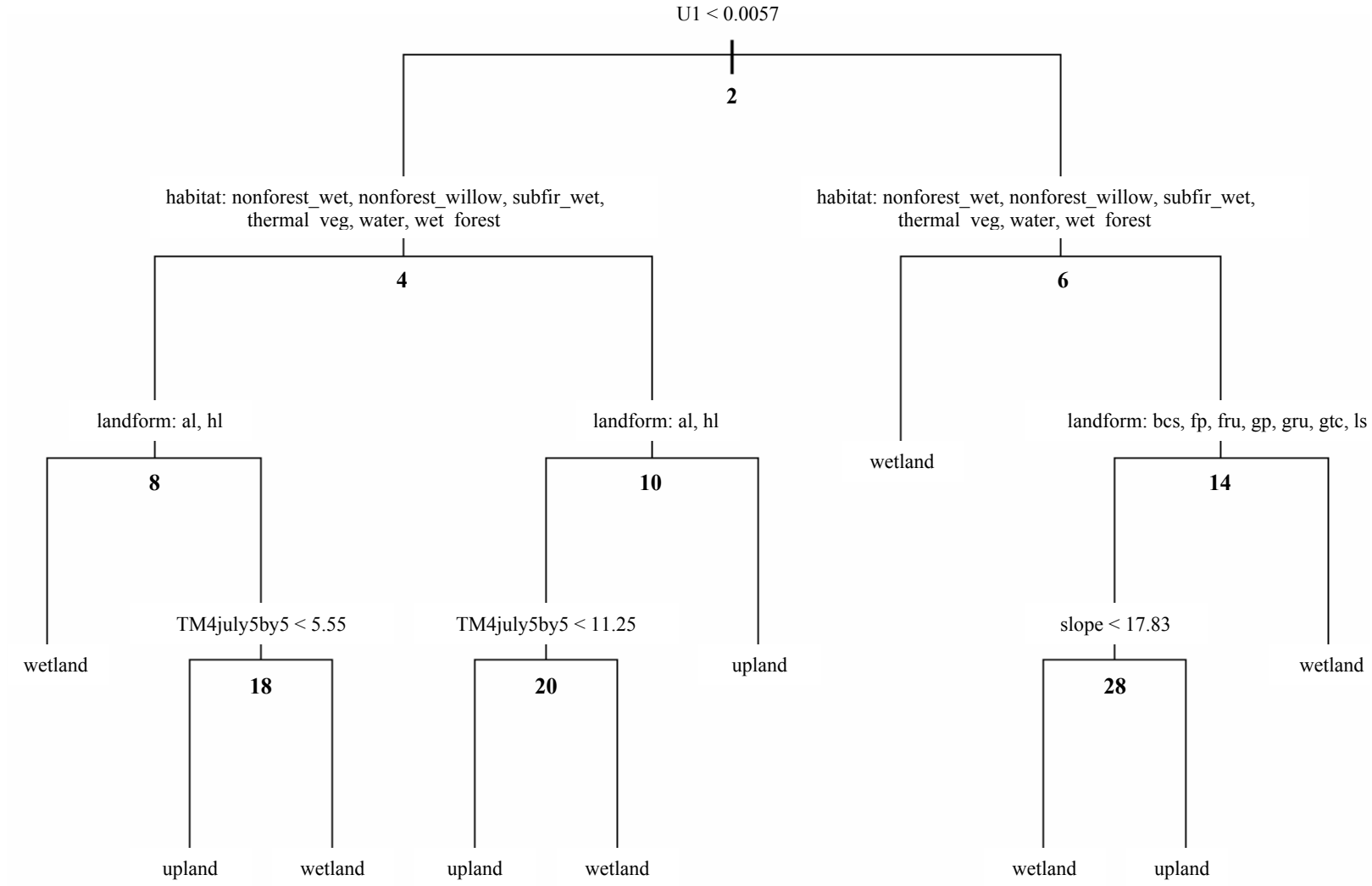

Figure 3.3. 1997 palustrine wetland/upland simple classification tree.

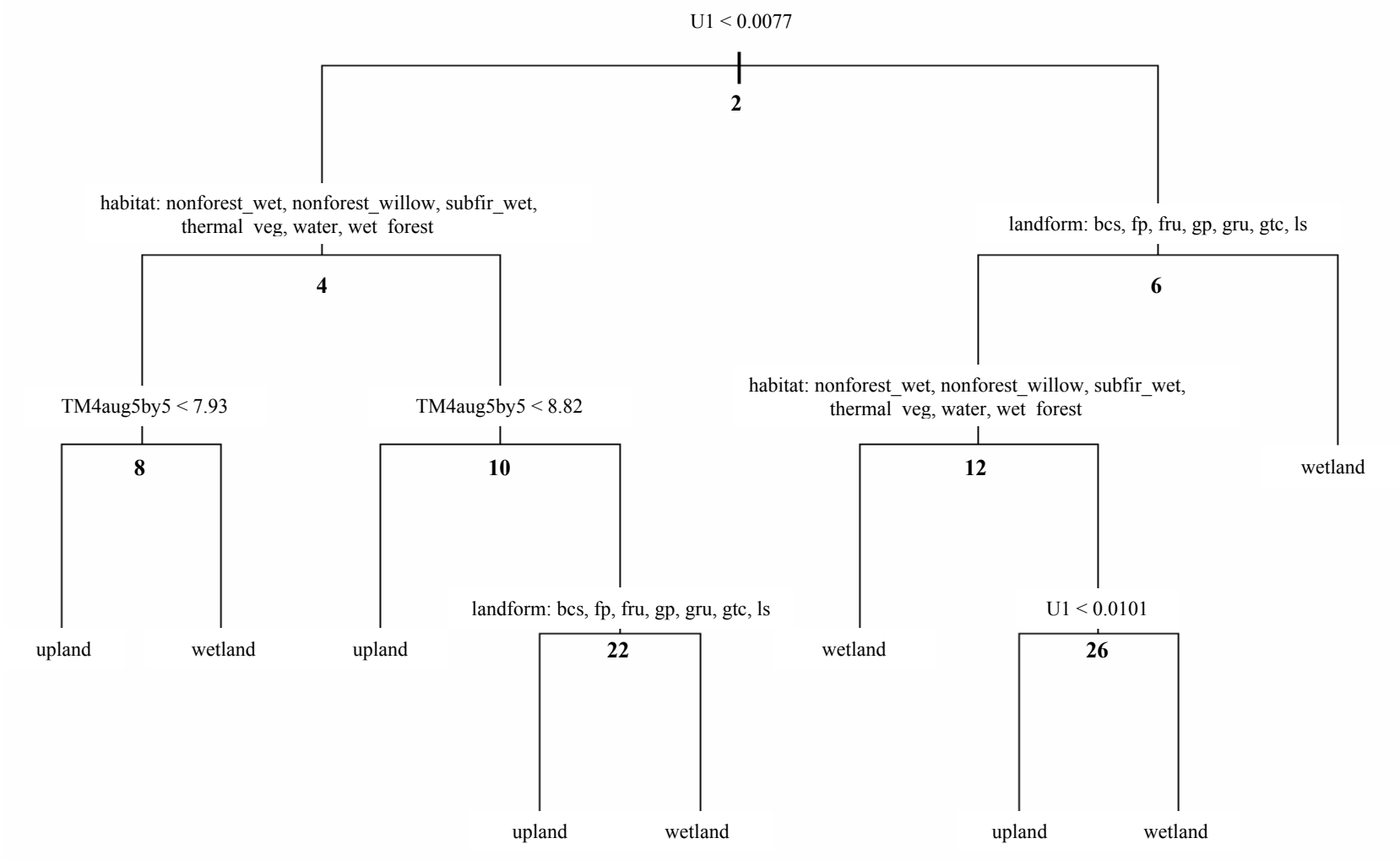

Figure 3.4. 1999 palustrine wetland/upland simple classification tree.

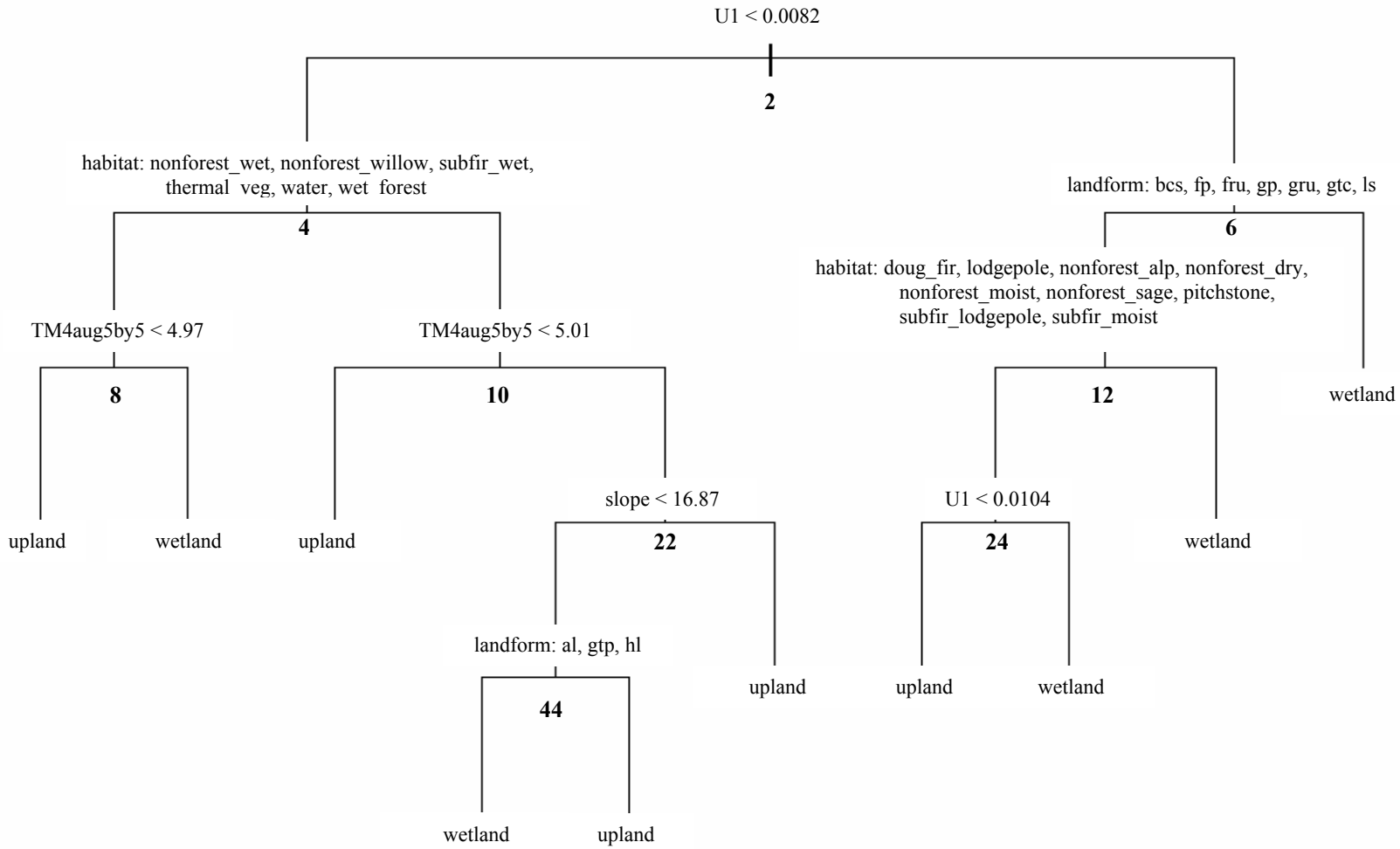

Figure 3.5. 2000 palustrine wetland/upland simple classification tree.

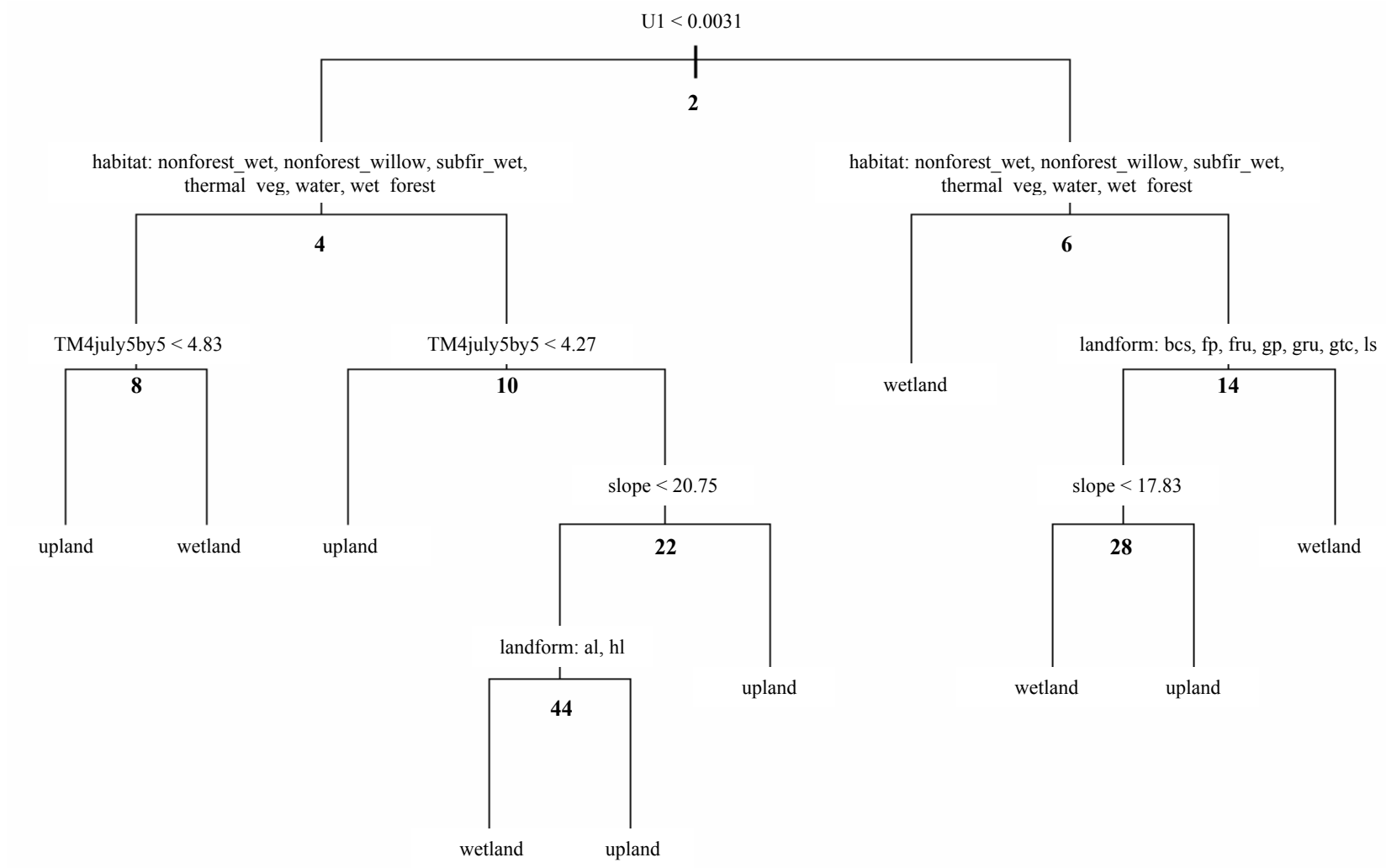

Figure 3.6. 2001 palustrine wetland/upland simple classification tree.

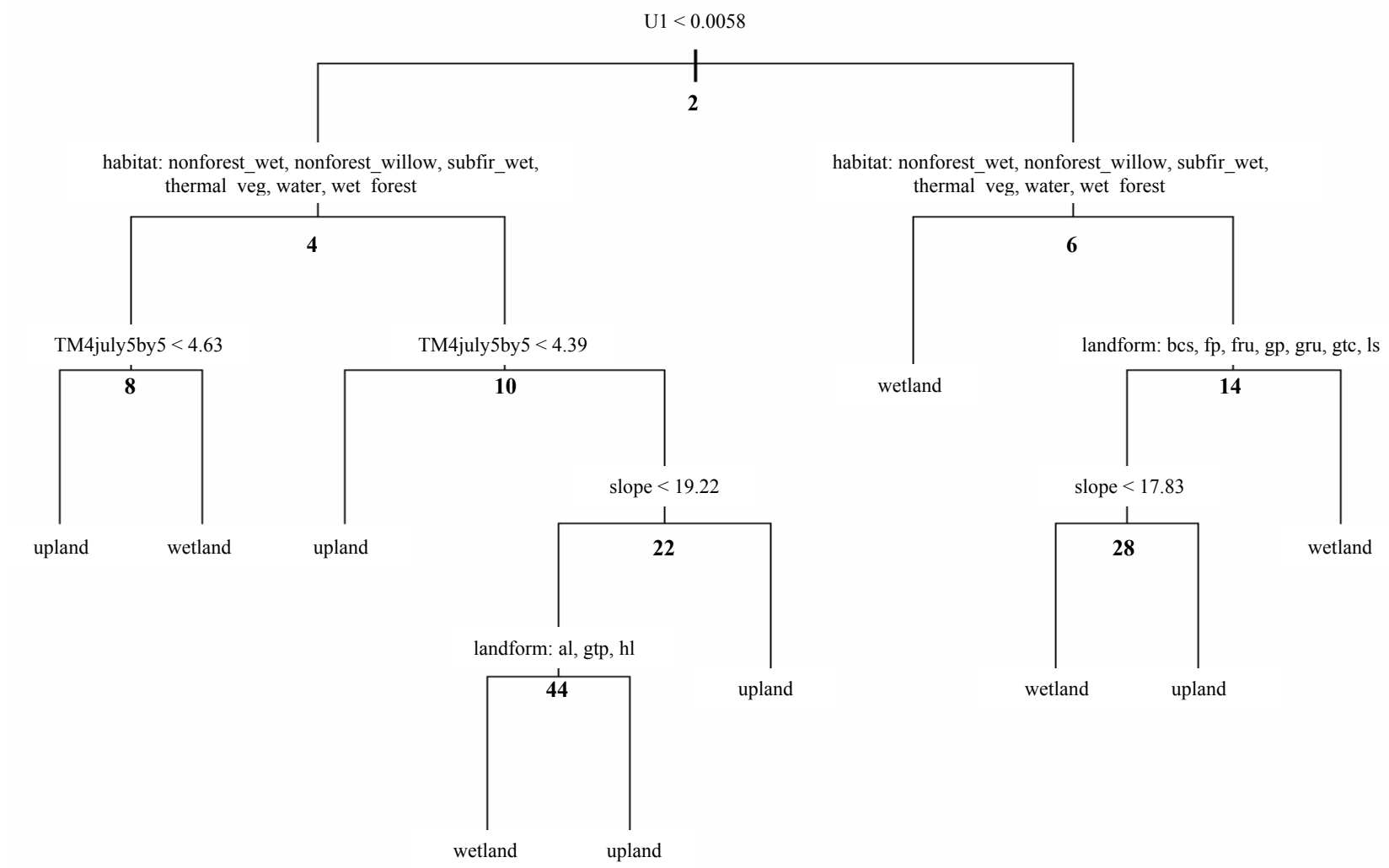

Figure 3.7. 2002 palustrine wetland/upland simple classification tree.

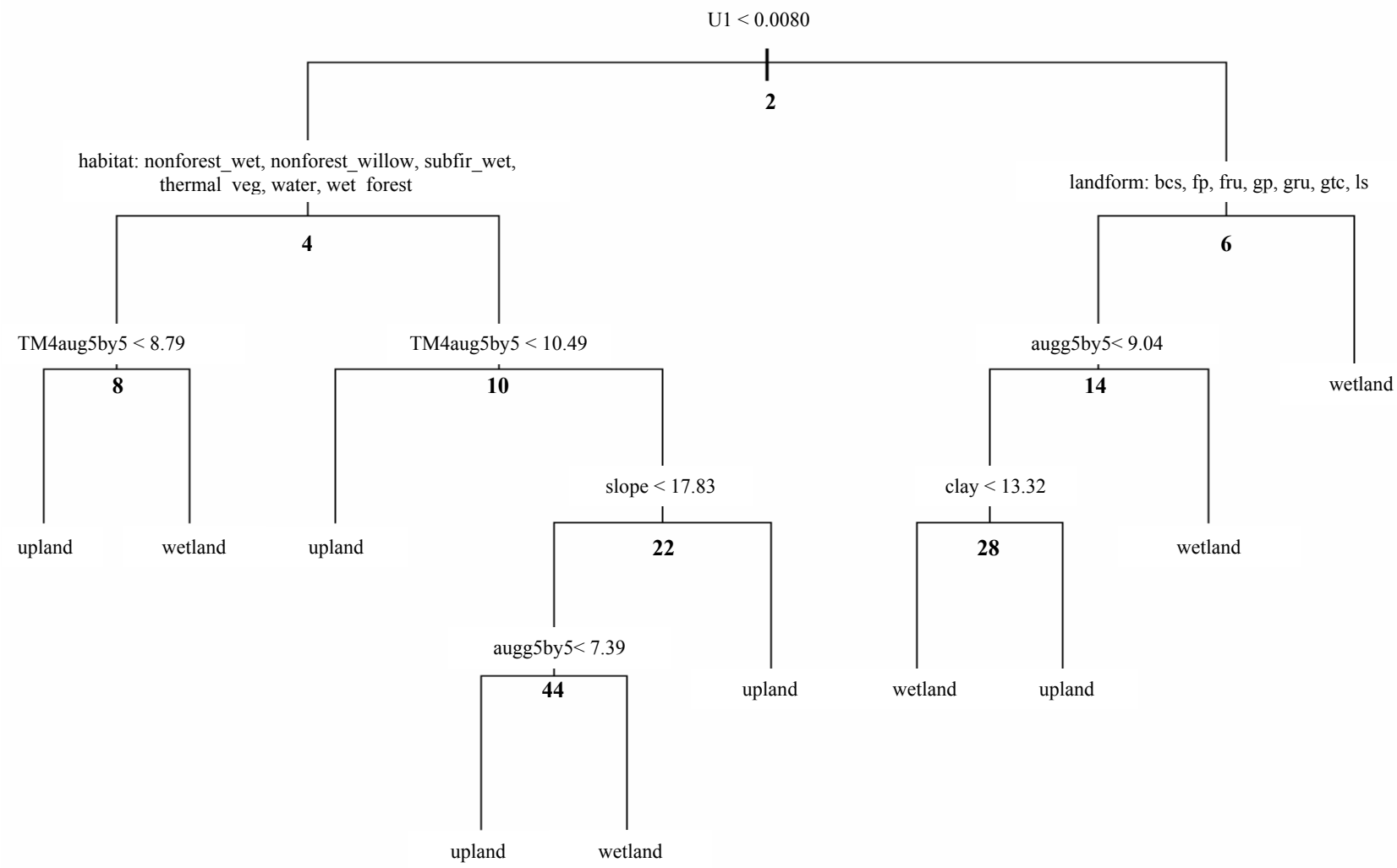

Figure 3.8. 2003 palustrine wetland/upland simple classification tree.

sending pixels not falling in alluvial or hydrothermal landforms to an upland terminal node (figure 3.3).

Along the right branch from node (10), the 2000-2003 trees make a split on slope at node (22) (figures 3.5-3.8). Critical slope values range between 16.87 and 20.75 percent, with greater slopes associated with upland pixels. By contrast, the 1988 and 1999 classification trees make a split on landform type at node (22) (figures 3.2 and 3.4). Here, pixels found in breaklands and colluvial slopes (bcs), fluvial plateaus (fp), fluvial rolling uplands (fru), glaciated rolling uplands (gru), glacial troughs and cirques (gtc), and landslides (ls) are sent to an upland terminal node.

The 1988 classification tree uses a split on tasseled cap greenness texture at node (46) to separate upland and wetland terminal nodes (figure 3.2). At node (44) the 2003 tree makes an equivalent split (figure 3.8). Similarly, at the lowest level in the upland main branch of the 1997 tree, node (20), TM band 4 texture is used to separate upland and wetland terminal nodes (figure 3.3). In the 2000-2002 trees, a low level split at node (44) is made on landform type (figures 3.5-3.8), with wetland associated with alluvial (al) and hydrothermal (hl) landforms and glaciofluvial terraces and plains (gtp).

Moving down the wetland main branch, the 1999, 2000, and 2003 trees make a split on landform type at node (6) (figures 3.4-3.5, 3.8). Wetland pixels are associated with alluvial (al), hydrothermal (hl), glaciofluvial terraces and plains (gtp), and other glaciofluvial (ogl) landforms. By contrast, the 1988, 1997, 2001, and 2002 trees make a split on habitat type at node (6) (figures 3.2-3.3, 3.6-3.7). Wetland pixels are associated with the nonforest wet, nonforest willow, subalpine fir wet, thermal vegetation, water,

and wet forest habitat types. In the 1997 and 1999-2002 classification trees, the split following node (6) is also made on landform or habitat type (figures 3.3-3.8). The choice of which mirrors the split made above, i.e. if the node (6) split was made on landform the next split is made on habitat type, if the node (6) split was made on habitat type the next split is made on landform.

At node (28) in the 1997, 2001, and 2002 classification trees a final split is made on slope, with a critical value of 17.83 percent for all three trees (figures 3.3, 3.6-3.7). The 1988 tree also makes a split on slope at node (28), but requires an additional split at node (56) to separate upland and wetland terminal nodes based on TM band 4 texture (figure 3.2). Final splits are made in the 1999 and 2000 trees at nodes (26) and (24), respectively, based on canonical discriminant scores (figures 3.4-3.5). Lastly, the 2003 classification tree makes a final split on % clay content at node (24) (figure 3.8). In this case, clay contents less than 13.32% are associated with a wetland terminal node.

Average overall error rates for palustrine wetland types classification trees were 23.32% for the TM only model, 20.51% for the TM+TXT model, 19.91% for the TM+TXT+DEM model, and 16.96% for the TM+TXT+DEM+GIS model (table 3. 8). Average error rates for the palustrine emergent (PEM) class were consistently the lowest among the five classes and declined from 12.35% for the TM only model to 8.80% for the TM+TXT model and 8.53% for the TM+TXT+DEM model. While the addition of image texture resulted in a decline of 3.55 percentage points in the average PEM error rate, little improvement was associated with adding terrain information (0.27 percentage points), and the error rate for the TM+TXT+DEM+GIS model actually increased to

Table 3.8. Producer's and overall error rates (%) for palustrine wetland types classification trees given four predictive models; 1988, 1997, 1999 2003.

Model	TM						TM+TXT					
Year	**PAB**	**PEM**	**PFO**	**PSS**	**PUS**	**Overall**	**PAB**	**PEM**	**PFO**	**PSS**	**PUS**	**Overall**
1988	61.94	12.78	29.71	92.07	23.54	21.54	60.64	8.82	23.73	89.76	31.90	17.57
1997	78.81	11.70	44.36	100.00	30.16	24.84	67.39	8.86	46.63	99.24	39.02	23.46
1999	57.79	12.42	40.59	92.49	29.35	23.84	76.56	8.41	38.54	92.00	26.50	20.74
2000	53.29	13.15	39.68	88.34	27.47	23.82	68.43	9.59	38.24	87.39	27.58	21.18
2001	63.58	11.88	35.71	79.57	37.60	21.98	72.75	8.64	32.83	69.95	44.34	18.90
2002	65.05	12.14	32.91	83.77	31.12	21.61	66.18	8.73	33.91	78.56	28.00	19.15
2003	55.97	12.39	49.77	88.40	28.43	25.60	54.41	8.58	45.72	86.87	52.39	22.60
Mean	**62.35**	**12.35**	**38.96**	**89.23**	**29.67**	**23.32**	**66.62**	**8.80**	**37.09**	**86.25**	**35.68**	**20.51**
Std. Error	**3.18**	**0.19**	**2.59**	**2.48**	**1.61**	**0.62**	**2.78**	**0.14**	**2.99**	**3.59**	**3.74**	**0.80**

Model	TM+TXT+DEM						TM+TXT+DEM+GIS					
Year	**PAB**	**PEM**	**PFO**	**PSS**	**PUS**	**Overall**	**PAB**	**PEM**	**PFO**	**PSS**	**PUS**	**Overall**
1988	56.49	7.75	29.57	75.15	27.00	17.19	59.26	8.13	24.79	42.51	27.20	14.72
1997	67.39	8.41	44.29	100.00	40.60	22.70	75.35	10.12	29.29	54.30	39.25	18.21
1999	77.77	8.66	37.32	87.81	28.74	20.49	77.77	8.62	34.66	39.05	27.85	17.30
2000	52.51	8.27	41.35	81.90	21.53	20.33	55.02	10.47	31.58	39.43	24.65	17.56
2001	89.19	8.93	29.84	73.87	25.19	18.33	82.00	8.93	29.77	38.84	26.89	16.44
2002	56.66	9.36	29.43	72.78	32.20	18.28	71.28	9.90	25.79	37.29	32.20	16.16
2003	59.08	8.32	47.77	82.21	27.97	22.06	61.51	10.59	32.83	45.01	27.31	18.36
Mean	**65.58**	**8.53**	**37.08**	**81.96**	**29.03**	**19.91**	**68.88**	**9.54**	**29.82**	**42.35**	**29.34**	**16.96**
Std. Error	**5.08**	**0.20**	**2.89**	**3.64**	**2.29**	**0.78**	**3.90**	**0.37**	**1.36**	**2.22**	**1.86**	**0.49**

9.54%. Average error rates for the palustrine scrub-shrub class (PSS) were very high for the TM, TM+TXT, and TM+TXT+DEM models, over 80%, but dropped substantially to 42.35% when ancillary thematic information was added in the TM+TXT+DEM+GIS model. For the palustrine forested class (PFO), average error rates were similar across the first three models, nearly 40%, while the average error rate for the TM+TXT+DEM+GIS model was approximately 30%. Average error rates for the palustrine unconsolidated shore class (PUS) were consistent for the TM, TM+TXT+DEM, and TM+TXT+DEM+GIS models, approximately 30%, but the error rate for the TM+TXT model was somewhat larger, 35.68%, largely due to a 52.39% error rate for the PUS class in 2003. Average error rates for the palustrine aquatic bed class (PAB) were consistently high across the four models, over 60%.

Compared to wetland/upland models, substantially more predictors were retained by TM+TXT+DEM+GIS wetland types classification trees (tables 3.9 and 3.10). Cover type is the first predictor used in 1997, 1999-2000, and 2003 trees, while habitat type is used at level two in all years but 1988. The first split in the 1988 tree is on tasseled cap brightness while brightness is first used at levels four and five in all other years. The 2001 and 2002 trees use per-pixel differences in TM bands 3 and 5 as initial criteria while band 5 differences are used at level three in 1999 and 2000. Image texture is used at a high level across all years; brightness texture at level two in 1988, TM band 4 texture at levels two or three in all other years. TM band 3 reflectance is first selected at levels two through five for all years, TM band 4 reflectance is first selected at levels three through five, and TM band 5 reflectance is used at levels three through eight. Tasseled cap

Table 3.9. Predictors retained by wetland types classification trees, 1988, 1997, and 2003.

Level	1988	1997	2003
1	JULY brightness	Cover type	Cover type
2	JULY brightness texture	Habitat type	Habitat type
2	JULY greenness	JULY TM4 texture	AUG TM4 texture
3	Cover type	Elevation	Elevation
3	Elevation	JULY TM3	AUG TM3
3	Habitat type	JULY greenness	AUG TM4
3			AUG greenness
4	JULY TM4	Precipitation	Precipitation
4	Landform type	JULY brightness	AUG TM5
4	JULY TM2	JULY TM4	AUG brightness texture
4		% Clay	AUG TM1
5	JULY TM7	Elevation	AUG brightness
5	JULY TM3	JULY TM5	% Clay
5			
6	JULY TM4 texture	JULY TM5 texture	AUG wetness texture
6	JULY wetness texture	Landform type	AUG greenness texture
7	JULY wetness	JULY TM1	Snow
7	JULY TM5	JULY brightness texture	Landform type
7	Snow		
7	JULY TM1		
8	Precipitation	JULY greenness texture	AUG wetness
8			Slope
9	% Rock	Snow	
10	% Clay	% Rock	Depression fill depth
11		Depression fill depth	

greenness is first used at levels two through four for all years but 2001. Elevation is first used at levels three through four over all years. Landform type, average annual precipitation, and percent clay content are used at intermediate to lower levels, between levels four and ten. TM bands 1 or 2 are first used at levels three through seven in all years but 2002. Image texture in various tasseled cap bands is typically used across years at intermediate depths between levels five and eight. Tasseled cap wetness also appears between levels five and eight in all years but 1997 and 2002. Low-level predictors in single-date classification trees include average annual snowfall, percent rock fragments,

Table 3.10. Predictors retained by wetland types classification trees, 1999-2002.

Level	1999	2000	2001	2002
1	Cover type	Cover type	TM3 difference	TM5 difference
2	Habitat type	Habitat type	Habitat type	Habitat type
2	SEPT TM4 texture	JULY TM4 texture	JULY TM3	JULY TM3
3	SEPT TM5	Elevation	SEPT wetness	SEPT TM5
3	SEPT TM2	JULY greenness	Cover type	Cover type
3	TM5 difference	TM5 difference	SEPT TM4 texture	SEPT TM4 texture
3	SEPT TM1	JULY TM3	SEPT TM1	JULY greenness
4	Elevation	AUG TM5	Elevation	Elevation
4	SEPT TM3	AUG brightness	SEPT brightness	SEPT TM3
4	AUG greenness	JULY TM4		JULY TM4
4	TM3 difference			
5	AUG wetness texture	Bedrock geology	TM5 difference	Slope
5	AUG TM3	AUG TM3	JULY TM4	JULY brightness
5	Landform type	JULY TM5	JULY wetness	SEPT TM2
5	TM5 difference	JULY brightness	SEPT TM2	JULY brightness texture
5	SEPT TM4	AUG TM4 texture	Landform type	
5	AUG TM4			
6	TM4 difference	Precipitation	JULY brightness	Landform type
6	Brightness difference	AUG TM4	SEPT TM3	JULY brightness
6	SEPT wetness	% Clay	JULY greenness texture	JULY TM4 texture
6	% Clay	Landform type		
6		Wetness difference		
7	Precipitation	Snow	% Clay	Precipitation
7	SEPT brightness texture	JULY TM2	TM3 difference	JULY greenness texture
7		JULY TM1	Snow	
7		AUG TM5 texture	JULY TM4 texture	
7		AUG brightness texture		
8	AUG greenness texture	Brightness difference	Precipitation	Snow
8	SEPT greenness	AUG wetness	SEPT TM5	TM4 difference
8		JULY brightness texture	Brightness difference	% Clay
8			JULY brightness texture	
9	AUG brightness	Greenness difference	TM4 difference	Bedrock geology
9		Slope	Greenness difference	SEPT brightness
9		Depression fill depth	JULY TM5	
10				SEPT TM4
10		JULY greenness texture		Greenness difference
10				JULY TM5 texture

slope, and depression fill depth. Low-level predictors in two-date classification trees include per-pixel differences in TM band 4 and in terms of tasseled cap brightness and greenness.

The seven wetland types classification trees also exhibit similar high-level structure. Figure 3.9 shows that a substantial portion of the total deviance in the 1988 and 1999 optimal wetland types trees is accounted for by a relatively small number of high-level splits.

The 1997, 1999, 2000, and 2003 simple wetland types trees all make a first split on cover type (figures 3.10-3.11, 3.13). Pixels associated with aspen, Douglas fir post-disturbance, pygmy lodgepole pine, and nonforest cover types are sent down the left main branch. Pixels associated with Douglas fir climax, Engelmann spruce-subalpine fir, lodgepole pine climax, lodgepole pine successional, water, whitebark pine climax, whitebark pine post-disturbance, and whitebark pine successional cover types are sent down the right main branch. The 2001 and 2002 trees achieve a similar result in the first split, using July-September differences in TM bands 3 and 5 (figure 3.12). The 1988 tree makes a first split on July tasseled cap brightness, with values greater than 79.5 sent down the right main branch and largely associated with palustrine emergent wetland (figure 3.10).

The 1997-2003 classification trees all make a split on habitat type at node (4) (figures 3.10-3.13). Pixels found in Douglas fir, lodgepole pine, and nonforest willow

1988 Palustrine Wetland Types Optimal Tree

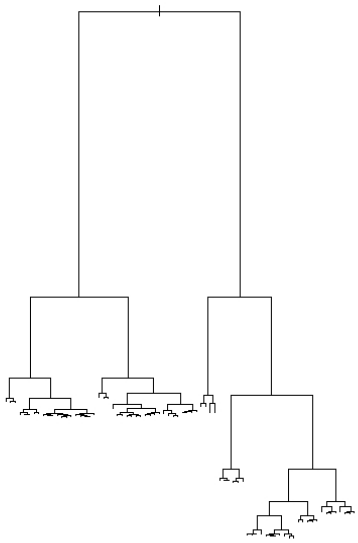

1988 Palustrine Wetland Types Simple Tree

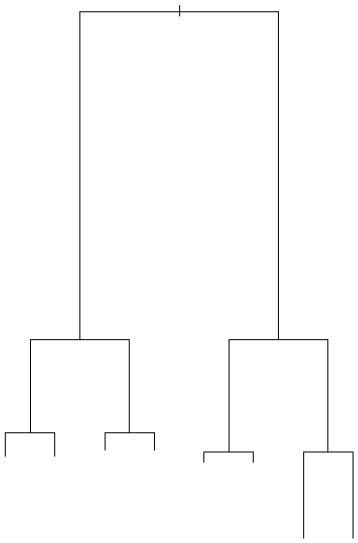

1999 Palustrine Wetland Types Optimal Tree

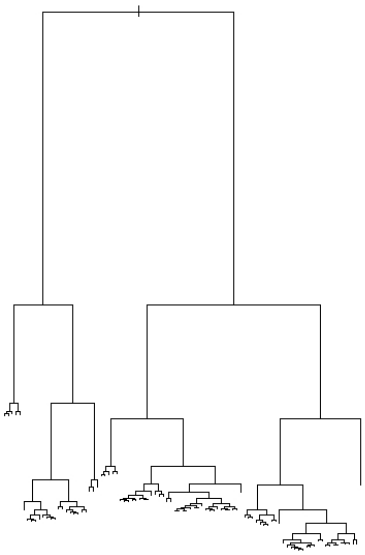

1999 Palustrine Wetland Types Simple Tree

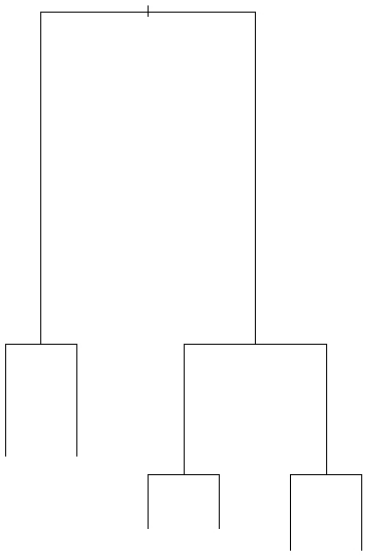

Figure 3.9. Optimal and simple palustrine wetland types classification trees, 1988 and 1999.

1988 Palustrine Wetland Types Simple Tree

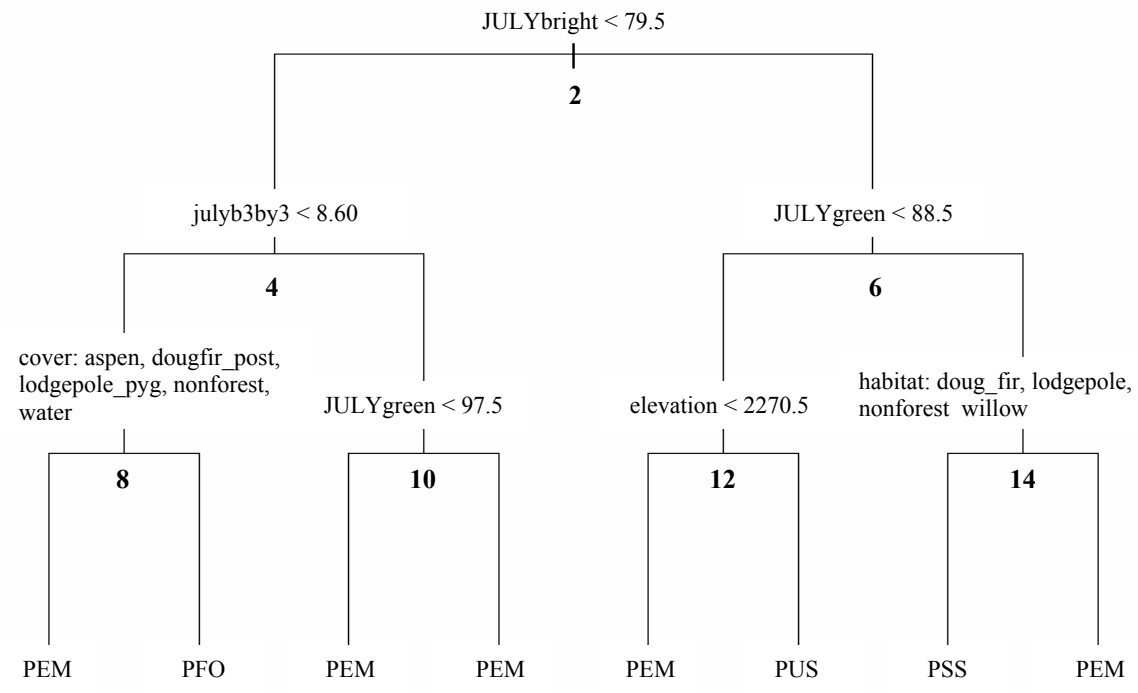

1997 Palustrine Wetland Types Simple Tree

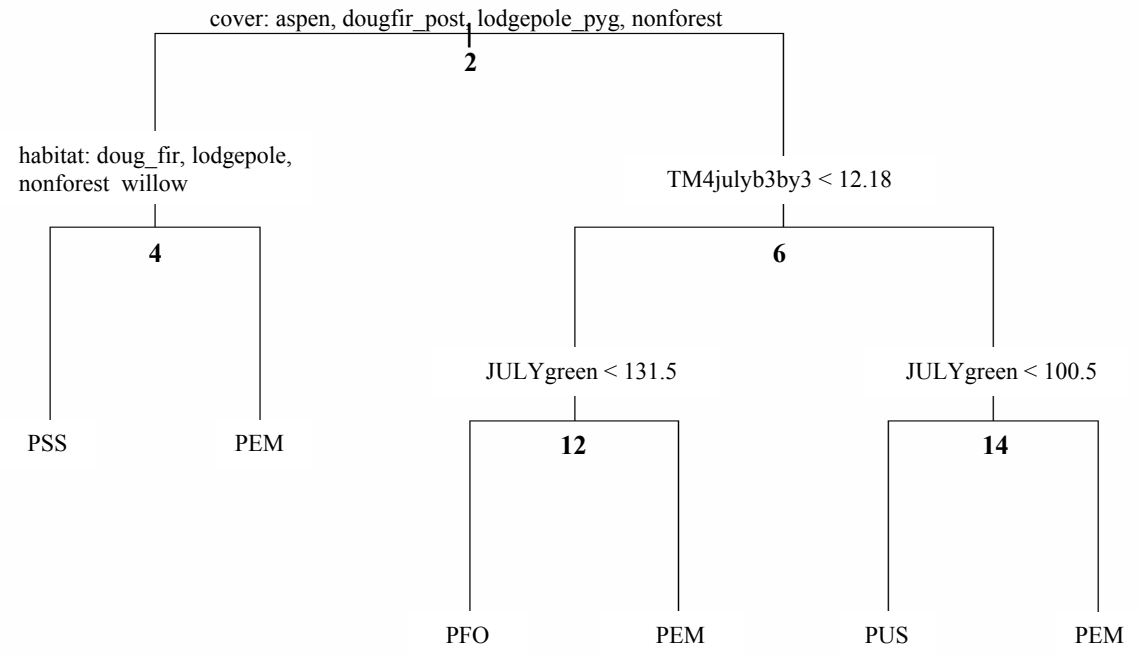

Figure 3.10. Simple palustrine wetland types classification trees, 1988 and 1997.

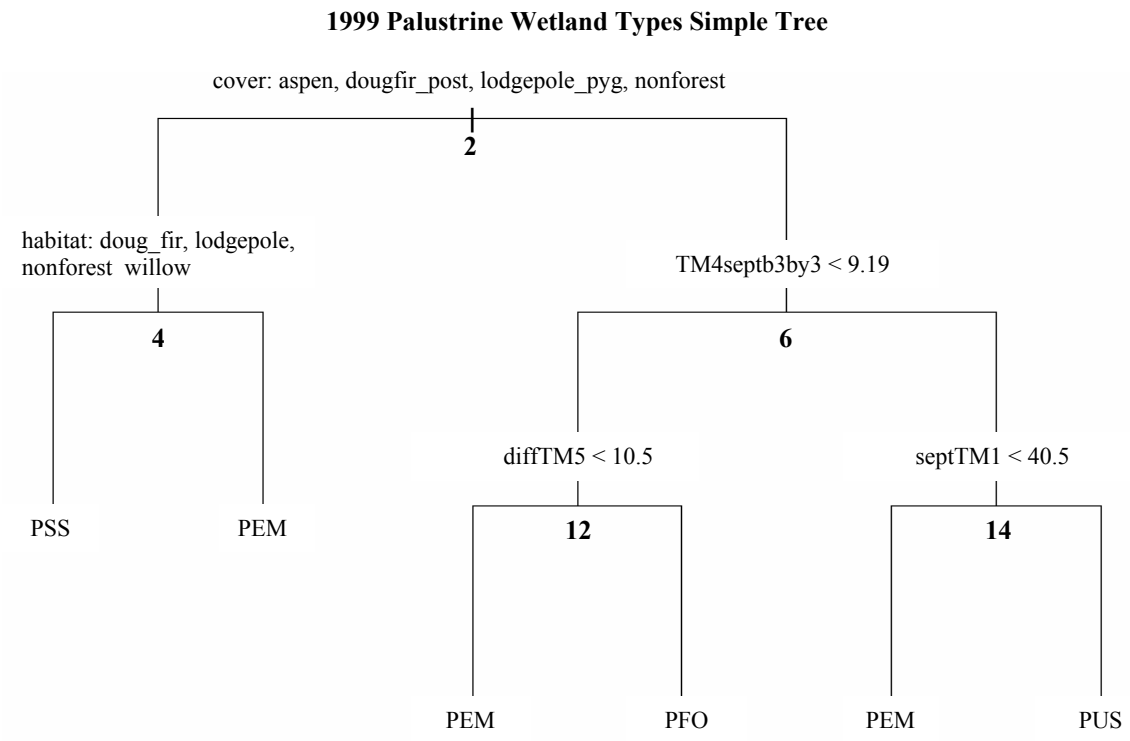

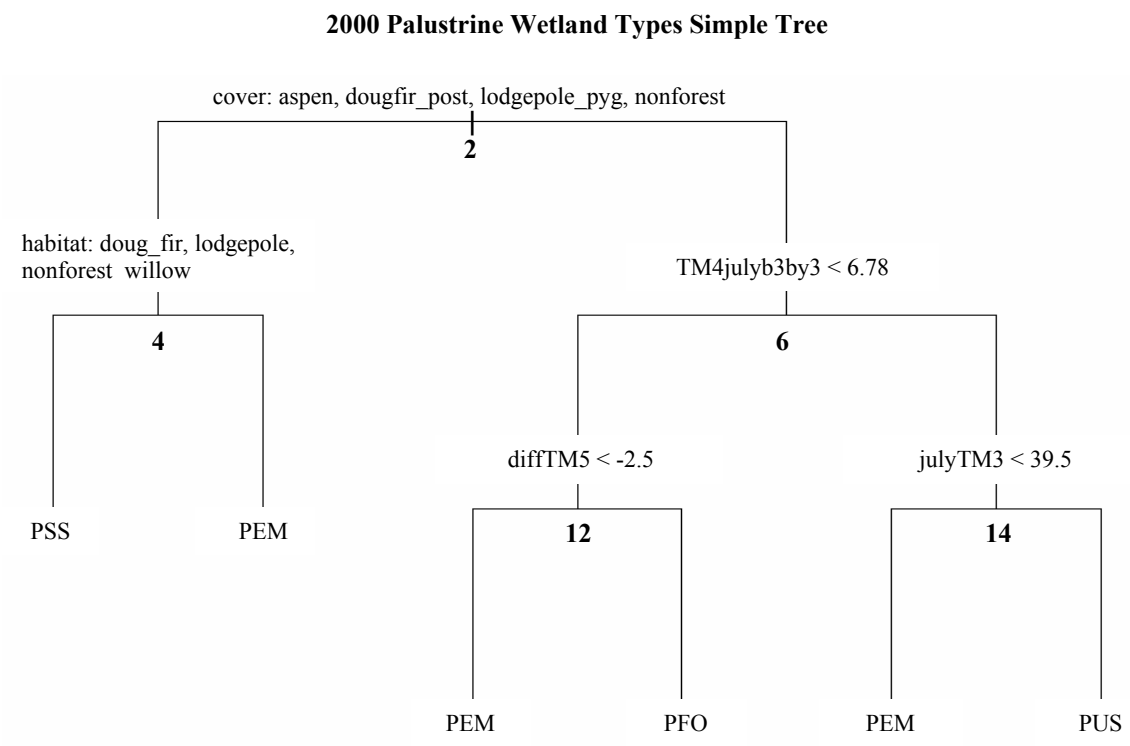

Figure 3.11. Simple palustrine wetland types classification trees, 1999 and 2000.

2001 Palustrine Wetland Types Simple Tree

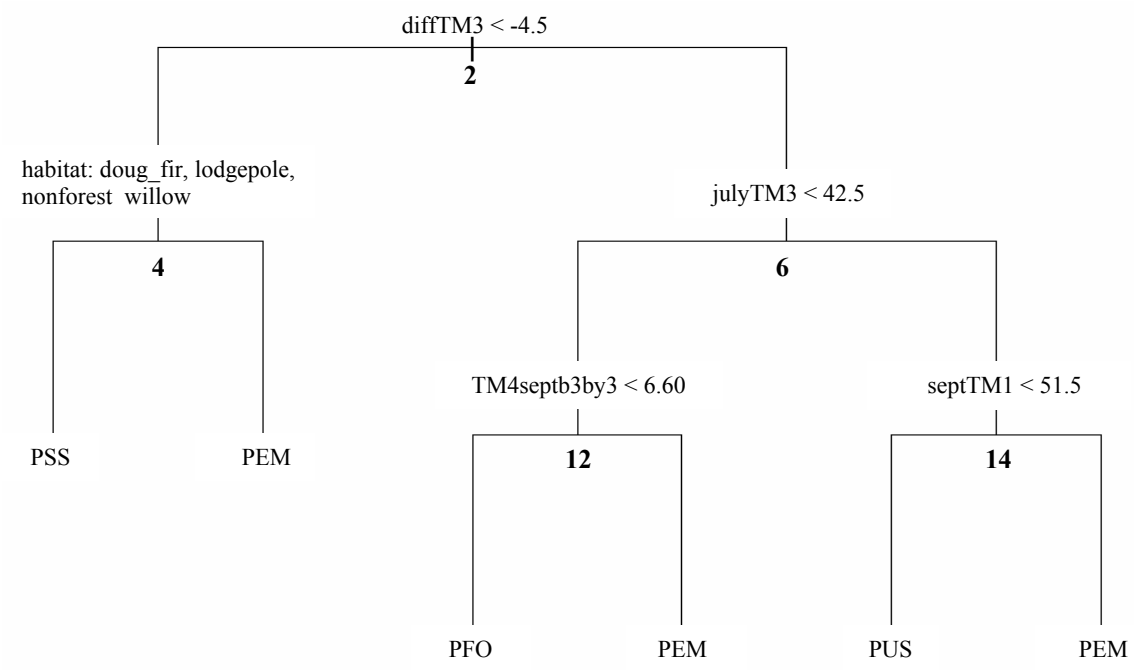

2002 Palustrine Wetland Types Simple Tree

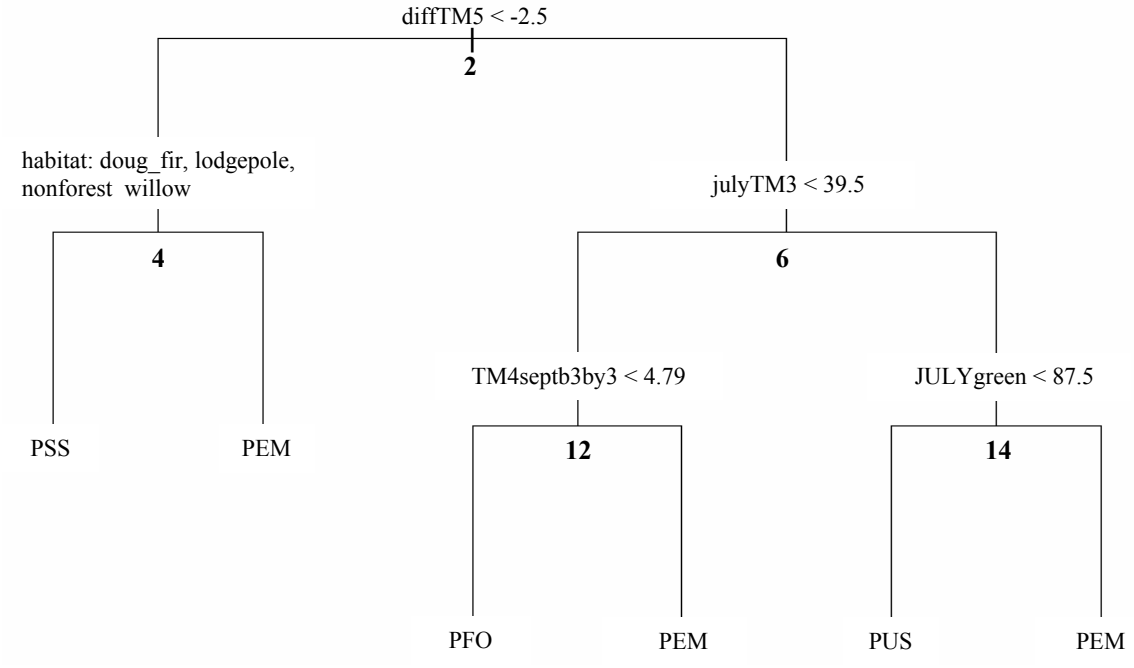

Figure 3.12. Simple palustrine wetland types classification trees, 2001 and 2002.

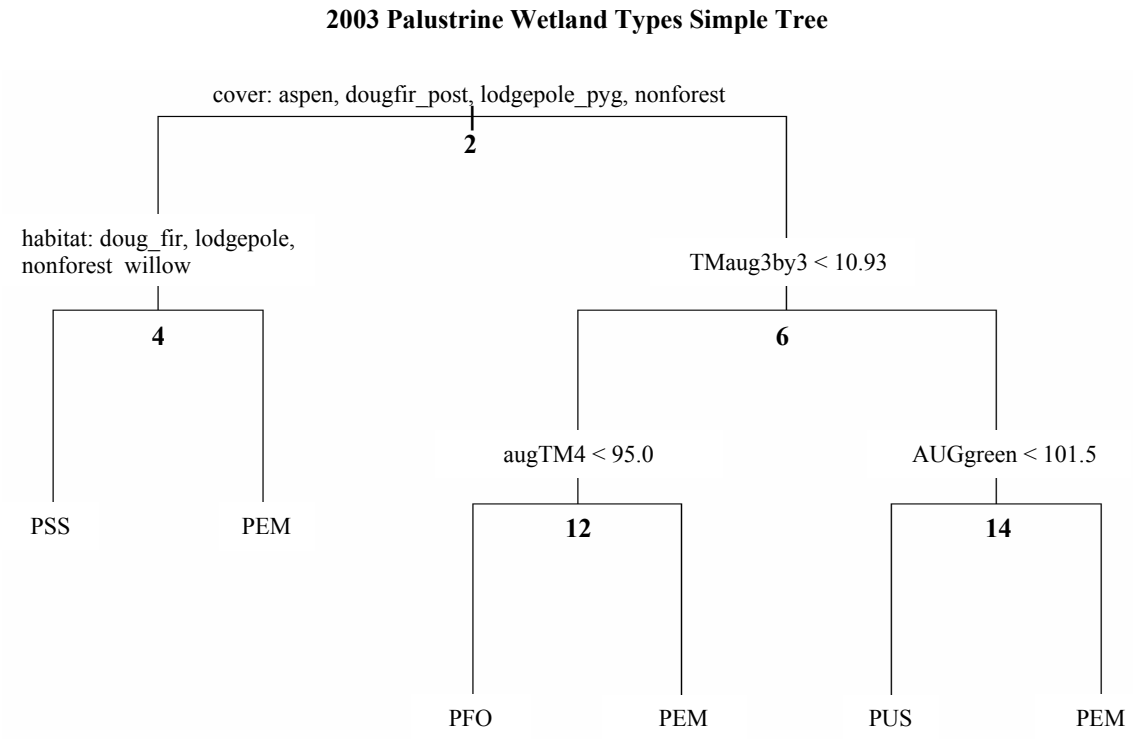

Figure 3.13. Simple palustrine wetland types classification trees, 2003.

habitat types are sent to a palustrine scrub-shrub terminal node. All other habitat types are sent to a PEM terminal node. In the 1997, 1999, 2000, and 2003 trees, the split at node (6) is made on TM band 4 texture (figures 3.10-3.13). In 2001 and 2002 the node (6) split is made on TM band 3 reflectance (figures 3.12-3.13). An equivalent split is made on tasseled cap brightnesstexture at node (4) in 1988 (figure 3.10). In all cases, smaller textures and smaller band 3 reflectance are associated with the forested wetland class while larger values are associated with emergent wetland.

At node (12) in the 1997 and 1999-2003 trees, PFO and PEM wetland types are further differentiated (figures 3.10-3.13). An equivalent split is made at node (8) in the 1988 tree (figure 3.10). The variables used in these splits are somewhat inconsistent over

the different trees. In 1988, cover type is used; with aspen, post-disturbance Douglas fir, pygmy lodgepole pine, nonforest, and water classes sent to a PEM terminal node and all other cover types sent to a PFO terminal node. In 1997, July greenness values greater than 131.5 at node (12) are associated with PEM wetlands, values less than 131.5 are associated with PFO wetlands. Similarly, the 2003 classification tree uses TM band 4 reflectance at node (12), with larger values sent to a PEM terminal node. In the 2001 and 2002 trees, the difference in TM band 5 reflectance between mid and late-summer is the criterion. More negative values are associated with the PEM class, likely indicative of drying occurring in PEM wetlands. In the 2001 and 2002 models, the node (12) split is based on TM band 4 image texture, with smaller values associated with forested wetland and larger values associated with emergent wetland.

The last splits to be considered in simple wetland types trees separate palustrine unconsolidated shore wetland from the PEM class. Unconsolidated shore wetlands in Yellowstone National Park are almost exclusively associated with hydrothermal features where a bright white substrate reflects strongly in the visible spectra. In the 1999-2001 simple trees, PUS pixels are distinguished from PEM pixels at node (14) based on high reflectance in TM bands 1 and 3 (figures 3.11-3.12). Higher reflectance in the visible spectra also translates to smaller tasseled cap greenness, and the PUS class is separated from the PEM class based on tasseled cap greenness at node (14) in the 1997, 2002, and 2003 trees (figures 3.10, 3.12-3.13).

The highest overall accuracy rate among palustrine wetland types trees, approximately 85%, was observed for the 1988 TM+TXT+DEM+GIS model (table 3.8).

The full error matrix for this model is included in table 3.11. Producer's accuracy for the PEM class was very high, nearly 92%. In terms of errors-of-commission for PEM predictions, the 1988 tree tends to misidentify forested wetland as emergent wetland more than any other class, with smaller error rates for the PSS, PUS, and PAB classes. Conversely, the dominance of the PEM class is reflected in the fact that the majority of misclassifications of PAB, PFO, PSS, and PUS pixels are as emergent wetland. While producer's accuracies for aquatic bed and scrub-shrub wetlands are relatively low, 0.4074 and 0.5749, respectively, user's accuracies for the PAB and PSS classes are substantially higher, 0.6488 and 0.7228, respectively. This difference stems largely from the fact that the model classifies PEM wetland so well. While PEM wetland is the most prevalent class, the relatively small number of pixels from the PAB and PSS classes that are misidentified as PEM leads to higher user's accuracies. Less dramatic differences between producer's and user's accuracies are seen for the PFO and PUS classes.

Table 3.11. Error matrix for the 1988 palustrine wetland types classification tree.

Actual Class	Predicted Class					Producer's accuracy
	PAB	PEM	PFO	PSS	PUS	
PAB	471	497	125	59	4	**0.4074**
PEM	134	63182	3885	956	617	**0.9187**
PFO	84	5288	16728	439	3	**0.7521**
PSS	34	2047	133	3008	10	**0.5749**
PUS	3	695	8	0	1890	**0.7280**
User's accuracy	**0.6488**	**0.8811**	**0.8012**	**0.7228**	**0.7488**	Overall accuracy **0.8528**

Discussion

This study demonstrates substantially improved wetland detection and wetland class identification when ancillary spatial information is combined with satellite remote sensing. Image texture, terrain measures, and thematic GIS layers reduced the producer's error rate for the palustrine wetland class by approximately 37% (figure 3.14). The overall error rate for palustrine wetland class identification by the TM+TXT+DEM+GIS model was 27% smaller than the error rate for the TM-only model (figure 3.15). Overall error rates for TM+TXT+DEM models were not substantially larger than error rates for classification trees including GIS information (figures 3.14 and 3.15), indicating that

.

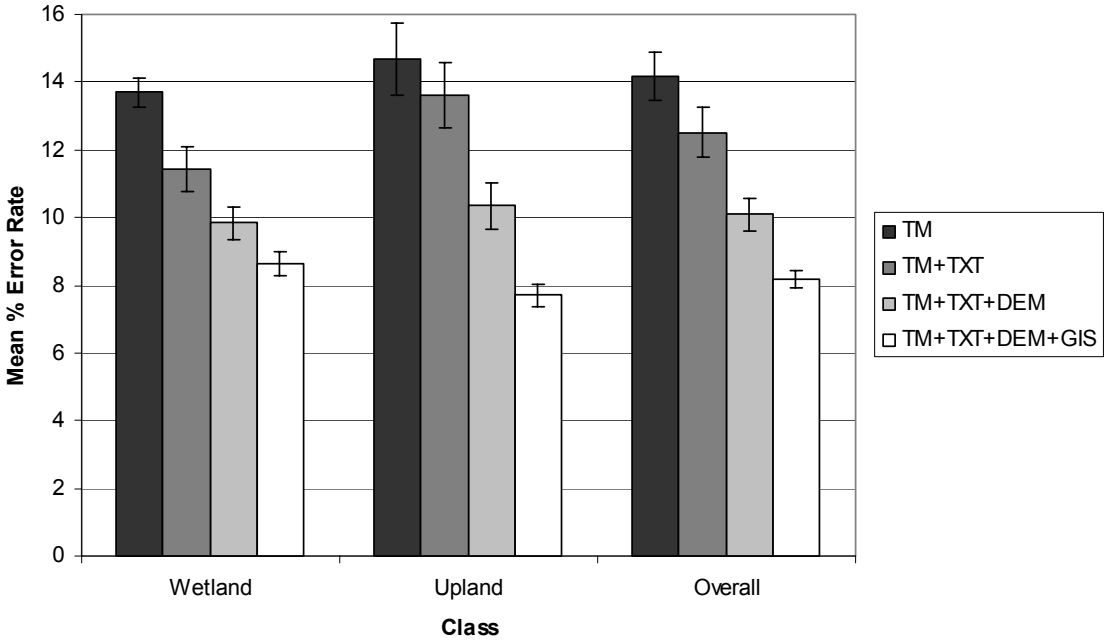

Figure 3.14. Mean error rates for optimal palustrine wetland/upland classification trees (+/- standard error) given four combinations of training data.

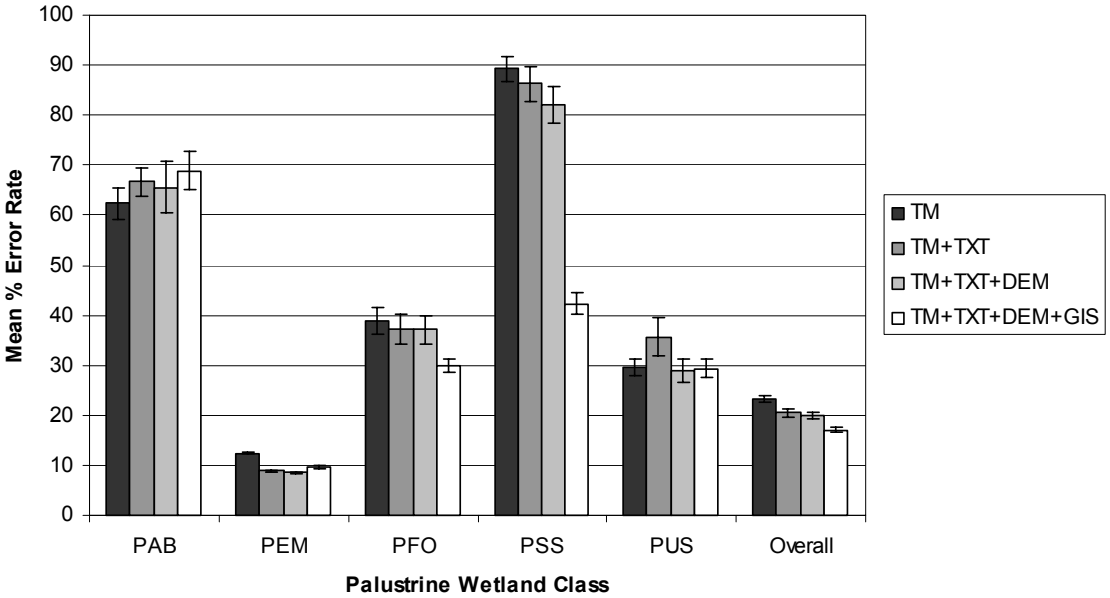

Figure 3.15. Mean error rates for optimal palustrine wetland types classification trees (+/- standard error) given four combinations of training data.

classification trees trained in Yellowstone could be effectively applied outside the park in areas where equivalent GIS layers are not available

Given a demonstrated ability to detect, on average, nearly 92% of pixels classified as wetland by the Yellowstone NWI, the developed methodology should detect a majority of true wetland pixels not delineated by the NWI. Model error rates were consistent among years (tables 3.5 and 3.8), indicating that the developed method could be applied to annual wetland monitoring in Yellowstone.

Role of Texture Measures, Terrain Information, and Thematic GIS Data

Building classification trees given different subsets of predictors allows an assessment of the role and importance of different types of variables in predicting

wetland occurrence as well as providing an indication of how models might be expected to perform when some predictors are not be available.

While an incremental decline in overall error rates is observed as more predictors are added to wetland/upland models (figure 3.14), overall error rates for the TM+TXT and TM+TXT+DEM palustrine wetland types models were similar (figure 3.15). This suggests that terrain information was useful in separating wetland from upland, but did not confer added predictive power when used to distinguish among wetland types. In Yellowstone, terrain attributes, especially slope, indicate areas on the landscape where wetlands are hydrologically more likely to occur. But once wetlands are present, terrain attributes may be less important in determining wetland type, or terrain effects may be masked by stronger associations between different wetland types and spectral and GIS information.

The topographic wetness index was retained as a predictor in only the 1988 classification tree. Recall, that the topographic wetness index is calculated as the natural log of (upstream contributing area / tan slope), and as such is larger for pixels with equivalent upstream contributing areas but lesser slopes. The observation that slope was a more effective predictor than the topographic wetness index, even though slope is a component of the index, may reflect the fact that the topographic wetness index is based on a steady-state assumption that the entire upstream contributing area contributes to the flow reaching any arbitrary point on the landscape (Wilson and Gallant 2000). In drier environments in Yellowstone, the velocity of subsurface water flow may be very slow, with points receiving contributions of water from only a small proportion of their

upstream contributing area. In this case, the steady-state assumption would be incorrect, and higher values of the topographic wetness index would not necessarily correspond to areas where water is expected to collect.

In general, image texture information was more useful for identifying wetland than upland (figure 3.14). Nominally equivalent TM band 4 and tasseled cap greenness textures were the dominant texture measures used. This reflects an expectation that abrupt wetland/upland transitions would be observed in a number of spectral bands, especially in the near infrared (TM band 4), and that these abrupt transitions would translate to larger variances in moving windows straddling boundaries between wetland and upland. Within wetlands, one might also expect to observe more image texture as a result of variability in soil water content, variability in the vigor of vegetation, the presence of patches of open water, and clumped distributions of wetland vegetation.

In terms of palustrine wetland class discrimination, texture information was most effective in discriminating emergent wetland from the four other palustrine classes (figure 3.15). Generally, PEM wetland was associated with greater texture in TM band 4, while forested wetlands were associated with smaller band 4 textures. Forested wetland canopies may have textures similar to that of adjoining upland forest, with more abrupt transitions occurring between emergent wetland and upland grasslands, or between emergent wetland and upland forests. Forested wetland canopies also are likely to obscure variability in soil water content. Differences in plant vigor within wetland forests may not be as pronounced, or as spectrally apparent, as differences in vigor within emergent wetlands.

Larger moving windows, 5 pixels by 5 pixels, were used to compute image texture for wetland/upland classification trees, while smaller 3 pixel by 3 pixel moving windows were to used to compute image texture for wetland types classification trees. Though overall misspecification error rates were similar for 3-by-3, 5-by-5, and 7-by-7 moving windows (table 3.3), it seems reasonable that differences between wetland and upland might be reflected in image textures at a larger scale than texture differences between different wetland types. One might expect texture differences between different wetland types to occur typically within wetland patches at finer scales, while texture differences between wetland and upland patches are dominated by the wetland/upland transition at larger scales. Weak evidence that the 5 pixel by 5 pixel window was optimal for wetland/upland models, may reflect a tradeoff between greater noise sensitivity of 3 pixel by 3 pixel windows and the greater smoothing tendency of 7 pixel by 7 pixel windows. Given the effectiveness of image texture in reducing average wetland classification errors across the seven years, further examination of the role of texture using other measures, e.g. measures derived from grey level co-occurrence matrices, Fourier analysis, or geostatistical analysis, may be warranted.

Smaller overall misclassification rates for TM+TXT+DEM+GIS wetland type models are attributable to improved identification of the palustrine forested and palustrine scrub-shrub classes when thematic GIS information was made available to the classification tree algorithm (figure 3.15). In simplified wetland types trees (figures 3.10-3.13), the PSS class is identified by its association with nonforest willow, lodgepole pine, and Douglas fir habitat types. Cover type information contributed to improved

identification of forested wetland. At node (8) in the simplified 1988 wetland types tree (figure 3.10), aspen, Douglas fir post-disturbance, pygmy lodgepole pine and nonforest cover types are sent to a PEM terminal node. Qualitatively, these are cover types where forested wetland is likely to *not* be found. All other cover types are sent to a PFO terminal node.

Histograms of 1999 TM band 4 texture before and after the split on cover type at the root node illustrate how cover type information contributes to separation of PFO wetland in the 1999 tree (figure 3.16). The distribution of September TM band 4 texture among PFO training pixels at the root node before the split is virtually identical to the distribution at node (6) following the split, demonstrating that forested wetland is typically not found in the aspen, Douglas fir post-disturbance, pygmy lodgepole pine and nonforest cover types. By contrast, the split on cover type eliminates a large number of non-PFO pixels with image textures less than 10. As a result, the distribution of image texture among smaller values at node (6) is weighted toward the PFO class, and PFO pixels are isolated by the node (6) split with a critical value of approximately 9.19 (figure 3.11).

Misclassification error rates for the aquatic bed class were uniformly high across the four models, on the order of 65% (figure 3.14). This may have resulted from the fact that the proportion of PAB pixels in the training data was very small, approximately 1.2% of the total. However, reasonably low error rates are observed for the palustrine unconsolidated shore class, around 30%, given only approximately 2.6% of the total training data. Lower error rates for the PUS class likely result from the spectrally

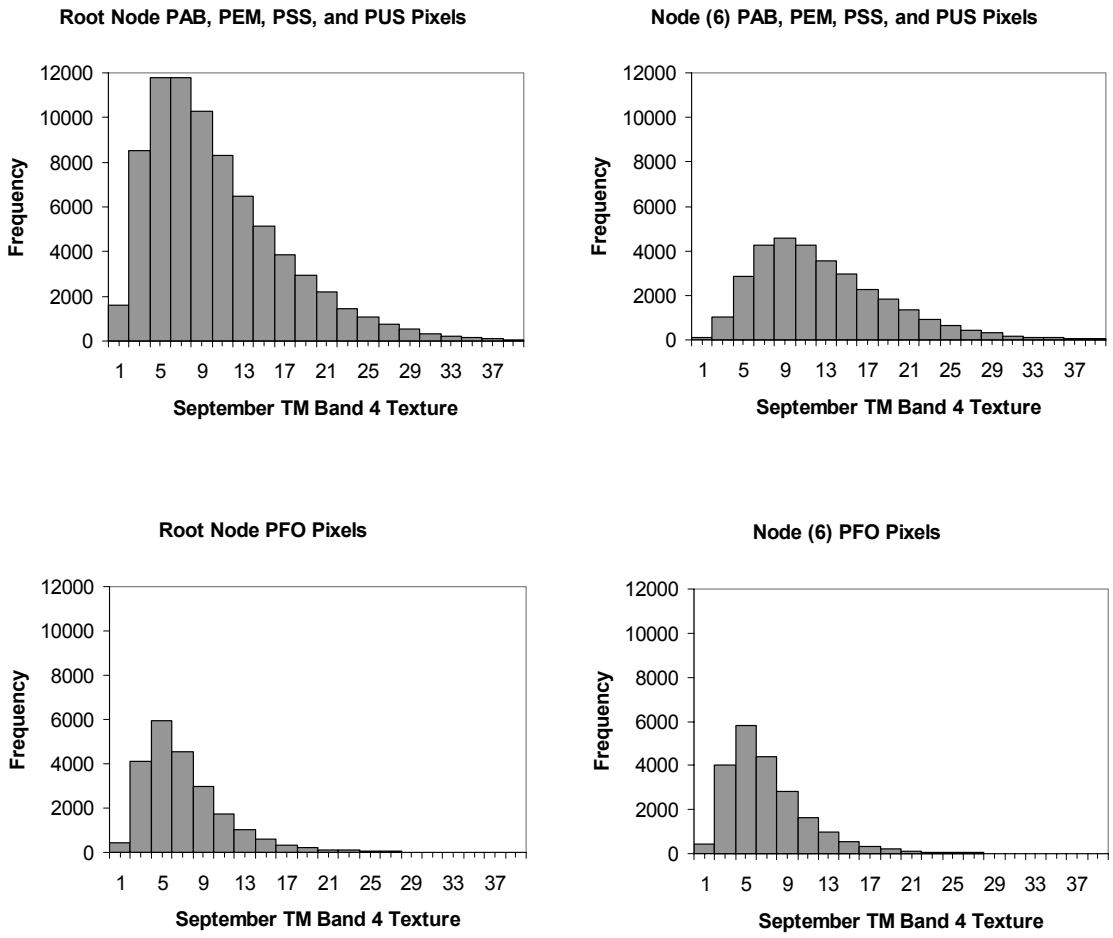

Figure 3.16. Distribution of 1999 September TM band 4 texture at the root node and node (6) with respect to PFO training pixels and not-PFO training pixels.

easy to resolve bright substrate found at hydrothermal sites. Aquatic bed wetlands were classified at levels lower than those presented in simple wetland type trees. The PAB class was typically associated with lower reflectance in the near infrared (band 4), lower tasseled cap greenness, and greater tasseled cap wetness, but tended to be confused with emergent wetland.

Similar high-level structure across years in simplified TM+TXT+DEM+GIS wetland/upland classification trees (figures 3.2-3.8) suggests that the classification tree algorithm made consistent use of terrain and thematic information when presented with spectral data from different years, different dates within the growing season, and two different TM instruments. In discriminating wetland from upland at the highest levels, ancillary information was used in a supporting role. Wetland/upland models used a spectral variable, the canonical discriminant score, as a criterion for the initial split before making subsequent splits on habitat type and landform. This suggests that the information encapsulated in the TM data was more useful than the information encapsulated in ancillary data, and also indicates that the classification tree methodology is more sensitive to temporally varying spectral data than temporally invariant ancillary information, something one might hope for in using this method to assess wetland temporal variability

An example of ancillary thematic information being substituted for spectral information is illustrated by a comparison of the 1988 and 1997 wetland/upland classification trees (figures 3.2-3.3). 1988 was a very dry year while, as mentioned above, 1997 was a very wet year. The two trees make identical splits at nodes (2) and (4). But at node (8) the 1988 tree is able to isolate an upland node after making a split on tasseled cap greenness texture, whereas the 1997 tree makes a split on landform type at node (8) and is unable to separate wetland from upland. Histograms of tasseled cap greenness texture illustrate why the two trees respond differently (figure 3.17). Among wetland pixels, 1988 and 1997 histograms of July greenness texture at node (8) are very

similar (figure 3.17). However, among upland pixels, the 1988 distribution of greenness texture at node (8) is shifted to the left, with more upland pixels with greenness textures less than 4.0. Subsequently the 1988 classification tree is able to isolate upland pixels with greenness textures less than approximately 4.03. The best split available to the 1997 tree at node (8) is on landform type, and in this case wetland pixels associated with alluvial and hydrothermal landforms are isolated with high accuracy but it is not possible

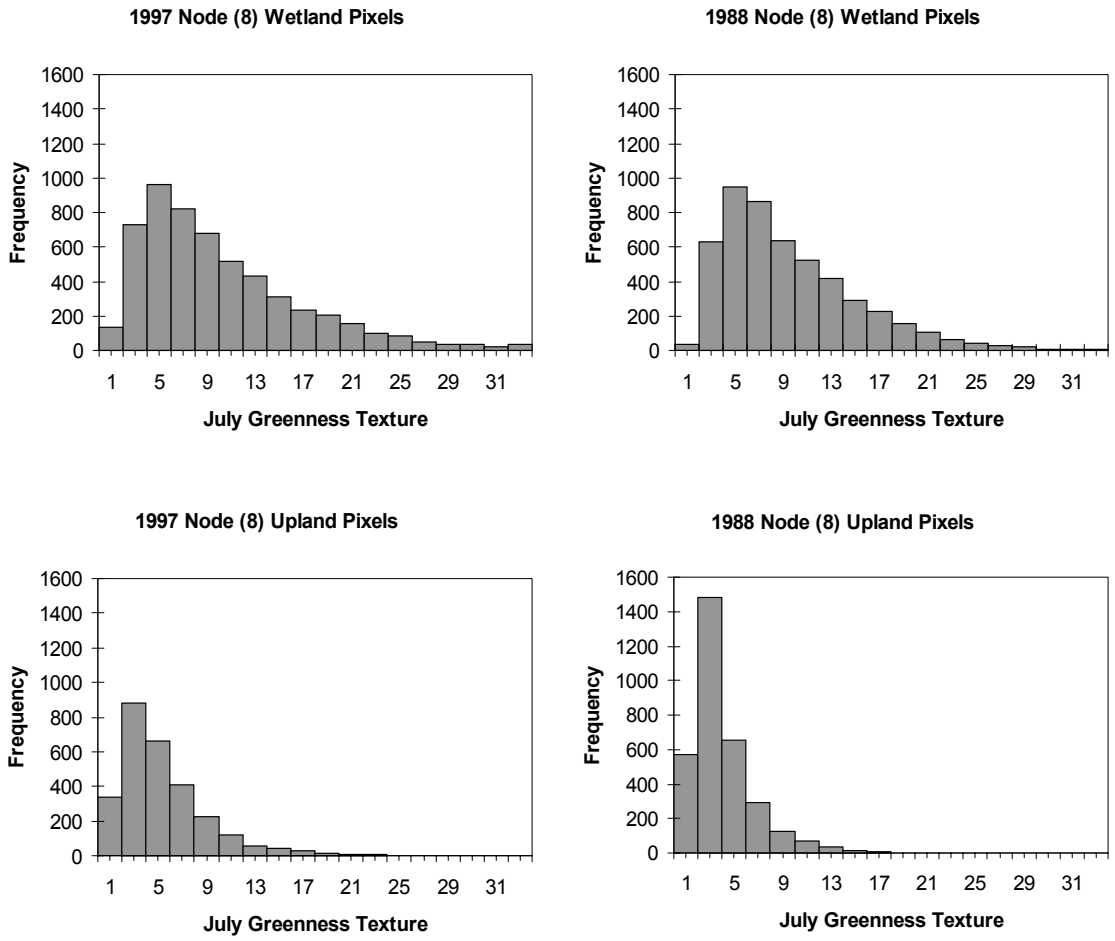

Figure 3.17. Distribution of July tasseled cap greenness texture at node (8) in 1988 and 1997 wetland/upland classification trees with respect to upland and wetland training pixels.

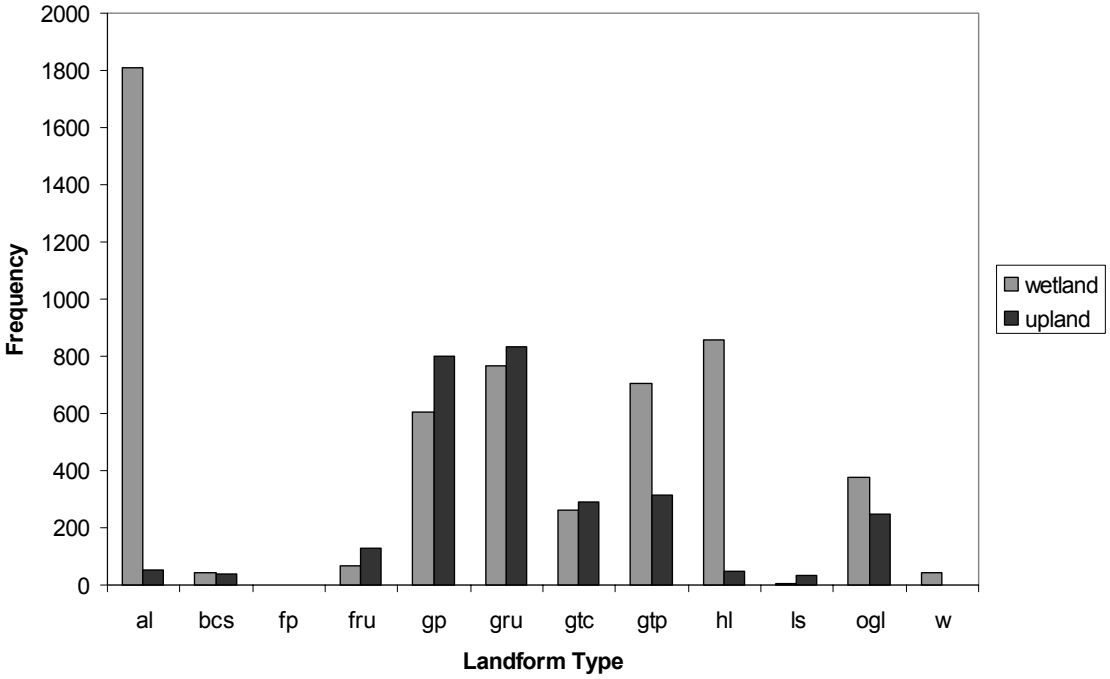

Figure 3.18. Distribution of landform type at node (8) in the 1997 wetland/upland classification tree with respect to wetland and upland training pixels.

to separate out upland, since there is not a landform type where upland pixels are more predominant (figure 3.18). It appears that in a very dry year, less texture is observed among upland pixels, making it easier to separate them from typically larger-textured wetland pixels. Intuitively this makes sense, as one might expect Yellowstone uplands to be more uniformly dry by mid-July in a dry year than in a wet year, where patches of green upland vegetation might be expected to persist into mid-July.

Model Training Issues

Use of the Yellowstone NWI to identify training and model verification data allowed a large number of training pixels to be presented to the classification tree algorithm while making large sample sizes available for model verification. Obviously reliance on the Yellowstone NWI to build and evaluate classification trees is predicated on presumed accuracy of the NWI. As discussed above, the rarity of palustrine wetlands on the Yellowstone landscape should guarantee that the proportion of wetland pixels misidentified as upland by the NWI is relatively small within the upland training data. Conversely, if the NWI tends to err more by omission than by commission, the proportion of wetland training pixels identified by the NWI that are actually upland should be small.

More generally, use of the Yellowstone NWI in the model training and evaluation process exemplifies an approach where a large number of training locations identified from a static GIS layer are used to extract useful information from that layer while, at the same time, potentially addressing shortcomings of that GIS layer; e.g. identification of wetlands not included in the Yellowstone NWI, or development of a capacity for monitoring temporal variability of Yellowstone wetlands.

Application Outside of Yellowstone National Park

Given that the average overall error rate for the TM+TXT+DEM model, 10.09%, is not substantially larger than the average error rate for classification trees also using thematic GIS information, 8.18% (figure 3.5), it appears that this model could be successfully applied in areas outside of Yellowstone National Park; say where a 30 m

DEM is available but the types and quality of thematic ancillary information might not be equivalent to that available for the park. For example, using the same TM scenes that Yellowstone models were trained on, digital maps of palustrine wetland likelihood could be developed for a substantial portion of the Greater Yellowstone Region surrounding the park.

The average producer's error rate for the palustrine emergent class in TM+TXT+DEM models is 8.53%, and is actually smaller than the average error rate observed for the TM+TXT+DEM+GIS model, 9.54% (table 3.8). Assuming that Yellowstone emergent wetlands are representative of emergent wetlands found in the Greater Yellowstone Region, models trained in Yellowstone could be successfully applied to identifying PEM wetlands outside the park. Higher error rates for the PSS and PFO classes when GIS information is not available suggests that it might be necessary to train TM+TXT+DEM models with greater proportions of training data from these two classes or to develop models capable of using GIS information available from areas outside the park, e.g. cover or habitat type maps, that resemble, but are not identical to thematic information used in Yellowstone models.

Wetland Monitoring

The low overall error rate for TM+TXT+DEM+GIS palustrine wetland classification trees suggests that the developed method could be used for wetland monitoring in Yellowstone National Park. Note, however, that high producer's accuracies for both a rare and a common land cover type can be accompanied by low user's accuracy for the rare class given the compounding effect of errors-of-commission

spread over the common class. Over Yellowstone, the upland training data were drawn from 7,822,088 pixels, which for an average producer's accuracy of 92.29%, corresponds to an estimated 603,083 upland pixels misidentified as wetland over the entire sampling frame. The estimated total number of wetland pixels correctly identified, equal to the known number of palustrine wetland pixels from NWI polygons greater than 1 ha times the average producer's accuracy for the wetland class is (462,844)(0.9135) = 422,808 pixels. In turn, the estimated average user's accuracy for the wetland class is then 422,808 / (422,808 + 603,083) = 0.4121.

While the estimated user's accuracy for the palustrine wetland class is low, note that it was calculated on a per-pixel basis. Many incorrectly identified wetland pixels are expected to be found on the margins of true wetlands, where, contextually, models correctly identify the presence of wetland but err in specifying exact boundaries. Also, recall that the objective of this study was to maximize producer's accuracy for the wetland class. By increasing the proportion of upland pixels in the training sample, one could expect to increase the producer's accuracy for the upland class, and in turn increase the user's accuracy for the wetland class. Thus, choices regarding the balance between wetland producer's and user's accuracies, can be tailored to an analyst's requirements. For example, if the objective is to locate wetlands not included in the Yellowstone NWI, one might choose a higher producer's accuracy over a smaller user's accuracy in order to minimize the number of true wetland pixels missed. With respect to annual wetland monitoring, higher user's accuracies might be preferred. With a greater degree of

certainty associated with pixels identified as wetland, inferences regarding changes over time can be made with greater certainty.

Demonstration of the detection of wetlands not included in the Yellowstone NWI obviously requires field verification. Preliminary fieldwork in 2003 showed that approximately 14% of pixels predicted to be palustrine wetland by a classification tree model derived from 1 August, 2003 Landsat-5 imagery actually were palustrine wetland and were not identified as wetland by the Yellowstone NWI (Wright, unpublished data). Application of the developed methodology to monitoring/evaluating spatio-temporal variability of Yellowstone wetlands has been limited. However, preliminary comparison of wetland likelihood maps for a dry year (1988) and a wet year (1997) indicates an expansion of the spatial extent of Yellowstone wetlands in 1997 (Wright, unpublished data).

Summary

This study demonstrates the utility of ancillary information in wetland remote sensing, as originally recommended by the Federal Geographic Data Committee (1992). Wetland classification trees are easily interpreted and conform to what one might expect in terms of where palustrine wetlands occur in Yellowstone National Park, what their spectral characteristics are, and how ancillary information facilitates the separation of different palustrine wetland types. The developed method is relatively easy to implement and could potentially be used to improve satellite remote sensing of wetlands in general.

CHAPTER 4

REMOTE SENSING OF PALUSTRINE WETLANDS IN YELLOWSTONE NATIONAL PARK AS PART OF THE AMPHIBIAN RESEARCH AND MONITORING INITIATIVE

Introduction

In the year 2000, the U.S. Department of the Interior was directed by executive order to develop a plan to monitor amphibians on lands managed by the department and to research causes of amphibian declines. Under the resulting Amphibian Research and Monitoring Initiative (ARMI), monitoring programs were instituted nationwide, including amphibian surveys in Yellowstone National Park (Peterson and Patla 2001). As part of the ARMI effort in Yellowstone, this study was initiated to map potential amphibian wetland habitat using a combination of satellite remote sensing and ancillary spatial information.

Classification trees were used to map the likelihood of palustrine wetland occurrence across the Yellowstone landscape. In combination with ancillary thematic data and terrain measures derived from a 30 m digital elevation model (DEM), an August 1, 2003 Landsat-5 Thematic Mapper (TM) image was used to develop wetland models for the entire park. Wetland predictions were subsequently verified by field visits during late-summer and early-autumn of 2003.

Methods developed in this study will be used to monitor annual variability of Yellowstone wetlands. An ability to relate amphibian presence to wetland habitat

variability over a large geographic extent would represent a powerful tool for amphibian researchers. More generally, coupled wetland-amphibian systems in Yellowstone may present an ideal model for studying relationships between spatio-temporal habitat variability and species persistence.

Lacustrine, palustrine and riverine wetlands cover an estimated 10% of the Yellowstone landscape (Elliott and Hectner 2000), similar to pre-European settlement wetland cover across the United State (Dahl 1990). Thus the park may represent an excellent null model for relating landscape-scale wetland attributes to amphibian population persistence. Lastly, methods developed in Yellowstone should be applicable to wetland mapping/monitoring in other physiographic settings, with obvious applications to amphibian conservation.

Methods

Wetlands in Yellowstone National Park are currently mapped by the National Wetland Inventory (NWI). The NWI classifies wetlands using the Cowardin system (Cowardin et al. 1979), where freshwater wetlands are divided into lacustrine, riverine, and palustrine systems. Palustrine wetland is the predominant wetland type in the Yellowstone NWI, (Elliott and Hektner 2000), and includes the vast majority of potential amphibian wetland habitat within the park. In the Cowardin scheme, palustrine wetlands are divided into classes, including emergent (PEM), forested (PFO), scrub-shrub (PSS), aquatic bed (PAB), and unconsolidated shore (PUS) types. Palustrine classes are further

described by water regime modifiers, e.g. intermittently flooded, seasonally flooded, saturated, semi-permanently flooded, etc.

Emergent wetlands in Yellowstone are typically dominated by sedges (*Carex spp.*), including water sedge (*Carex aquatilis*) and inflated sedge (*Carex vesicaria*). Drier emergent wetland typically consists of the tufted hairgrass (*Deschampsia cespitosa*)/sedge (*Carex spp.*) habitat type (Despain 1990). Scrub-shrub wetlands are dominated by willows (*Salix spp.*). Three wet forest habitat types common in the park are; Engelmann spruce (*Picea engellmannii*)/common horsetail (*Equisetum arvense*), Engelmann spruce (*Picea engellmannii*)/sweetscented bedstraw (*Galium trifidum*), and subalpine fir (*Abies lasiocarpa*)/bluejoint reedgrass (*Calamagrostis canadensis*) habitat types (Despain 1990). Other common tree species in Yellowstone National Park include lodgepole pine (*Pinus contorta*), whitebark pine (*Pinus albicaulis*), and Douglas fir (*Pseudotsua menziessi*). Aspen (*Populus tremuloides*) is a relatively rare tree species in the park.

Classification trees were constructed using S-Plus V6.1 software (Insightful Corporation, Seattle, WA). Following the Cowardin system, wetland classification trees were developed hierarchically. At the most general level, the likelihood of palustrine wetland occurrence was modeled. At the next level, classification trees were developed to distinguish between the five palustrine classes. At the finest level, water regime classification trees were independently generated for the PAB, PEM, and PFO classes.

Training data locations were identified using the Yellowstone NWI. Random sampling of palustrine wetland sites was limited to pixels falling inside palustrine

polygons larger than one ha (approximately 11 TM pixels) to reduce the likelihood of spatial errors and pixel mixing. To capture the wetland to upland transition, one stratum of upland training locations was randomly sampled from pixels located more than 60 meters and less than 120 meters distance from any lacustrine, riverine, or palustrine NWI polygon. To ensure adequate coverage of upland sites across the entire park, a second stratum was randomly sampled from all upland pixels greater than 120 meters distance from any NWI polygon.

A cloudless, terrain-corrected Landsat-5 image of Yellowstone from 1 August, 2003 was obtained from the U.S. Geological Survey Earth Resources Observation System (EROS) Data Center. TM digital numbers were tasseled cap transformed to brightness, greenness, and wetness bands using coefficients derived by Huang et al. (2002). Image texture was determined for the three tasseled cap bands by calculating variances in 3-by-3, 5-by-5, and 7-by-7 pixel moving windows using ERDAS IMAGINE V8.6 software (Leica Geosystems GIS & Mapping, Atlanta, GA).

A 30 meter digital elevation model (DEM) and thematic GIS layers were obtained from the Yellowstone Spatial Analysis Center (Mammoth, WY). Undrained depressions in the 30 meter DEM were filled using the algorithm of Planchon and Darboux (2002). Depression fill depth (in meters) was retained as an ancillary terrain variable while percent slope and a steady state topographic wetness index, $\log_e$(upstream contributing area/tan slope), were computed from the filled DEM using TAPES-G terrain analysis software (Wilson and Gallant 2000).

Thematic ancillary information included habitat types (potential climax vegetation), cover types (actual vegetation following the 1988 catastrophic fires in Yellowstone), landform types, bedrock geology, two soil attributes (% clay and % rock fragments), average annual snowfall, and average annual precipitation. Thematic classes and their abbreviations are summarized in table 4.1. Terrain and thematic data were re-sampled to coincide with the 30 meter TM grid using ArcInfo V8 software (Environmental Systems Research Institute, Redlands, CA).

Palustrine wetlands are relatively rare on the Yellowstone landscape, approximately 5.5% of the total land area (minus lacustrine and riverine wetlands), as estimated from the Yellowstone NWI. This rarity poses a problem for discrimination between upland and wetland pixels; classification trees presented with unbalanced data tend to focus predictive power on the common class (Breiman et al. 1984). Increasing the proportion of rare cases in the training sample is one way to increase classification accuracy for the rare class. However, while increasing the proportion of wetland training pixels can be expected to decrease the rate of errors-of-omission for the wetland class (wetland pixels classified as upland), an increase in the rate of errors-of-commission for the wetland class (upland pixels classified as wetland) can also be expected as the proportion of upland pixels in the training sample falls. In terms of mapping accuracy, classification trees trained with wetland and upland data approximately proportional to their true rate of occurrence can be expected to under-predict the true extent of palustrine wetland; or in other words, wetland maps generated by these classification trees would have relatively low producer's accuracies (high rate of false-negatives) and relatively

Table 4.1. Habitat type, cover type, landform type, and bedrock geology classes and corresponding variable abbreviations.

Habitat type		**Cover type**		**Landform type**		**Bedrock geology**	
Douglas fir	df	Aspen	as	Alluvial landforms	al	Cambrian sediments	cs
Lodgepole pine	lp	Douglas fir, climax	dc	Breaklands and colluvial slopes	bcs	Cretaceous sediments	crs
Nonforested, alpine	np	Douglas fir, post disturbance	dp	Fluvial plateaus	fp	Devonian sediments	ds
Nonforested, dry	nd	Douglas fir, successional	ds	Fluvial rolling uplands	fru	Mississippian sediments	ms
Nonforested, moist	nm	Engelmann spruce and subalpine fir, climax	es	Glacial troughs and cirques	gtc	Ordovician sediments	os
Nonforested, sagebrush	ns	Krummholz	kz	Glaciated plateaus	gp	Pennsylvanian sediments	ps
Nonforested, wet	nw	Lodgepole pine, climax	lc	Glaciated rolling uplands	gru	Permian sediments	prs
Nonforested, willow	nwl	Lodgepole pine, post disturbance	lp	Glaciofluvial terraces and plains	gtp	Precambrian metamorphics	pm
Pitchstone plateau complex	ps	Lodgepole pine, successional	ls	Hydrothermal landforms	hl	Quaternary basalt flows	qbf
Subalpine fir, lodgepole pine	sl	Nonforest	nft	Landslides	ls	Quaternary rhyolite flows	qrf
Subalpine fir, moist	sm	Pygmy lodgepole pine	lg	Other glaciofluvial landforms	ogl	Quaternary rhyolite tuffs	qrt
Subalpine fir, wet	sw	Water	wa	Water	w	Quaternary hydrothermal deposits	qh
Subalpine fir, whitebark pine	swb	Whitebark pine, climax	wc			Quaternary sediments	qs
Talus	ts	Whitebark pine, post disturbance	wp			Tertiary andesites	ta
Thermal area vegetation	tv	Whitebark pine, successional	ws			Tertiary andesites, basalts	tab
Water	wa					Tertiary basalts	tb
Wet forest	wf					Tertiary intrusives	ti
Whitebark pine	wb					Tertiary sediments	ts
						Triassic sediments	trs
						Water	wa

high user's accuracies (low rate of false-positives). Conversely, models produced from more equal-sized training samples would tend to over-predict the extent of palustrine wetland. In this case, producer's accuracy for the wetland class can be expected to be relatively high, while user's accuracy for the wetland class is relatively low.

In building 2003 palustrine wetland/upland classification trees, a balance between producer's and user's accuracy was sought. The formal objective was to achieve a minimum producer's accuracy of 80% for the wetland class, while simultaneously maximizing the user's accuracy for the wetland class. Classification trees were built using 50,000 common upland training pixels, with increasing numbers of wetland training pixels added to create different training data sets with increasing proportions of wetland data. The starting point was a training sample with 2,938 wetland pixels, or approximately 5.5% of the total, and representing the estimated true proportion of palustrine wetland pixels on the landscape.

Classification trees generated from different proportional training samples were cost-complexity pruned (Breiman et al. 1984). Accuracy rates of pruned sub-trees were estimated using a common, independent sample containing 2,938 wetland pixels and 50,000 upland pixels. These accuracy rates were treated as estimates of the true accuracy rates of maps generated from these trees. As the proportion of wetland training pixels increased, wetland producer's accuracy increased while wetland user's accuracy decreased (figure 4.1). A wetland proportion of 0.175 resulted in a pruned tree with an estimated producer's accuracy of 80.60% and an estimated user's accuracy

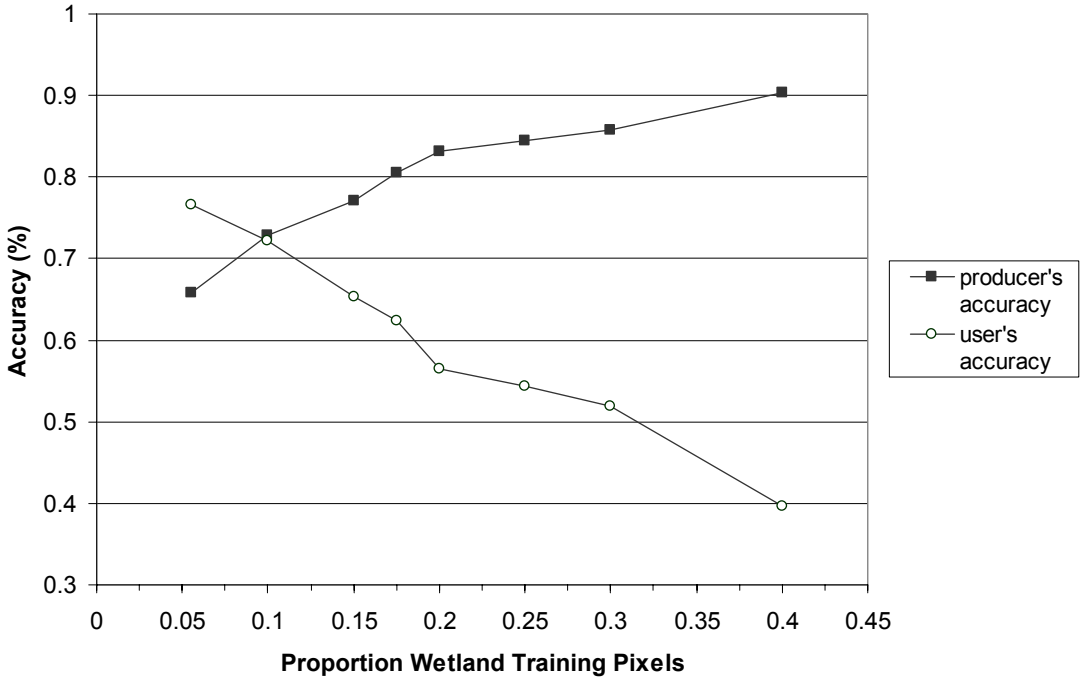

Figure 4.1. Wetland class producer's and user's accuracies of optimally pruned classification trees as a function of the proportion of wetland pixels in training data.

of 62.45%. This classification tree was determined to be optimal and was subsequently used to map palustrine wetland across Yellowstone Park.

Classification tree predictions were output as probabilities that individual pixels were palustrine wetland. However, note that because the proportion of wetland pixels in the training sample was no longer the same as the proportion of wetland pixels in the sampling frame, these probabilities do not represent unbiased estimates of the true probability of wetland occurrence. Thus it is more appropriate to describe classification tree predictions as relative likelihoods of palustrine wetland occurrence. For classification purposes, pixels with relative likelihoods greater than 0.5 were classified as palustrine wetland.

Training data for the palustrine wetland class model were randomly sampled from emergent (PEM), forested (PFO), scrub-shrub (PSS), aquatic bed (PAB), and unconsolidated shore (PUS) NWI polygons larger than 1 hectare. Relative proportions of the five classes in the training data set were also adjusted to achieve prescribed accuracy rates. Objectives were an 80% producer's accuracy for the PEM class, 70% producer's accuracies for the PFO and PSS classes, and producer's accuracies greater than 50% for the PAB and PUS classes. Instead of varying the number of pixels randomly sampled from all five classes, only the number of PEM pixels was varied. 2,000 pixels were sampled from PAB and PUS classes, 5,000 pixels were sampled from the PSS class, and 7,500 pixels were sampled from the PFO class. This fixed training data was combined separately with 10,000, 15,000, and 20,000 PEM pixels with corresponding PEM proportions of 0.37, 0.48, and 0.55, respectively. Accuracy rates of optimally pruned trees were assessed using a common sample of set-aside data where the numbers of pixels in each wetland class was proportional to the land area of each class in the Yellowstone NWI; 0.69 PEM, 0.22 PFO, 0.05 PSS, 0.03 PUS, 0.01 PAB.

The pruned classification tree obtained from a training dataset with a 0.48 proportion of PEM pixels satisfied the defined accuracy goals (figure 4.2) and was subsequently used to map palustrine wetland types. In mapping the PAB, PEM, PFO, PSS, and PUS classes across the Yellowstone landscape, predictions were generated for all pixels previously classified as palustrine wetland by the wetland/upland classification tree. Pixels were assigned to the palustrine class with the largest predicted likelihood.

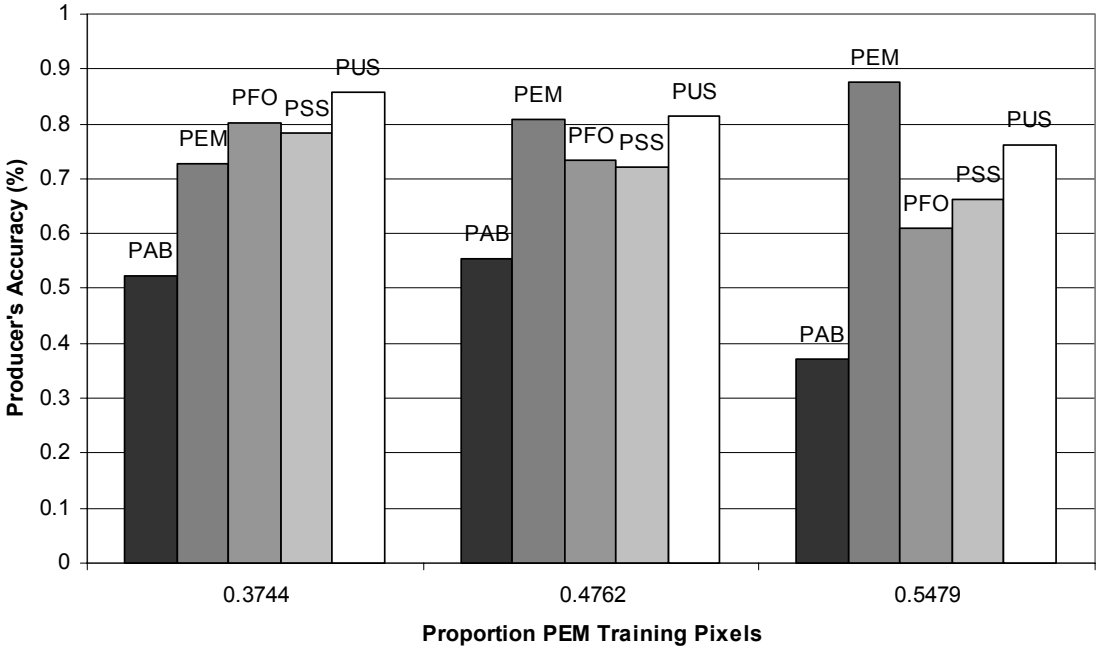

Figure 4.2. Producer's accuracies of optimally pruned classification trees for PAB, PEM, PFO, PSS, and PUS classes given different proportions of PEM pixels in training data.

Modeling of water regimes was limited to the PEM, PFO, and PAB classes. In the Yellowstone NWI, the seasonally flooded water regime dominates the scrub-shrub class (approximately 94% by area), while the PUS class is predominantly intermittently flooded (approximately 97% by area).

Palustrine emergent wetland almost exclusively falls into the saturated (PEMB) and seasonally flooded (PEMC) water regimes. In the saturated water regime, by definition: "The substrate is saturated to the surface for extended periods during the growing season, but surface water is seldom present (Cowardin et al. 1979)." In the seasonally flooded class, "Surface water is present for extended periods especially early

in the growing season, but is absent by the end of the season in most years. When surface water is absent, the water table is often near the land surface (Cowardin et al. 1979)."

Forested wetlands are dominated by the temporary flooded (PFOA) and saturated (PFOB) water regimes. In the temporary flooded water regime, "Surface water is present for brief periods during the growing season, but the water table usually lies well below the soil surface for most of the season (Cowardin et al. 1979)."

Aquatic bed wetlands are classified as semi-permanently flooded (PABF) or intermittently exposed (PABG). By definition, surface water persists throughout the growing season in most years in the semi-permanently flooded water regime. In intermittently exposed wetlands surface water is present the whole year, except during severe drought (Cowardin et al. 1979).

50,000 pixels were randomly sampled from PEM wetland polygons larger than one hectare and proportional to the relative cover of the PEMB (0.27) and PEMC (0.73) regimes. Two sets of identically sampled PEM pixels were set-aside for pruning and model verification. 50,000 pixels were proportionally sampled from PFO polygons; 0.43 from the PFOA class, 0.57 from the PFOB class. There were not enough training pixels available from polygons larger than one hectare to assemble similarly sized pruning and verification data sets, so two sets of 20,000 PFO pixels were proportionally sampled for these purposes. The number of PAB pixels available from NWI polygons larger than one hectare was small, 5,324 pixels. Half of these pixels were set-aside for model training (0.85 PABF, 0.15 PABG) while the other half was reserved for pruning and model verification. Given that water regime strata were sampled proportionally, model-

verification data were treated nominally as simple random samples. Maximum likelihood estimators of producer's and user's accuracy rates, and their estimated variances, were from Green et al. (1993).

The sampling frame for field verification was designed using ArcView V8 software (Environmental Research Institute, Redlands, CA) with the objective of limiting travel time to sites while ensuring reasonable coverage within the park. First, all segments of trails further than 5 kilometers from any road were erased from the Yellowstone trails coverage. A one kilometer buffer was placed around the remaining trail segments. Similarly, a one kilometer buffer was placed around all roads in the park, including primary roads, secondary roads, and maintenance roads. The two one kilometer buffers were then combined. Areas where the sampling frame intersected NWI riverine polygons or Yellowstone Lake, Shoshone Lake, or Lewis Lake (the three largest lakes in Yellowstone Park) were eliminated. Distribution of the field sampling frame across the Yellowstone landscape is illustrated in figure 4.3.

Individual field verification sites were randomly selected based on classification tree predictions. The objective was to visit 50 pixels from each of the five palustrine classes, 50 upland pixels falling outside any NWI polygon, and 50 upland pixels falling inside NWI palustrine wetland polygons, for a total of 350 sites. Upland sites were divided in this fashion given an expectation that the rate at which wetland pixels were erroneously identified as upland would be very small, and given an assumption that misidentified upland pixels would be more likely to be found where the NWI indicated palustrine wetland. Given an expectation that some sites would be inaccessible due to

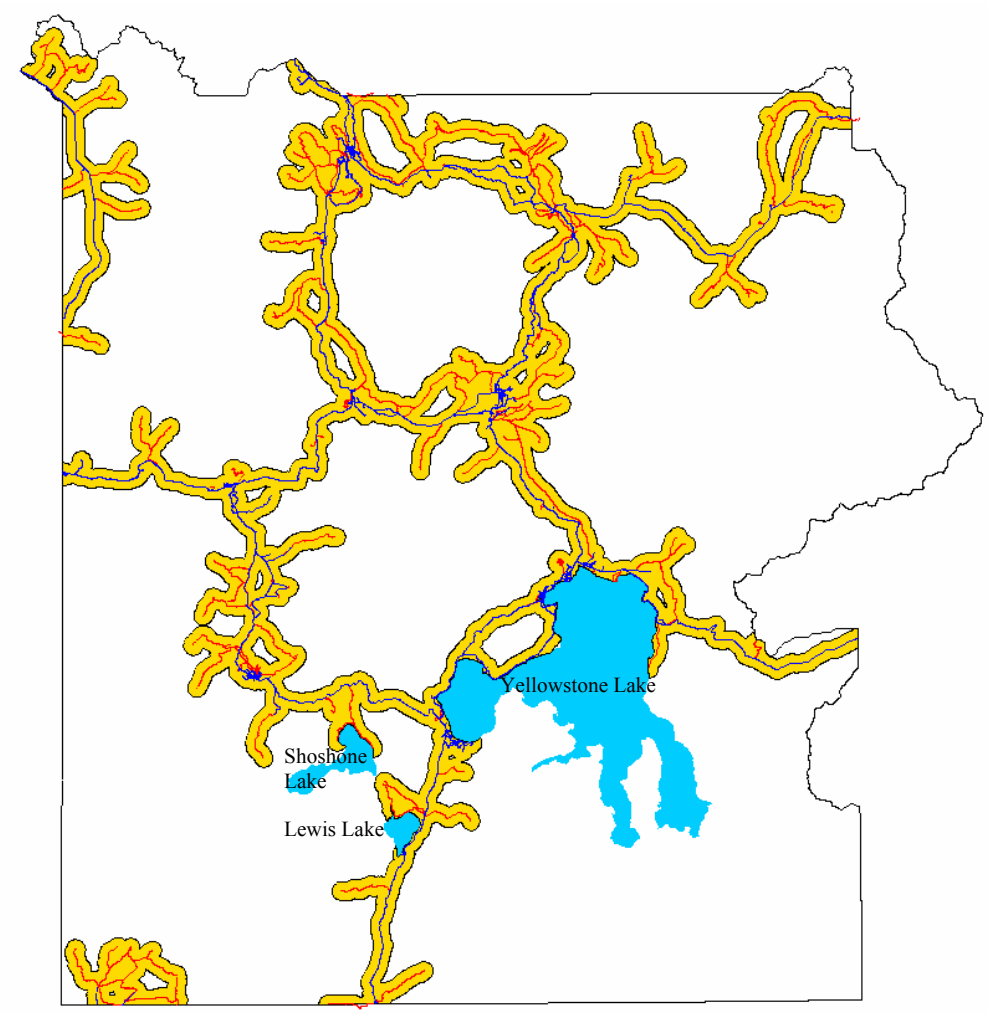

Figure 4.3. 2003 field sampling frame (tan colored areas) in Yellowstone National Park. Blue lines are park roads, red lines are trails.

terrain, road and trail closures, forest fire, etc., 75 pixels were randomly selected from each class, with extra sites rejected in the field when it became apparent that they were inaccessible.

Pixel centers were located using a Garmin eTrex Legend (Garmin International, Inc., Olath, KS) Global Positioning System (GPS). Accuracies indicated by the GPS were nearly always less than ten meters and typically four to six meters. Pixel boundaries

were located approximately by navigation in the four cardinal directions from pixel centers. Pixels were identified as palustrine emergent (PEM), palustrine forested (PFO), palustrine scrub-shrub (PSS), palustrine unconcsolidated shore (PUS), or palustrine aquatic bed (PAB) according to specifications of the Cowardin system (Cowardin et al. 1979), or as upland (UPL). A pixel was identified as one of the five palustrine wetland types if any part of the pixel contained palustrine wetland. Conversely, a pixel was identified as upland only if the entire pixel did not contain any wetland. Water regime modifiers were not determined in the field.

In a relatively small number of cases, field sites were identified as riverine or lacustrine wetland; of six predicted PAB pixels, five were riverine, one was lacustrine, while one PEM pixel and one upland pixel were riverine. Rather than adding riverine and lacustrine categories to the error analysis, the upland category was re-specified as "Not Palustrine wetland" which was considered general enough to include misclassified riverine and lacustrine pixels. Not Palustrine pixels were divided into pixels with centers falling inside NWI palustrine wetland polygons (Not Palustrine +NWI) and pixels falling outside NWI palustrine wetland polygons (Not Palustrine –NWI).

The stratified random sample from the seven predicted classes was used to generate a sample error matrix. Given that the total number of pixels falling in each of the predicted classes over the sampling frame was known, the sample error matrix was then used to estimate a population error matrix. Overall accuracy, and producer's and user's accuracies were estimated from the population error matrix (Stehman 1996).

Standard errors of accuracy rates were estimated using maximum likelihood estimators derived by Card (1982) for stratified random sampling.

Results

Classification Trees

A simplified version of the optimally pruned palustrine wetland/upland classification tree, including the first five levels, is plotted next to the full tree in figure 4.4. Branch lengths in each tree are proportional to the reduction in total deviance accounted for by the split they arise from, with the simple tree accounting for a substantial proportion of the total deviance resolved by the full tree. Labels of splits in

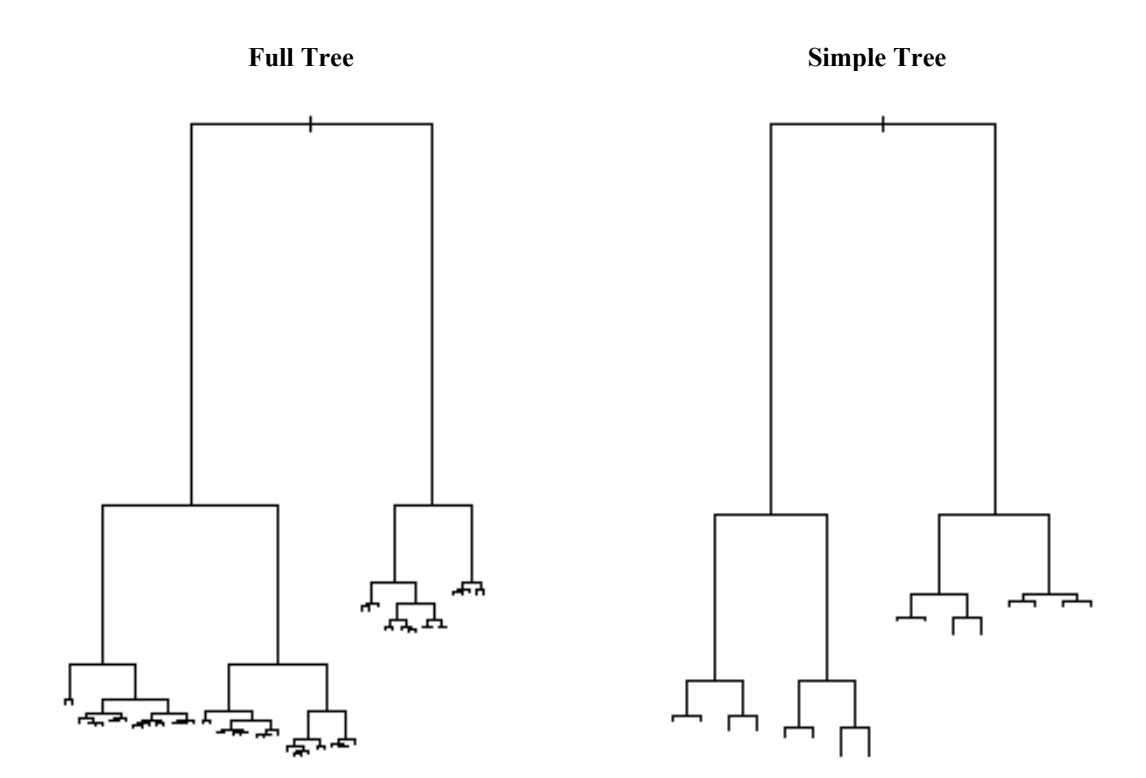

Figure 4.4. Palustrine wetland/upland classification trees. Full tree is the complete, optimally pruned tree. Simple tree consists of the first five levels of the full tree.

figure 4.5 indicate rules determining which pixels are sent to the left. Where splits are categorical, pixels sent to the right are not necessarily from all other categories, but may be a subset of the categories not sent to the left. Where important, these details will be noted in the text.

The first split in the palustrine wetland/upland tree is based on tasseled cap greenness (figure 4.5). Most upland training pixels had tasseled cap greenness values less than 119.5 and were sent down the left main branch of the tree. Separation of wetland pixels within the upland main branch is possible only after splits on habitat type and landform type. Palustrine wetland is associated with alluvial (al) and hydrothermal (hl) landforms and six habitat types: nonforest wet (nw), nonforest willow (nwl), subalpine fir wet (sw), thermal vegetation (tv), water (wa), and wet forest (wf). Within these wetter habitat types, upland pixels are more likely in breaklands and colluvial slopes (bcs), fluvial plateaus (fp), fluvial rolling uplands (fru), glaciated plateaus (gp), glaciated rolling uplands (gru), glacial troughs and cirques (gtc), glaciofluvial terraces and plains (gtp), landslides (ls), and other glaciofluvial landforms (ogl) (figure 4.5).

Returning to the initial split on tasseled cap greenness, pixels with greenness values greater than 119.5 are more likely to be palustrine wetland (figure 4.5). Within the right main branch dominated by wetland, upland pixels are separated by their association with drier habitat types, slopes greater than approximately 14% and smaller tasseled cap greenness texture (in both 5 pixel-by-5 pixel and 7 pixel-by-7 pixel moving windows). Wetland pixels are less likely in breaklands and colluvial slopes (bcs), fluvial plateaus

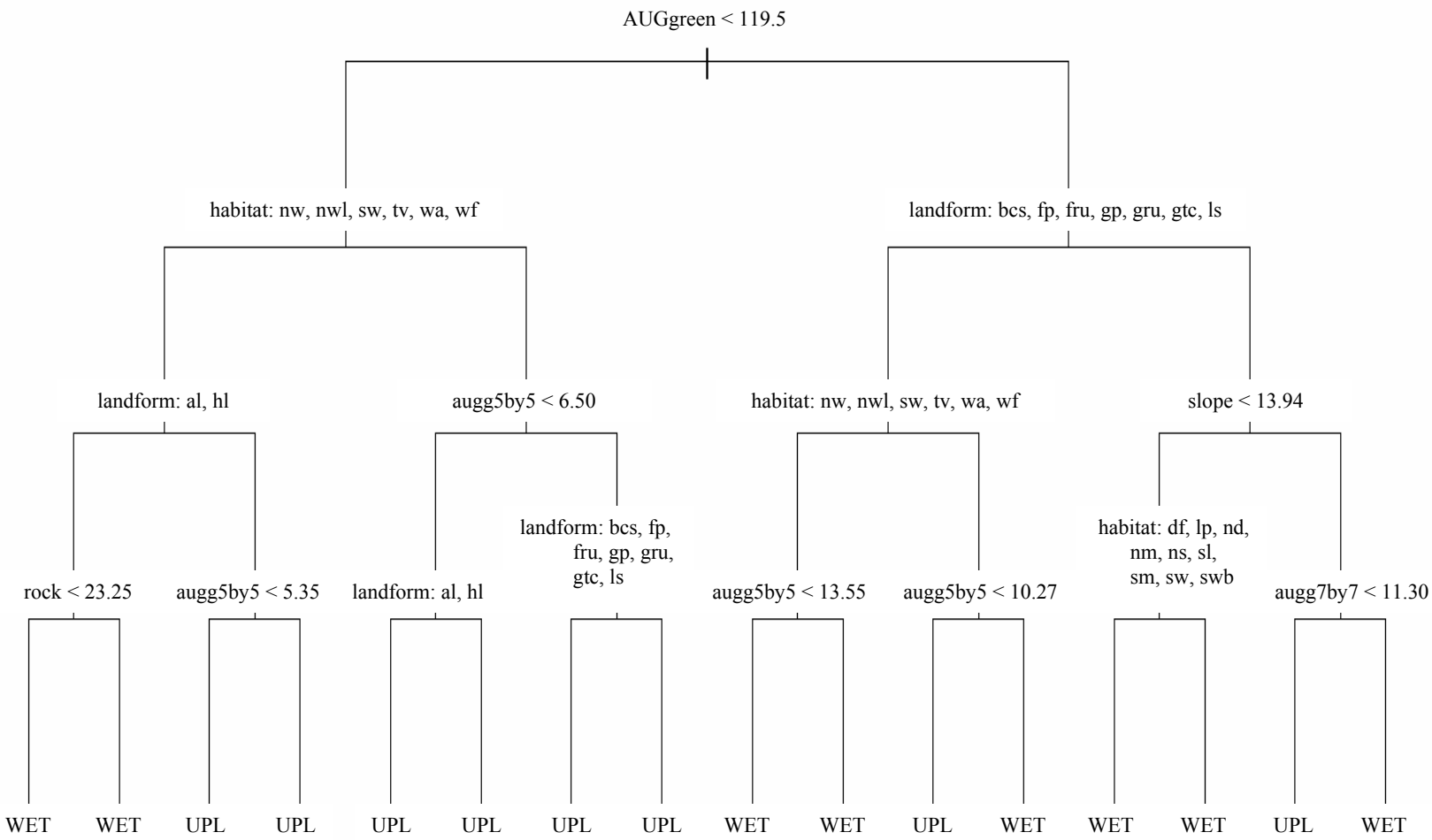

Figure 4.5. First five levels of the palustrine wetland/upland classification tree.

(fp), glaciated plateaus (gp), glaciated rolling uplands (gru), glacial troughs and cirques (gtc), and landslides (ls). And in these landforms they are associated with wetter habitat types: nonforest wet (nw), nonforest willow (nwl), subalpine fir wet (sw), thermal vegetation (tv), water (wa), and wet forest (wf). By contrast, in wetter landforms, i.e. alluvial (al), fluvial rolling uplands (fru), glaciofluvial terraces and plains (gtp), hydrothermal (hl), and other glaciofluvial landforms (ogl), wetland pixels with slopes less than approximately 14% are associated with both wetter habitat types and drier habitat types like nonforest dry (nd), and nonforest sage (ns) (figure 4.5).

In total, the full, optimally pruned palustrine wetland/upland classification tree retained 15 out of the 25 predictors presented to the classification tree algorithm (table 4.2). Variables are arranged in table 4.2 by the level at which they first appeared in the full tree, an approximate indicator of the relative importance of each variable in the classification process. Tasseled cap brightness, tasseled cap wetness texture, and greenness texture in 3 pixel-by-3-pixel windows were the only other spectral information included in the full tree. Additional ancillary GIS layers used in the full tree include percent clay content, cover type, bedrock geology, elevation, and depression fill depth.

The first five levels of the palustrine wetland types classification tree also resolve a substantial amount of the total deviance accounted for by the full, optimally pruned tree (figure 4.6). The first split in the wetland type tree is on cover type and, in general, emergent wetland (PEM) is associated with the aspen (as), Douglas fir post-disturbance (dp), nonforest (nf), and water (wa) cover types. Forested wetland (PFO) is generally associated with Douglas fir climax (dc), Engelmann spruce (es), subalpine fir (sf),

Table 4.2. Predictors retained by palustrine wetland/upland and palustrine wetland types optimally pruned classification trees.

Level	Palustrine Wetland/Upland Predictors	Level	Palustrine Wetland Types Predictors
1	Greenness (AUGgreen)	1	Cover type
2	Habitat type	2	Habitat type
2	Landform type	2	3 pixel-by-3 pixel greenness texture (augg3by3)
3	5 pixel-by-5 pixel greenness texture (augg5by5)	3	Elevation
3	Slope	3	Greenness (AUGgreen)
4	% Rock fragments	3	5 pixel-by-5 pixel greenness texture (augg5by5)
4	7 pixel-by-7 pixel greenness texture (augg7by7)	4	7 pixel-by-7 pixel wetness texture (augw7by7)
5	3 pixel-by-3 pixel greenness texture (augg3by3)	4	Brightness (AUGbright)
5	% Clay content	4	Wetness (AUGwetness)
6	Cover type	5	Landform type
6	Bedrock geology	6	% Clay content
6	Brightness (AUGbright)	6	3 pixel-by-3 pixel wetness texture (augw3by3)
6	3 pixel-by-3 pixel wetness texture (augw3by3)	7	Precipitation
7	Elevation	7	3 pixel-by-3 pixel brightness texture (augb3by3)
7	Depression fill depth	8	5 pixel-by-5 pixel wetness texture (augw5by5)
		9	5 pixel-by-5 pixel brightness texture (augb5by5)

lodgepole pine climax (lc), lodegepole pine pygmy (lg), lodgepole pine successional (ls), whitebark pine climax (wc), whitebark pine post disturbance (wp), and whitebark pine successional (ws) cover types (figure 4.7). Within these habitat types, the PEM class is separated from the PFO class largely by image texture, exhibiting greater texture in both brightness and greenness bands. Spectrally, PEM wetland is brighter than the palustrine scrub-shrub class (PSS) and greener than the unconsolidated shore (PUS) and aquatic bed (PAB) classes. PSS wetlands are isolated by association with the nonforest willow (nwl) and lodgepole pine (lp) habitat types. PAB pixels are distinguished by low tasseled cap

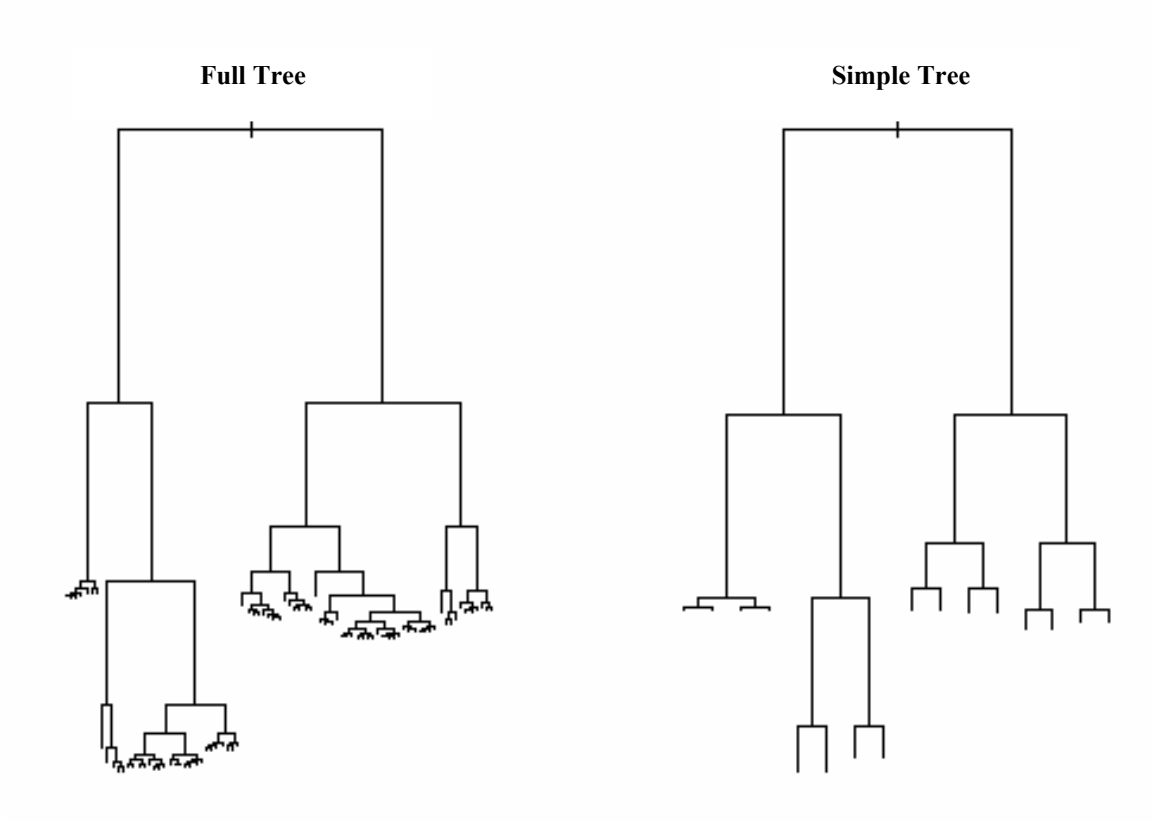

Figure 4.6. Palustrine wetland types classification trees. Full tree is the complete, optimally pruned tree. Simple tree consists of the first five levels of the full tree.

greenness and brightness, as would be expected from pixels containing open water, and also exhibit greater wetness texture. The PUS class is characterized by lesser greenness and greater brightness. In Yellowstone, PUS wetlands are typically found on bright white, geothermally formed substrates with little vegetation.

Additional ancillary predictors used in the full palustrine wetland types classification tree include landform type, percent clay content, and average annual precipitation (table 4.2). Spectrally, the full tree uses additional texture measures in the brightness and wetness tasseled cap bands in 3-by-3 and 5-by-5 moving windows.

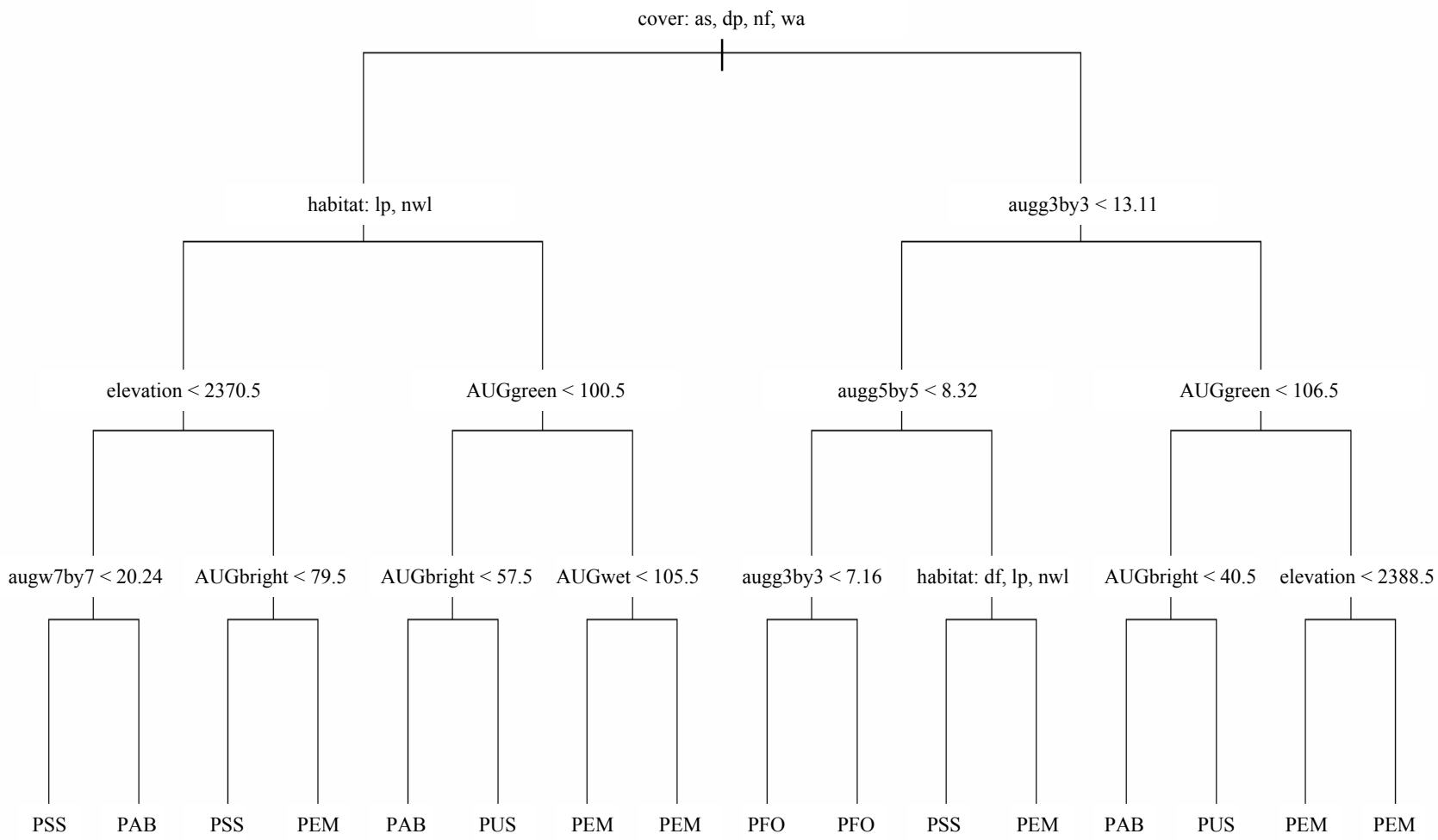

Figure 4.7. First five levels of the palustrine wetland types classification tree.

Optimally pruned water regime classification trees for the PEM, PFO, and PAB classes are plotted next to simple trees derived from them in figure 4.8. In all three cases, the first five levels of simple trees account for a large proportion of the total deviance resolved by full trees.

In the first split on landform type, the majority of seasonally flooded palustrine emergent (PEMC) training pixels were associated with alluvial (al), fluvial plateaus (fp), glaciated plateaus (gp), glaciofluvial terraces and plains (gtp), and hydrothermal (hl) landforms (figure 4.9). Saturated palustrine emergent (PEMB) training pixels were more evenly divided between these landforms and the set of landforms in the split to the right; breaklands and colluvial slopes (bcs), fluvial rolling uplands (fru), glaciated rolling uplands (gru), glacial troughs and cirques (gtc), landslides (ls), water (w), and other glaciofluvial landforms (ogl).

Within the PEMB dominated branch of the tree (the right main branch), saturated wetlands are strongly associated with elevations greater than 2,720.5 meters (figure 4.9). At lower elevations, saturated and seasonally flooded water regimes are separated based on percent rock fragments and cover type. PEMB pixels are associated with soils with percent rock fragments less than approximately 17% while PEMC pixels are more likely in soils with more rock fragments. In these coarser soils, the saturated water regime is more likely in aspen (ap), Engelmann spruce (es), and whitebark pine (wc, wp, ws) cover types.

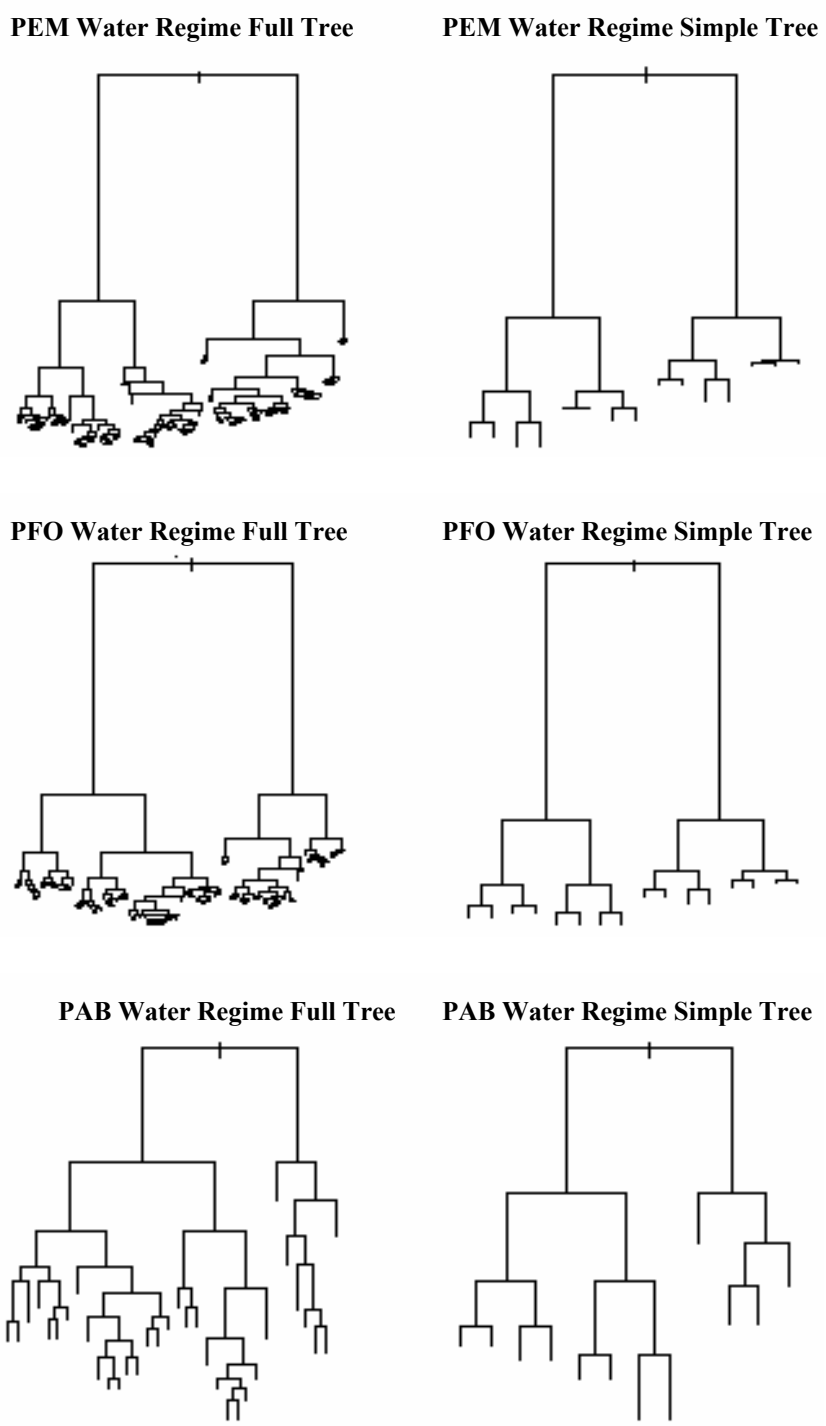

Figure 4.8. PEM, PFO, and PAB water regime classification trees. Full trees are complete, optimally pruned trees. Simple trees consist of the first five levels of full trees.

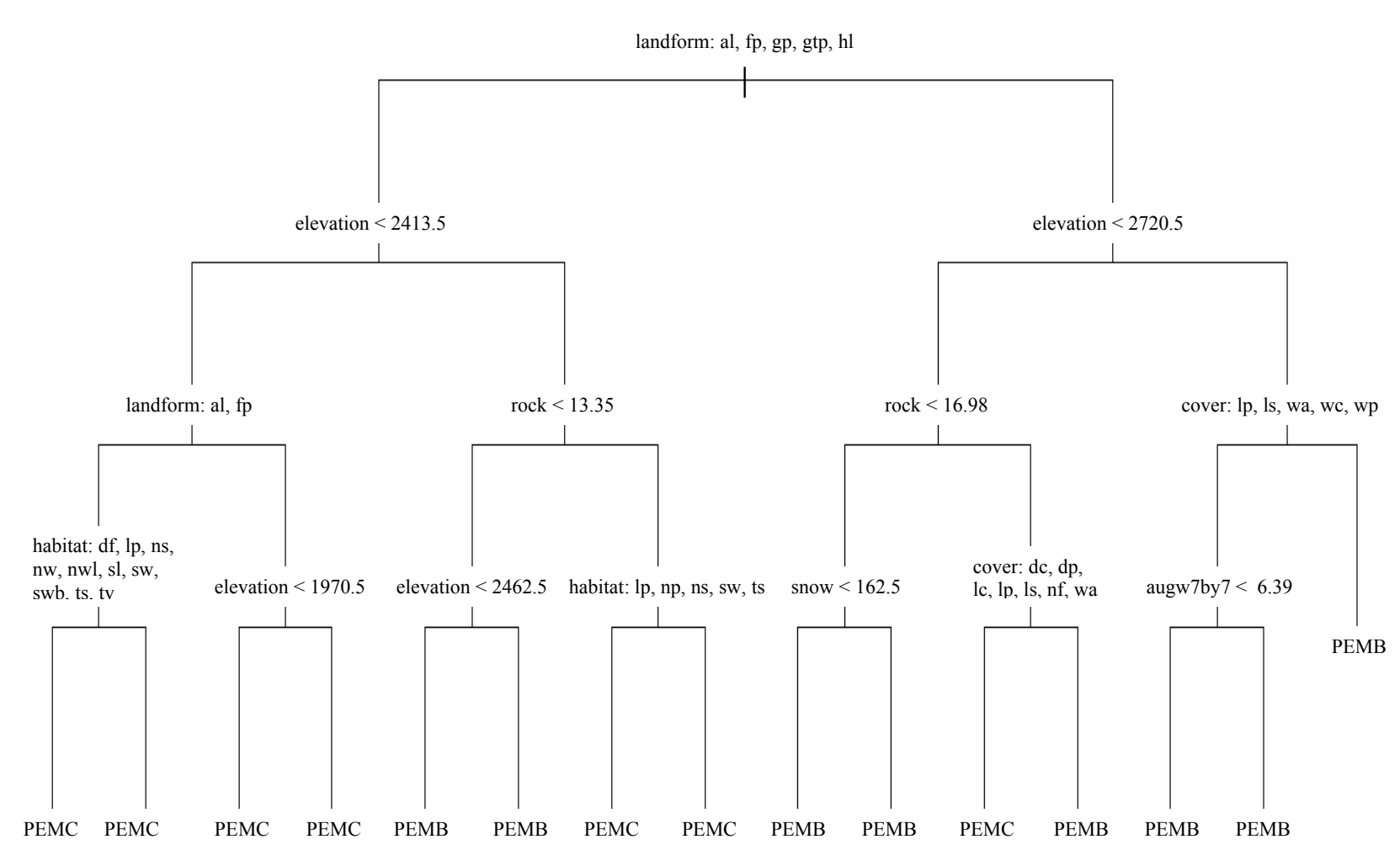

Figure 4.9. First five levels of the PEM water regime classification tree.

Along the PEMC dominated branch (the left main branch), the PEMB class is separable only at elevations above 2,413.5 meters and in soils with percent rock fragments less than 13.35%. Below 2,413.5 meters, most seasonally flooded pixels are found on fluvial plateaus (fp) and in alluvial (al) landforms. The rest are distributed on glaciated plateaus (gp), glaciofluvial terraces and plateaus (gtp), and hydrothermal landforms (hl) (figure 4.9).

The water regime classification tree for the PFO class also makes a first split on landform type (figure 4.10). Similar to the saturated water regime in emergent wetlands, saturated forested wetland (PFOB) is associated with breaklands and colluvial slopes (bcs), fluvial rolling uplands (fru), glaciated rolling uplands (gru), glacial troughs and cirques (gtc), landslides (ls), and other glaciofluvial landforms (ogl). Along the left main branch of the tree dominated by the temporary flooded (PFOA) regime, the PFOB class is separated by its association with elevations greater than 2,263.5 meters and slopes greater than 5.14%. Below 2,263.5 meters, most PFOA pixels are found in alluvial (al) landforms and on glaciofluvial terraces and plains (gtp). Over the right main branch, PFOB training pixels were relatively evenly divided between slopes less than 11.42% and slopes greater than 11.42%. But on lesser slopes, PFOA pixels are isolated at elevations less than 2010.5 meters.

The first split in the PAB water regime classification tree is on brightness texture (figure 4.11). A majority of semi-permanently flooded (PABF) pixels had textures less than 23.94 while intermittently exposed (PABG) pixels were more evenly distributed. PABG pixels in the left main branch of the tree are restricted to elevations higher than

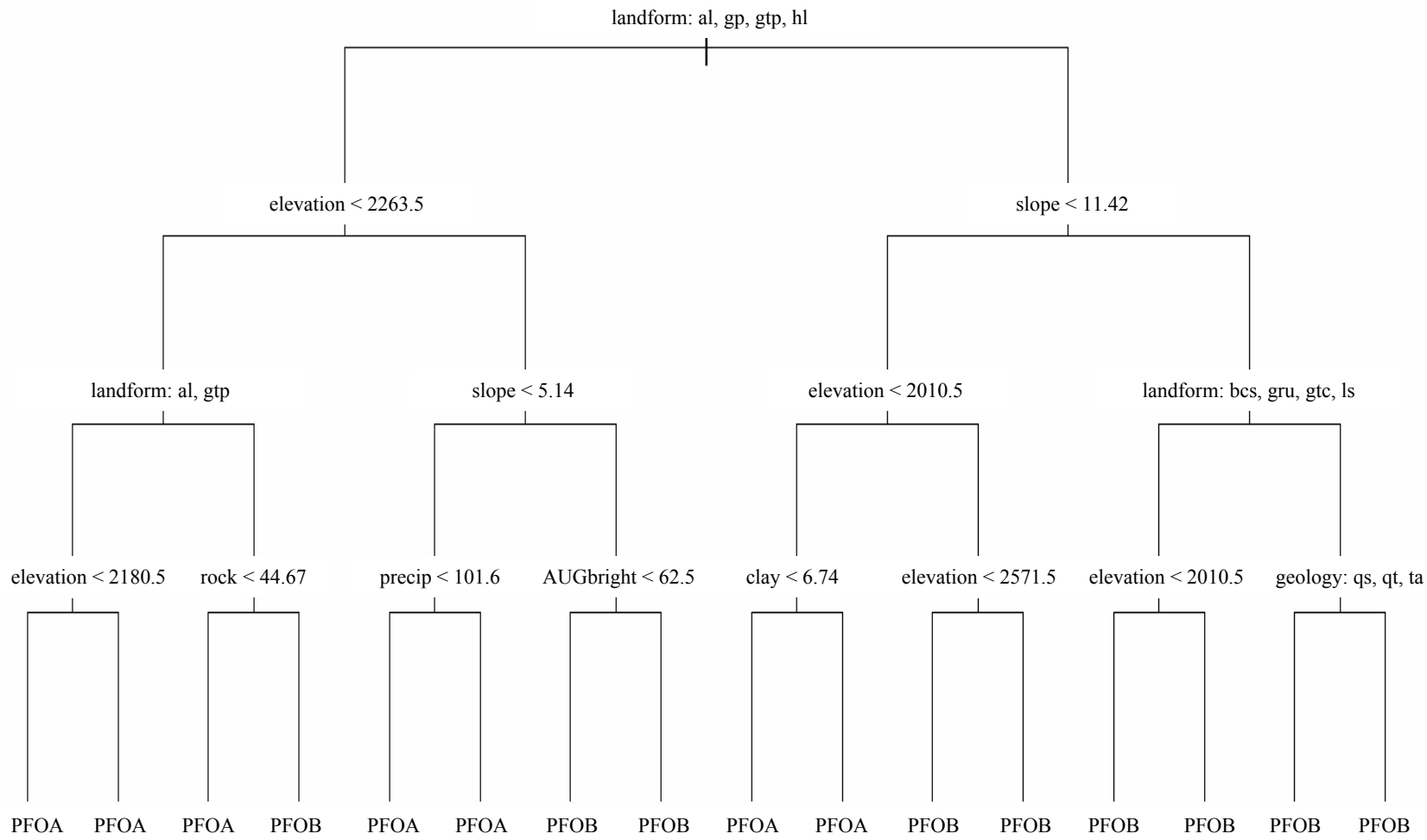

Figure 4.10. First five levels of the PFO water regime classification tree.

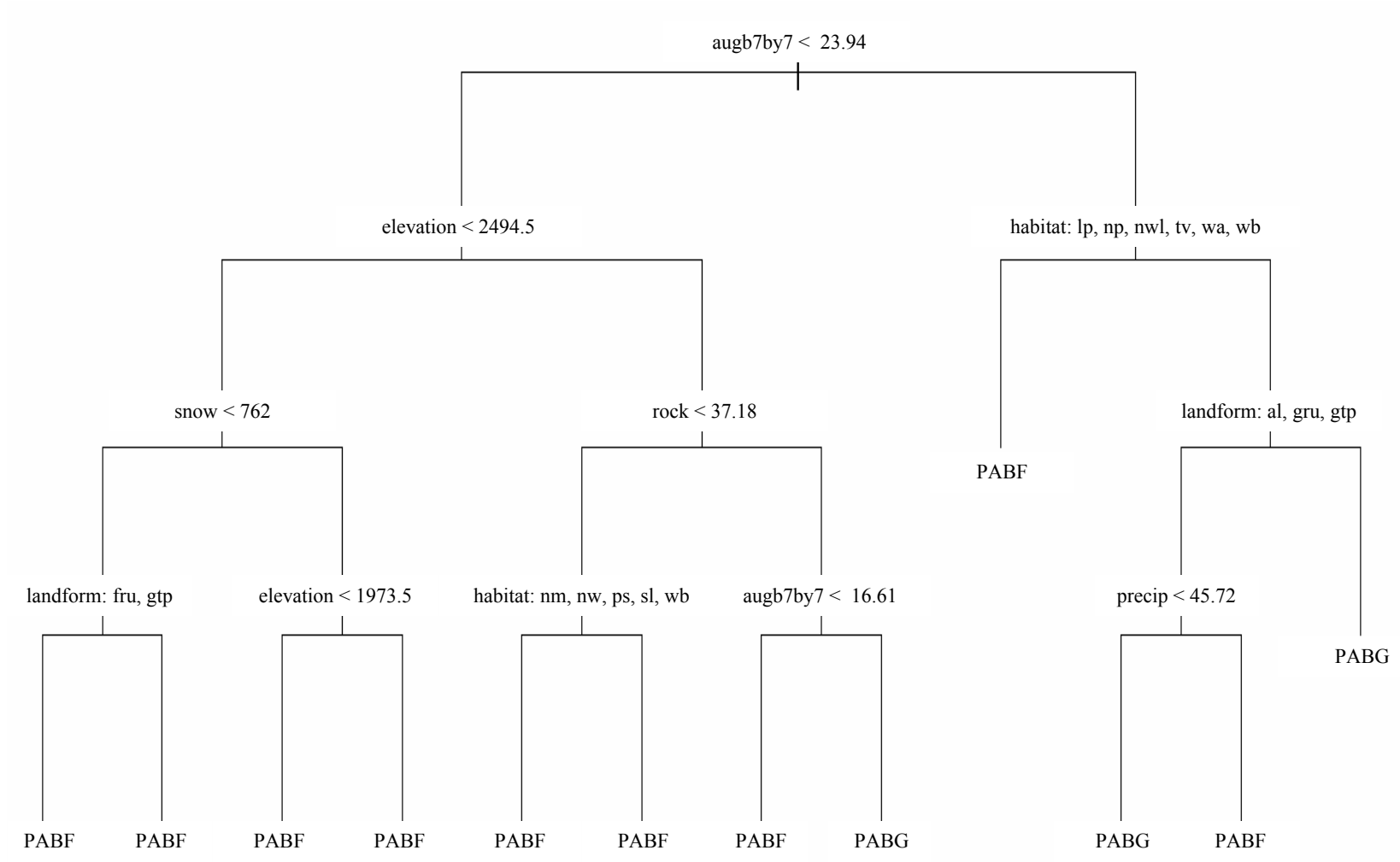

Figure 4.11. First five levels of the PAB water regime classification tree.

2,494.5 meters, percent rock fragments greater than approximately 37%, and brightness textures larger than 16.61. Down the right main branch, PABG pixels are isolated in fluvial rolling uplands (fru), glacial troughs and cirques (gtc), and landslides (ls), or in alluvial landforms (al), glaciated rolling uplands (gru), and glaciofluvial terraces and plateaus (gtp) with mean annual precipitation less than 45.72 cm. (figure 4.11).

Variables retained by full water regime classification trees are summarized in table 4.3. Additional ancillary variables used by the PEM water regime tree include percent clay content, depression fill depth, bedrock geology, slope, average annual precipitation and the topographic wetness index. Additional spectral information used by the PEM tree includes tasseled cap greenness, brightness, and wetness and texture measures derived from the three tasseled cap bands. Additional ancillary variables used by the PFO water regime tree include percent clay and rock fragments, bedrock geology, habitat type, depression fill depth, average annual precipitation and snowfall, and cover type. The PFO tree in addition to raw wetness and greenness retained image textures in all three tasseled cap bands. Additional ancillary variables used by the full PAB water regime tree include bedrock geology, percent clay content, depression fill depth, and cover type. The full PAB tree also made use of image texture in greenness and wetness bands in addition to raw wetness.

Table 4.3. Predictors retained by optimally pruned PEM, PFO, and PAB water regime classification trees.

Level	PEM predictors	Level	PFO predictors	Level	PAB predictors
1	Landform type	1	Landform type	1	7 pixel-by-7 pixel brightness texture (augb7by7)
2	Elevation	2	Elevation	2	Elevation
3	% Rock fragments	2	Slope	2	Habitat type
3	Cover type	4	% Rock fragments	3	Snow
4	Habitat type	4	Precipitation	3	% Rock fragments
4	Snow	4	Brightness (AUGbright)	3	Landform type
4	7 pixel-by-7 pixel wetness texture (augw7by7)	4	% Clay	4	Precipitation
5	% Clay	4	Bedrock geology	5	Bedrock geology
5	Greenness (AUGgreen)	5	Habitat type	5	% Clay
5	7 pixel-by-7 pixel greenness texture (augg7by7)	5	% Rock fragments	6	Depression fill depth
5	Depression fill depth	5	Depression fill depth	6	Cover type
5	Bedrock geology	5	Precipitation	6	7 pixel-by-7 pixel greenness texture (augg7by7)
6	5 pixel-by-5 pixel wetness texture (augw5by5)	5	Snow	7	3 pixel-by-3 pixel greenness texture (augg3by3)
7	Brightness (AUGbright)	7	7 pixel-by-7 pixel wetness texture (augw7by7)	7	3 pixel-by-3 pixel wetness texture (augw3by3)
7	Slope	7	7 pixel-by-7 pixel brightness texture (augb7by7)	9	Wetness (AUGwet)
7	7 pixel-by-7 pixel brightness texture (augb7by7)	7	Cover type		
8	Wetness (AUGwet)	8	7 pixel-by-7 pixel greenness texture (augg7by7)		
9	Precipitation	12	Wetness (AUGwet)		
13	Wetness index	18	Greenness (AUGgreen)		
14	5 pixel-by-5-pixel wetness texture (augw5by5)				

Accuracy Assessment

The sample error matrix for the five palustrine wetland classes and the two not palustrine classes (table 4.4) was used to estimate the population error matrix for the entire sampling frame (table 4.5). The total number of predicted pixels in each stratum is known and summarized in the row totals of table 4.5. Rates at which predicted pixels from individual classes were correctly or incorrectly identified are estimated from the sample error matrix and multiplied by the known number of pixels in each stratum to estimate the total number of pixels falling in each element of the population error matrix. From these totals, overall accuracy was estimated, in addition to producer's and user's accuracies for individual classes (Stehman 1997).

Table 4.4. Field sample error matrix.

		Actual							
		PAB	PEM	PFO	PSS	PUS	Not Palus. (-NWI)	Not Palus. (+NWI)	Row Sum
Predicted	PAB	15	7	0	0	1	25	0	48
	PEM	0	24	2	5	0	19	0	50
	PFO	1	6	22	0	0	21	0	50
	PSS	0	13	0	32	0	5	0	50
	PUS	0	7	0	0	28	15	0	50
	Not Palus. (-NWI)	0	1	0	0	0	49	0	50
	Not Palus. (+NWI)	1	23	7	2	1	0	14	48
	Column Sum	17	81	31	39	30	132	16	346

Table 4.5. Estimated population error matrix.

		Estimated Actual Number of Pixels in Sampling Frame									
		PAB	PEM	PFO	PSS	PUS	Not Palus. (-NWI)	Not Palus. (+NWI)	Known Row Sum	User's Accuracy	Std. Error
Predicted	PAB	5452	2544	0	0	363	9086	0	17445	0.3125	0.0669
	PEM	0	81160	6763	16908	0	64252	0	169084	0.4800	0.0707
	PFO	1476	8857	32476	0	0	31000	0	73809	0.4400	0.0702
	PSS	0	2833	0	6973	0	1090	0	10896	0.6400	0.0679
	PUS	0	2918	0	0	11673	6253	0	20844	0.5600	0.0702
	Not Palus. (-NWI)	0	30041	0	0	0	1471988	0	1502029	0.9800	0.0198
	Not Palus. (+NWI)	811	18656	5678	1622	811	0	11356	38935	0.2917	0.0656
	Estimated Column Sum	7739	147010	44917	25504	12847	1582942	11356	1833042		
	Producer's Accuracy	0.7044	0.5521	0.7230	0.2734	0.9086	0.9299	1.0000		Overall Accuracy 0.8844	0.0178
	Std. Error	0.1582	0.1188	0.0879	0.0806	0.0631	0.0077	----			

Relatively low estimated user's accuracies for the PAB, PEM, and PFO classes, less than 0.50 (table 4.5), are largely due to over-prediction within these classes, where a substantial number of predicted wetland pixels (from 19 to 25) were actually not palustrine wetland (table 4.4). Over-prediction was also evident in the PUS class, with an estimated user's accuracy of 0.56. Over-prediction in the predicted PSS class was limited to five pixels, but because scrub-shrub wetland was confused with emergent wetland at a relatively high rate (13 pixels out of 50), the estimated user's accuracy for the PSS class was 0.64. Estimated standard errors of user's accuracies for the five palustrine classes ranged between 0.0669 and 0.0707 (table 4.5).

Outside of NWI palustrine polygons, only one pixel in the predicted Not Palustrine (-NWI) class, was actually wetland (table 4.4), with a resulting estimated user's accuracy of 0.98 for the class and a small estimated standard error, 0.0198 (table 4.5). A large number of failures to identify wetland at pixels with centers falling inside NWI palustrine polygons contributed to a very low estimated user's accuracy for the Not Palustrine (+NWI) class, approximately 0.29, with an estimated standard error of 0.0656. However, all true Not Palustrine (+NWI) pixels were correctly identified (table 4.4), resulting in an estimated producer's accuracy of 1.0 for the class (table 4.5).

Among actual PAB and PUS pixels in the field sample, only two pixels were misclassified in each class (table 4.4). Estimated producer's accuracy for the PAB and PUS classes were approximately 0.70 and 0.91, respectively, though the estimated standard error of the PAB accuracy was relatively large, 0.1582 (table 4.5), given that

only 17 true PAB pixels were identified in the field sample. The estimated standard error for the PUS producer's accuracy was 0.0631 (table 4.5).

Two true PFO pixels were misclassified as PEM while seven true PFO pixels were falsely identified as not wetland (table 4.4), with a resulting producer's accuracy of 0.7230 estimated for the PFO class (table 4.5). The low producer's accuracy for the PSS class, approximately 0.27, resulted from the tendency of scrub-shrub wetland to be misclassified as emergent wetland (table 4.4). Standard errors of producer's accuracy for the PFO and PSS classes were similar, 0.0879 and 0.0806, respectively (table 4.5).

The estimated producer's accuracy for the PEM class was approximately 0.55 (table 4.5). Given that PEM wetland is the dominant palustrine class in Yellowstone, more true PEM sites were sampled in the field, a total of 81 pixels (table 4.4). Misclassified true PEM pixels were spread across the four other palustrine classes and the two Not Palustrine classes. Given the overwhelming prevalence of the Not Palustrine (-NWI) class in the sample frame, over 1.5 million pixels, the one true PEM pixel that was misidentified as not wetland played a dominant role in determining the PEM producer's accuracy, an estimated 30,041 misidentified pixels out of the estimated total of 147,010 true PEM pixels (table 4.5). While the predicted Not Palustrine (+ NWI) class is relatively rare (a total of approximately 39,000 pixels), the large number of PEM pixels misidentified in this class led to an estimated 18,656 misclassified true PEM pixels (table 4.5). Note that failure to identify palustrine wetland inside NWI polygons also made substantial impacts on estimated accuracy rates for the PFO and PSS classes (table 4.5).

Given the overall dominance of the Not Palustrine (-NWI) class within the sampling frame and the high producer's accuracy for this class, 0.9377, the estimated overall classification accuracy was 0.8844 with a small estimated standard error, 0.0178 (table 4.5).

Combination of the five palustrine classes (table 4.6) allows an assessment of the accuracy at which palustrine wetland pixels were distinguished from not palustrine wetland pixels. The estimated producer's accuracy for the combined palustrine wetland class is 0.7691 (table 4.7), and is within one standard error (0.0920) of the producer's accuracy found in the model training process, approximately 0.81 (figure 4.1). Estimated user's accuracy for the palustrine class is 0.6573 (table 4.7), slightly larger than the rate estimated during model training, 0.6245 (figure 4.1).

Table 4.6. Field sample error matrix for combined palustrine classes.

		Actual			
		Palustrine	Not Palustrine (-NWI)	Not Palustrine (+NWI)	Row Sum
Predicted	Palustrine	163	85	0	248
	Not Palustrine (-NWI)	1	49	0	50
	Not Palustrine (+NWI)	34	0	14	48
	Column Sum	198	132	16	346

Table 4.7. Estimated population error matrix for combined palustrine classes.

		Estimated Actual Number of Pixels in Sampling Frame					
		Palustrine	Not Palus. (-NWI)	Not Palus. (+NWI)	Known Row Sum	User's Acc.	Std. Error
Predicted	Palustrine	191971	100107	0	292078	0.6573	0.0301
	Not Palustrine (-NWI)	30041	1471988	0	1502029	0.9800	0.0198
	Not Palustrine (+NWI)	27579	0	11356	38935	0.2917	0.0656
	Estimated Column Sum	238017	1582942	11356	1833042		
	Producer's Accuracy	0.7691	0.9377	1.0000		Overall Acc. 0.9140	0.0170
	Std. Error	0.0920	0.0054	--------			

When the five palustrine classes are combined, the estimated number of predicted wetland pixels that actually are not wetland, 100,107 pixels, was smaller than the total over the five palustrine classes in table 4.5, 111,680 pixels (table 4.7). As a result, estimated producer's accuracy for the Not Palustrine (-NWI) class is higher, 0.9377, with a smaller standard error, 0.0054 (table 4.7), than the corresponding estimates in table 4.5. By extension, combining the five palustrine classes resulted in a larger estimated overall accuracy, 0.9140, with a smaller standard error, 0.0170 (table 4.7).

Note that accuracy rates reported for the five palustrine wetland classes in table 4.5 actually represent the accuracy of two separate classification procedures; first, classification of pixels as palustrine wetland; second, reclassification of wetland pixels as

one of the five palustrine wetland types. As a result, one would anticipate that accuracies estimated from field data would be smaller than accuracies estimated during model training with data identified from the Yellowstone NWI. This is true for producer's accuracy in the PEM and PSS classes. The field-estimated producer's accuracy for the PEM class, 0.5521 (table 4.5), is smaller than the value computed from NWI data, 0.8066 (figure 4.2). The field-estimated producer's accuracy for the PSS class, 0.2734 (table 4.5), is much smaller than the value estimated from NWI data, 0.6995 (figure 4.2). By contrast, estimated producer's accuracies for the PAB, PFO, and PUS classes in table 4.5 are similar to or larger than producer's accuracies calculated from NWI model verification data (figure 4.2).

Note in table 4.4, that in only the actual PEM class were pixels misclassified over the four other palustrine classes. In the actual PAB class, no pixels were misclassified as PEM, PSS, or PUS wetland (table 4.4). Similarly, no true PFO pixels were misclassified as PAB, PSS, or PUS, and no true PUS pixels were misclassified as PEM, PFO, or PSS (table 4.4). There also was a fairly large difference in the total number of pixels observed in each actual class in the field; 81 pixels in the PEM class, but only 17 in the PAB class, 31 in the PFO class, and 30 in the PUS class.

Relatively low numbers of actual pixels in the PAB, PFO, and PUS classes resulted from over-prediction in these classes. Given that substantial numbers of pixels predicted to be PAB, PFO, and PUS wetland actually were not palustrine wetland (table 4.4), sample sizes for pixels truly falling in these classes were reduced. Subtracting true PAB, PFO, and PUS pixels that were not classified as wetland in the first classification

step, the sample sizes for true PAB, PFO, and PUS pixels that were correctly identified as wetland are: PAB, 16 pixels; PFO, 24 pixels; PUS, 29 pixels.

An error matrix for the palustrine wetland type classification tree determined from NWI data (table 4.8) shows that true PAB, PFO and PUS pixels are misclassified as types other than PEM at low absolute rates. Maximum likelihood estimates of the proportion of true pixels in each class that are classified in each of the five predicted classes (table 4.9) are calculated simply by dividing each element of the error matrix by the corresponding column sum (Green et al. 1993).

Table 4.8. Palustrine wetland types error matrix given model verification data from the Yellowstone NWI.

		Actual					
		PAB	PEM	PFO	PSS	PUS	Row Total
Predicted	PAB	298	592	132	18	89	1129
	PEM	165	27735	2585	656	149	31290
	PFO	46	3986	8207	111	9	12359
	PSS	62	1439	156	1830	0	3487
	PUS	7	635	41	1	1501	2185
	Column Total	578	34387	11121	2616	1748	50450

Table 4.9. Classification rates for palustrine wetland types estimated from table 4.8.

		Actual				
		PAB	PEM	PFO	PSS	PUS
Predicted	PAB	0.5156	0.0172	0.0119	0.0069	0.0509
	PEM	0.2855	0.8066	0.2324	0.2508	0.0852
	PFO	0.0796	0.1159	0.7380	0.0424	0.0051
	PSS	0.1073	0.0418	0.0140	0.6995	0.0000
	PUS	0.0121	0.0185	0.0037	0.0004	0.8587

Estimated numbers of misclassified pixels that would be expected to be observed in the field sample error matrix (table 4.10) given observed sample sizes for each of the actual classes, and given similar misclassification rates observed with NWI data, are calculated by multiplying proportions in table 4.9 by respective sample sizes for each of the actual classes.

The estimated number of misclassified pixels needed to observe classification rates similar to those found with NWI data are very small for the PAB, PFO, and PUS classes (table 4.10). In the actual PFO class, the estimated number of true pixels expected to be misidentified given a sample size of 24 true PFO pixels was less than one pixel in the predicted PAB, PSS, and PUS classes. In the actual PUS class, the expected number of pixels misclassified as PFO and PSS is less than one, while approximately three PUS pixels were expected to be misclassified as PEM. In the actual PAB class, the expected number of pixels misclassified as PEM was approximately five pixels, the expected number of pixels misclassified as PSS was approximately two pixels, and the expected number of pixels misclassified as PUS was less than one (table 4.10).

Table 4.10. Numbers of pixels expected to be observed in the field sample error matrix.

		Actual				
		PAB	PEM	PFO	PSS	PUS
Predicted	PAB	8.25	0.98	0.28	0.25	1.48
	PEM	4.57	45.97	5.58	9.28	2.47
	PFO	1.27	6.61	17.71	1.57	0.15
	PSS	1.72	2.39	0.34	25.88	0.00
	PUS	0.19	1.05	0.09	0.01	24.90
	Known Column Total	16	57	24	37	29

Given the low number of misclassified pixels expected for the true PAB, PFO, and PSS classes, the failure to observe these misclassifications in the field appears to be less unlikely. Over-prediction in these classes resulted in sample sizes that were probably too small to accurately estimate producer's accuracies. Subsequently, the estimates in table 4.5 should be treated as positively biased. This vulnerability to over-prediction illustrates one drawback of the stratified sampling approach to accuracy estimation, especially when working with rare classes.

Recall that the estimated producer's accuracy for the scrub-shrub (PSS) class is quite low, 0.2734. This estimate may be negatively biased by the fact that the total predicted number of PSS pixels, 10,986, is much smaller than the total predicted number of PEM pixels, 169,084 pixels (table 4.5). While only five pixels out of 39 true PSS pixels were misclassified as PEM (table 4.4), they translated to an estimated 16,908 true PSS pixels misclassified as PEM (table 4.5). If a substantial amount of over-prediction is occurring in the PEM class, as table 4.4 suggests, the actual number of PSS pixels misclassified as PEM should be smaller than 16,908. Note, as well, that in the predicted Not Palustrine (+NWI) class, only two PSS pixels were not detected (table 4.4), contributing an estimated 1,622 additional misclassified pixels to the producer's accuracy calculation (table 4.5). This suggests that true PSS pixels are being classified as palustrine wetland at a high accuracy rate, and that the first step in the wetland mapping process is not making a substantial contribution to the low producer's accuracy estimated for the PSS class.

When the five palustrine classes are combined, field accuracy estimates appear to be more in agreement with values found during model training. The producer's accuracy for the palustrine wetland class estimated from the field sample, 0.7691 (table 4.7), is smaller than the 0.8060 value estimated from NWI data (figure 4.1). Given that model training data was sampled from NWI polygons larger than one hectare, one would expect a smaller accuracy rate from field data including pixels falling in palustrine wetlands smaller than one hectare and approaching the resolution limits of the Thematic Mapper. A slightly higher user's accuracy for the palustrine wetland class estimated from field data, 0.6573 (table 4.7), versus the 0.6245 accuracy rate estimated from NWI data, may result from the observed tradeoff between producer's and user's accuracy for the palustrine wetland class (figure 4.1).

Accuracy rates for the three water regime classification trees were estimated using set-aside data from the Yellowstone NWI. In this case, the sampling frame encompassed the entire park. Given that water regimes were not evaluated in the field, reported accuracies summarize the ability of classification trees to duplicate the NWI.

Emergent wetlands in Yellowstone fall predominantly in the seasonally flooded water regime (PEMC). The estimated producer's accuracy for the PEMC class, 0.8929, reflects this dominance, with a 0.6501 producer's accuracy rate estimated for the saturated water regime (PEMB) (table 4.11). Estimated user's accuracies were 0.6962 for the PEMB class and 0.8712 for the PEMC class, while corresponding standard errors were small, ranging between 0.0016 and 0.0041. The estimated overall accuracy rate for the PEM water regime classification tree was 0.8264 (table 4.11).

Table 4.11. Palustrine emergent water regimes error matrix.

		Actual			
		PEMB	PEMC	User's Accuracy	Standard Error
Predicted	PEMB	8906	3887	0.6962	0.0041
	PEMC	4794	32413	0.8712	0.0017
	Producer's Accuracy	0.6501	0.8929	Overall Accuracy 0.8264	
	Standard Error	0.0041	0.0016		

Among forested wetlands, the temporary flooded (PFOA) and saturated (PFOB) classes are more evenly distributed. Estimated producer's accuracies were 0.7837 for the PFOA class and 0.8565 for the PFOB class, with user's accuracies of 0.8037 and 0.8407, respectively (table 4.12). Estimated standard errors of these accuracies ranged between 0.0033 and 0.0044. The estimated overall accuracy rate for the PFO water regime classification tree was 0.8253 (table 4.12).

Table 4.12. Palustrine forested water regimes error matrix.

		Actual			
		PFOA	PFOB	User's Accuracy	Standard Error
Predicted	PFOA	6719	1641	0.8037	0.0043
	PFOB	1854	9786	0.8407	0.0034
	Producer's Accuracy	0.7837	0.8564	Overall Accuracy 0.8253	
	Standard Error	0.0044	0.0033		

Within aquatic bed wetlands, the semi-permanently flooded water regime (PABF) was classified with high accuracy, with producer's and user's accuracies of 0.9755 and 0.9572, respectively (table 4.13). Producer's accuracy for the intermittently exposed

class (PABG) was lower, 0.7559, with a corresponding user's accuracy of 0.8407. Standard errors of producer's and user's accuracies ranged between 0.0059 and 0.0336. The estimated overall accuracy for the PAB water regime classification tree was 0.8523 (table 4.13).

Table 4.13. Palustrine aquatic bed water regimes error matrix.

		Actual			
		PABF	PABG	User's Accuracy	Standard Error
Predicted	PABF	676	31	0.9562	0.0077
	PABG	17	96	0.8496	0.0336
	Producer's Accuracy	0.9755	0.7559	Overall Accuracy 0.9415	
	Standard Error	0.0059	0.0381		

Wetland Maps

The palustrine wetland/upland classification tree was used to map the likelihood of palustrine wetland occurrence across the Yellowstone landscape on a 30-meter grid (figure 4.12). Generally, the likelihood of wetland occurrence is low across the park, as would be expected for a rare land cover class. A number of areas of higher wetland likelihood are observed. Prominent among these are the Hayden, Pelican, and Lamar Valleys, Slough Creek, the Bechler Meadows, the South Entrance, the Yellowstone River flowing into Yellowstone Lake, and the Norris, Lower, and Upper Geyser Basins. Higher wetland likelihoods also tend to coincide with lesser drainage courses. Wetland likelihoods for Yellowstone, Lewis, and Shoshone lakes are less than 0.5, indicating that deep open-water does not strongly resemble palustrine wetland spectrally (figure 4.12).

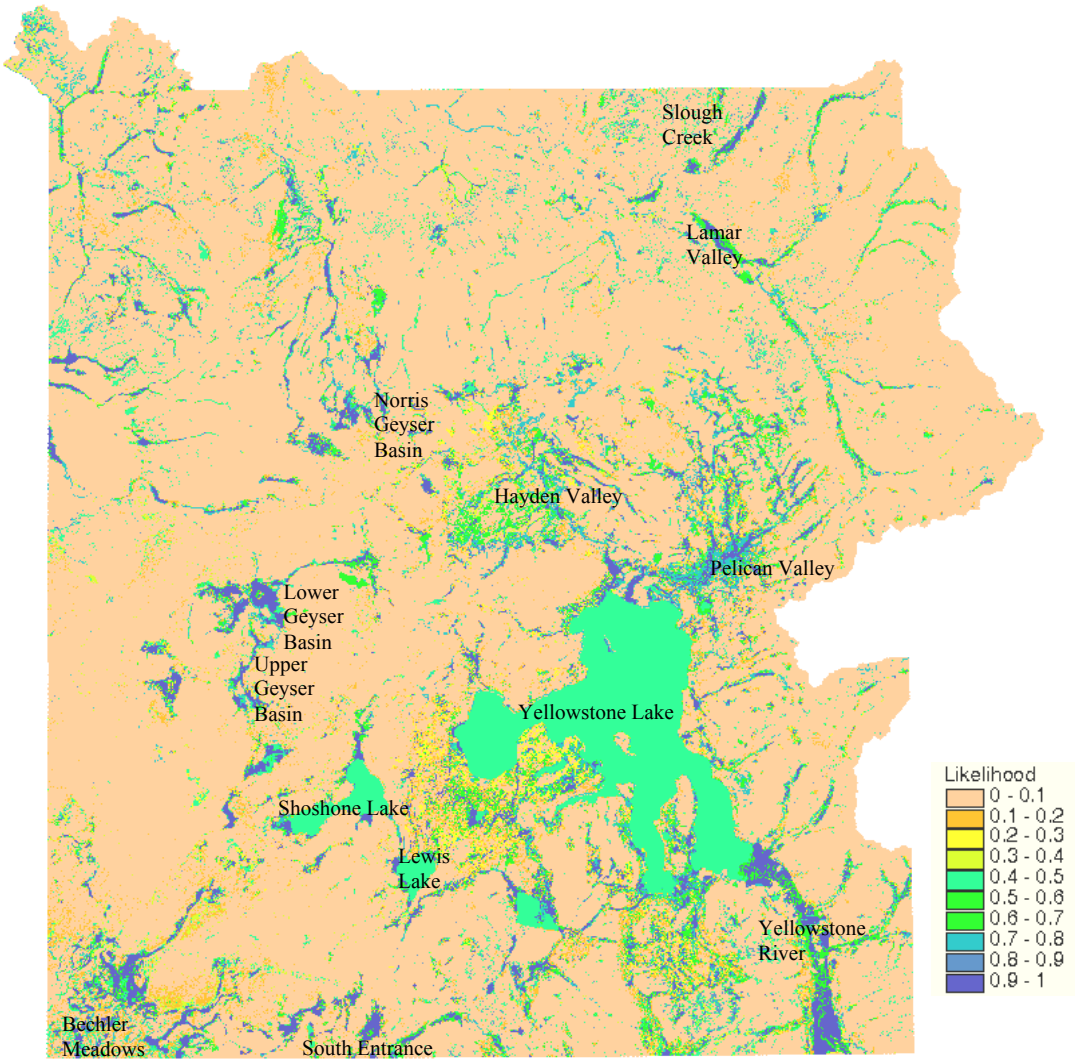

Figure 4.12. Palustrine wetland likelihood, Yellowstone National Park.

Over the smaller extent of the lower Slough Creek drainage (figure 4.13), palustrine wetland likelihoods and subsequent classification are illustrated in figure 4.14. Pixels with higher wetland likelihoods are concentrated in the Slough Creek floodplain, generally coinciding with the flooded area in figure 4.13. Pixels with likelihoods greater

Figure 4.13. Lower Slough Creek, spring flooding May, 2002.

than 0.5 in the left half of figure 4.14 are classified by palustrine wetland type in the right half of the figure.

Most pixels in the Slough Creek floodplain are classified as PEM wetland and generally coincide with PEM polygons delineated by the NWI (figure 4.14). However, predicted PEM wetland tends to extend beyond the margins of NWI polygons. Wetland likelihoods in these areas are typically 0.5 to 0.7 (green tones in the left half of figure 4.14), while higher wetland likelihoods (blue tones) are found inside PEM polygons. Though the classification tree may be over-predicting PEM extent around the margins of NWI polygons, the gradient of wetland likelihood indicates that pixels are increasingly less similar to wetland moving away from the Slough Creek floodplain.

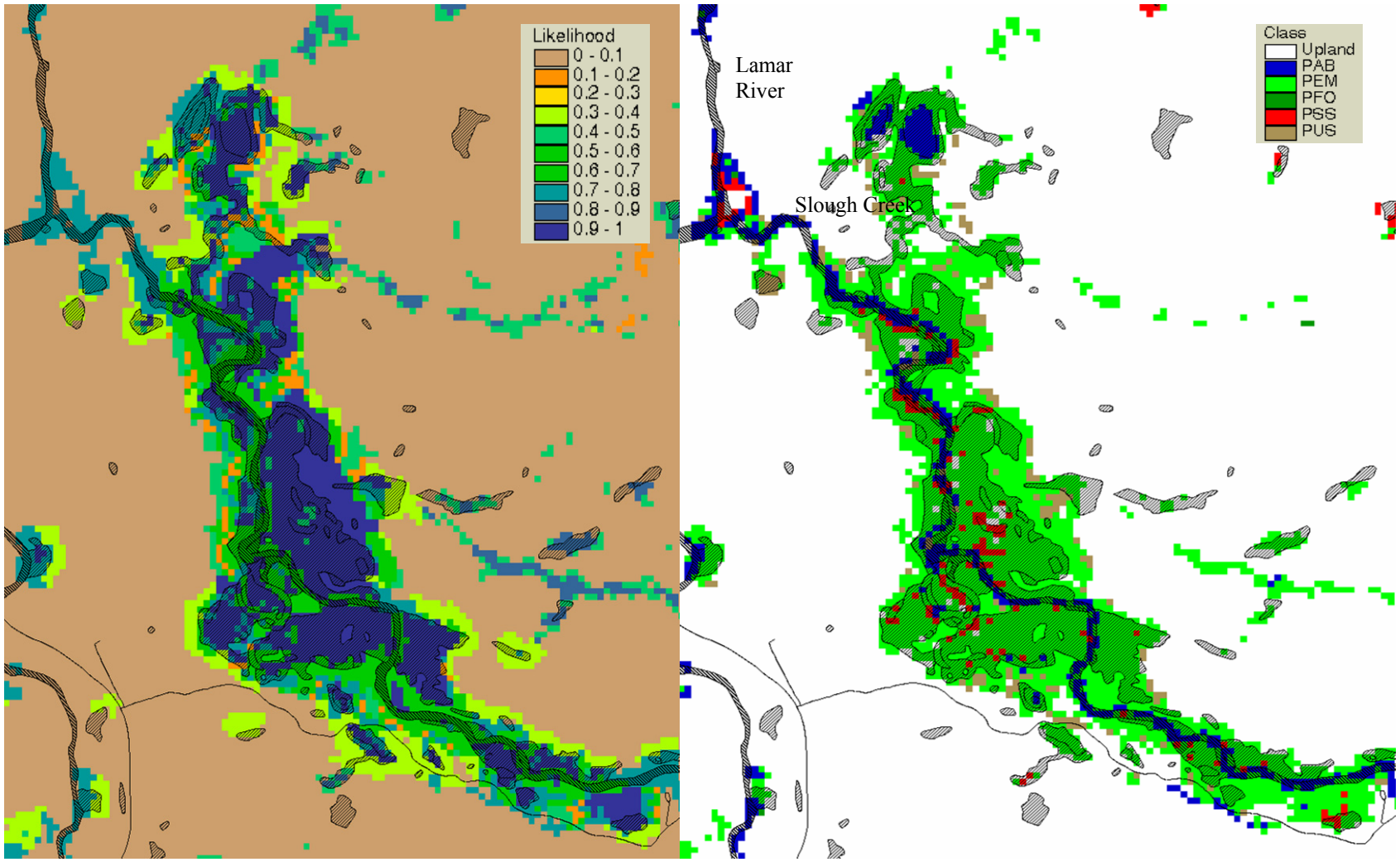

Figure 4.14. Palustrine wetland likelihood and classes in the lower Slough Creek drainage. Diagonal lines indicate NWI polygons.

A number of smaller wetlands delineated by the NWI were not identified as wetland by the classification tree (figure 4.14). In one instance, however, the model indicates a narrow PEM wetland in the lower right hand quadrant of figure 4.14 where no NWI polygon is drawn.

Pixels falling in the Slough Creek stream channel are typically classified as aquatic bed (PAB) wetland (figure 4.14). In general, the classification tree algorithm classified shallow stream channels as aquatic bed wetland across Yellowstone National Park. Palustrine wetland classification was not excluded from NWI riverine polygons and it may be prudent to mask out PAB pixels falling inside riverine polygons to avoid confusion. Two ponds near the confluence of Slough Creek and the Lamar River are correctly identified as PAB wetland (figure 4.14).

Predicted scrub-shrub pixels (PSS) are scattered across the Slough Creek floodplain. Small clusters or single PSS pixels tend to fall within larger palustrine emergent NWI polygons, suggesting that the classification tree classifies wetlands at a finer grain size than the NWI. Predicted unconsolidated shore (PUS) pixels are relatively rare and tend to occur along the margins of the large area in the Slough Creek floodplain classified as PEM (figure 4.14).

Harlequin Lake is a small lake perched above the Madison River. The Yellowstone NWI classifies the central portion of the lake as lacustrine aquatic bed with two adjacent PEM polygons while the wetland classification tree classifies the central portion of the lake as PAB wetland surrounded by emergent wetland (figure 4.15). The model also appears to accurately represent the patch of open water along the bottom of

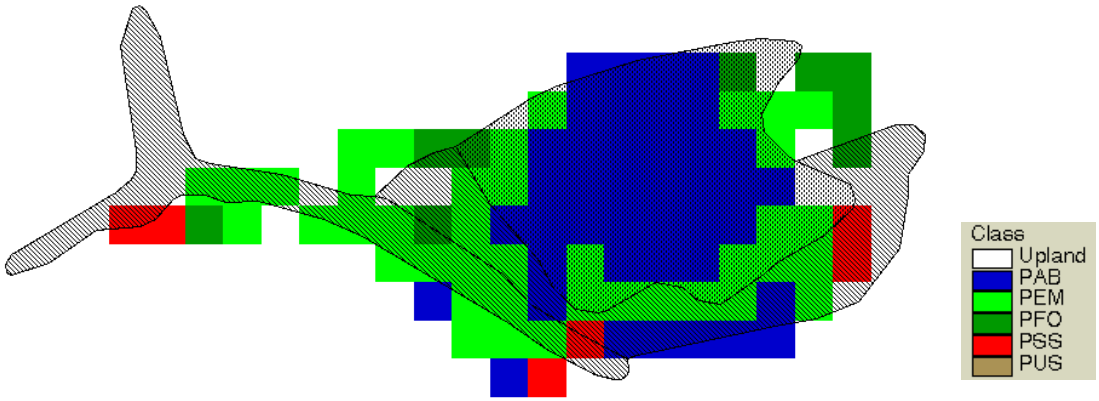

Figure 4.15. Wetland classification at Harlequin Lake. Diagonal lines indicates NWI palustrine emergent polygons, central polygon is classified as lacustrine aquatic bed by the NWI.

the photograph of Harlequin Lake, with a strip of PAB pixels isolated from the main water body by a band of PEM wetland. Additional habitat complexity not represented in the Yellowstone NWI, but indicated by the model, can be seen in the three PSS patches predicted around the edge of Harlequin Lake (one clump of willows can be seen in the lower right corner of the photograph in figure 4.15). The model also predicts some smaller patches of forested wetland around the margin of the lake.

Extensive palustrine emergent wetlands are found in the Pelican Valley (figure 4.16). Seasonally flooded (PEMC) NWI polygons tend to be concentrated in the floodplain of Pelican Creek and along synthetic streamlines leading to the creek. Predicted PEMC pixels generally tend to coincide with NWI PEMC polygons, though the model predicts saturated wetland (PEMB) in the central portion of figure 4.16 south of Pelican Creek where the NWI delineates a branching network of PEMC polygons. North of Pelican Creek, in the left one-third of figure 4.16, predicted PEMB pixels generally coincide with PEMB polygons delineated by the NWI. However, in general it appears that the classification tree is over-predicting the true extent of PEMB wetland.

Intermittently flooded forested wetland (PFOA) and saturated forested wetland (PFOB) is classified along the upper Bechler River (figure 4.17). Water regime predictions generally agree with PFOA wetlands delineated by the Yellowstone NWI in the lower left part of figure 4.17 and with PFOB wetlands delineated further upstream. In terms of wetland boundaries, model predictions are relatively consistent with the NWI, though the model predicts slightly more PFOA wetland in the lower left of figure 4.17 and slightly less PFOB wetland upstream.

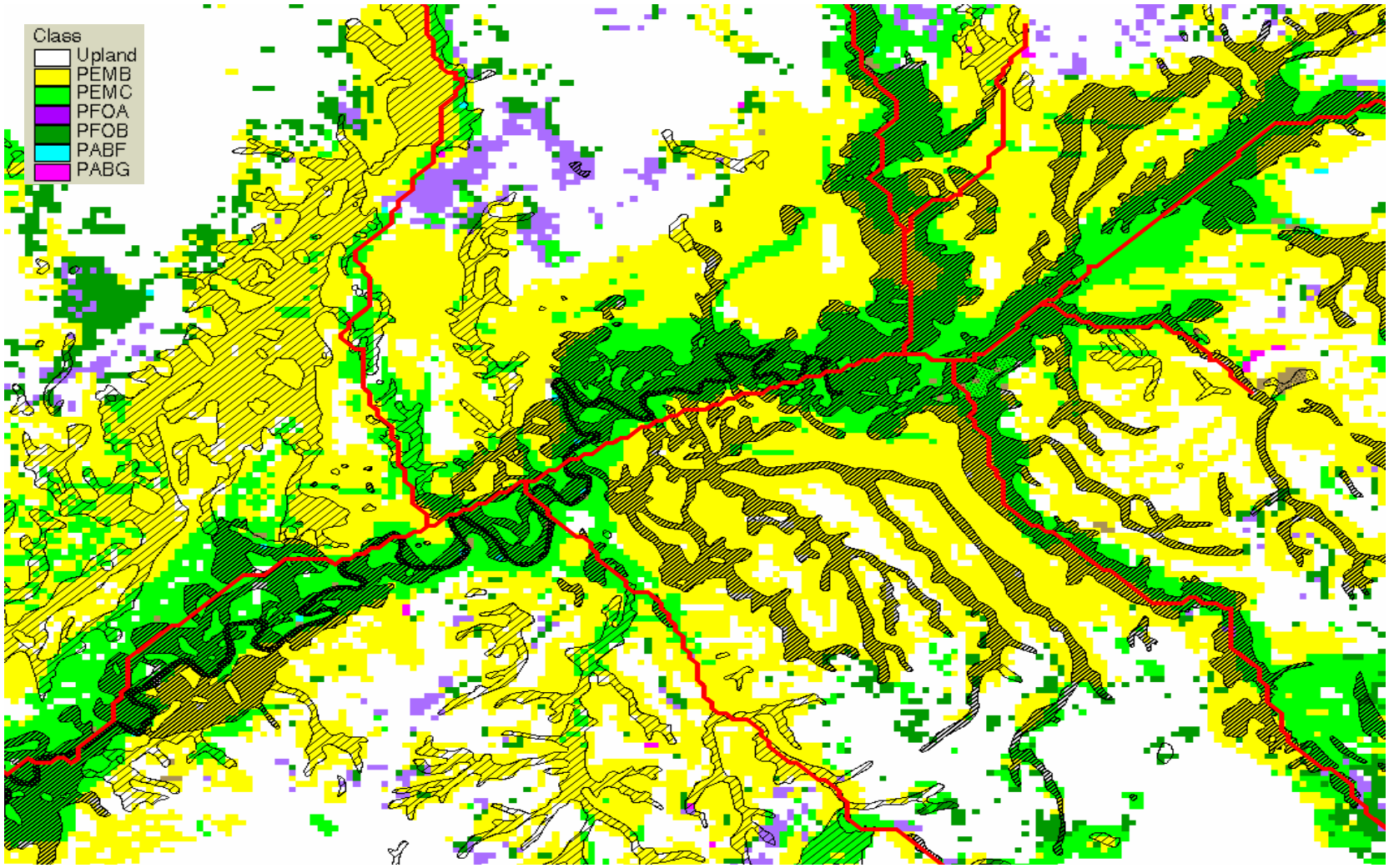

Figure 4.16. Palustrine emergent wetland in the Pelican Valley. Light diagonal lines indicate PEMB polygons, dense diagonal lines indicate PEMC polygons, dense cross-hatching identifies riverine polygons, and red lines are synthetic streamlines.

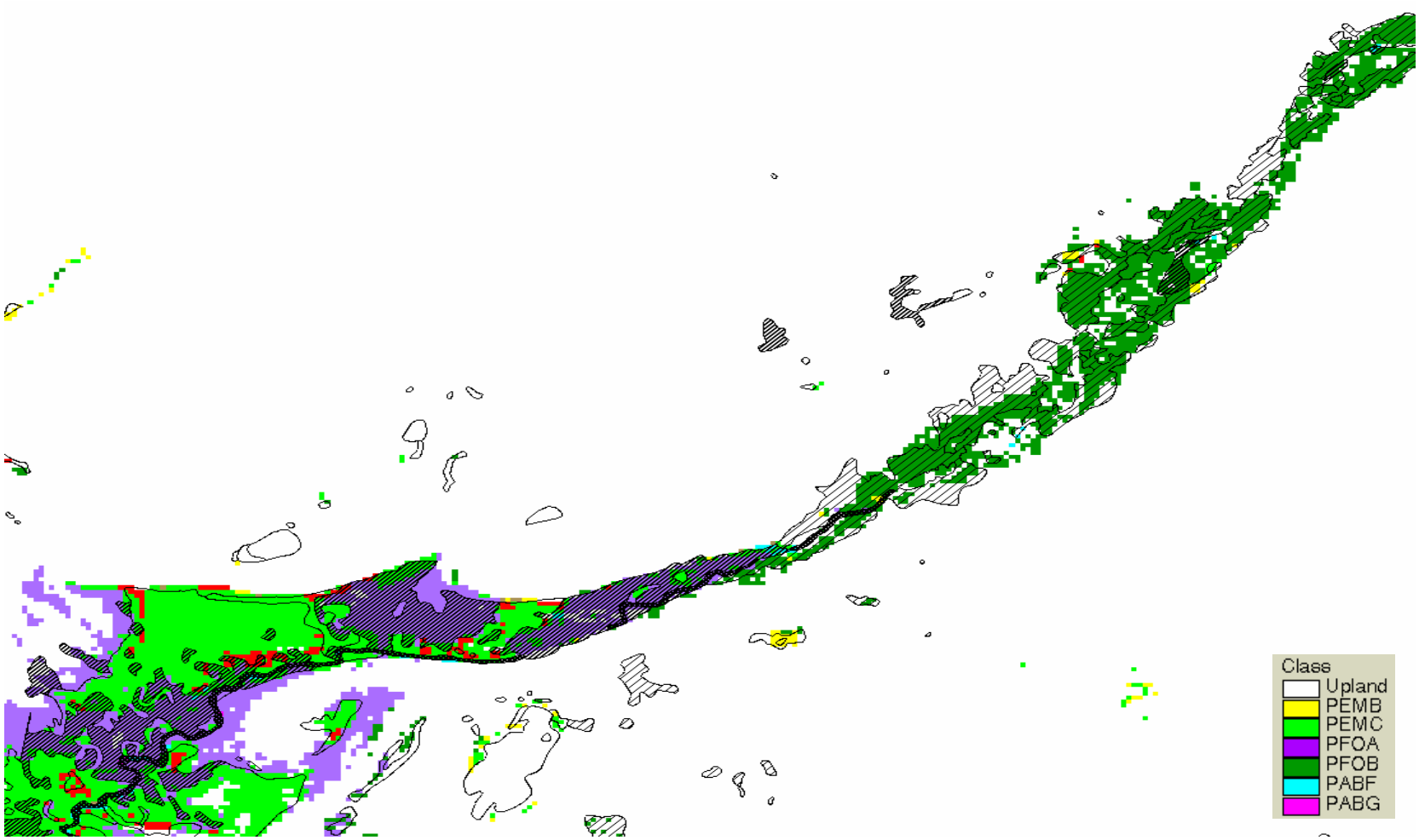

Figure 4.17. Palustrine forested wetland along the upper Bechler River. Dense diagonal lines indicate PFOA polygons, light diagonal lines indicates PFOB polygons, dense cross-hatching represents riverine polygons, and unfilled polygons are other palustrine wetland types. Red pixels are classified as PSS.

145

Discussion

Classification tree models derived from a combination of TM imagery and ancillary information are readily interpretable in terms of the spectral attributes of palustrine wetlands and how ancillary variables are associated with wetland occurrence. The ability to identify true wetland at a relatively high rate while simultaneously limiting the rate of false-positives suggests that the developed methodology would be effective identifying amphibian habitat not included in the Yellowstone NWI, and would be capable of monitoring wetland habitat variability with a reasonable degree of confidence.

The palustrine wetland/upland classification tree uses a predictor derived from TM imagery, tasseled cap greenness, in an initial split determining where wetland and upland pixels are most likely (figure 4.5). From a monitoring perspective, this result is encouraging in indicating that the wetland/upland dichotomy is most distinct in terms of a temporally varying predictor. The role of ancillary variables like habitat type, landform type, and slope then becomes one of setting the context in which TM-derived predictors can further refine discrimination between wetland and upland. For example, in the wetland dominated branch of figure 4.5, the initial split on landform type tends to isolate settings where very green pixels (i.e. values greater than 119.5) are more or less likely to be palustrine wetland or upland. Very green pixels found in alluvial (al), fluvial rolling upland (fru), hydrothermal (hl), and other glaciofluvial rolling upland (ogl) landforms, and on slopes greater than approximately 14%, tend to be upland if their greenness texture is less than approximately 11.3. By contrast, wetland pixels in this setting tend to exhibit greater image texture (figure 4.5).

Compared to the wetland/upland model, spectral variables appear to have less ability to discriminate between palustrine classes. For example, separation of the scrub-shrub (PSS) class is possible only after a high scrub-shrub likelihood space has been isolated in the intersection of two sets; {aspen, Douglas fir post-disturbance, nonforest, water} cover types and {lodgepole pine, nonforest willow} habitat types (figure 4.7). Above 2370.5 meters, PSS pixels falling in this combination of cover and habitat types tend to have tasseled cap brightness values less than 79.5 while PEM pixels tend to be brighter (figure 4.7). From a monitoring perspective, a transition from the PEM class to the PSS class would only be detectable by remote sensing over a limited subset of the landscape, i.e. pixels falling in the intersection between two subsets of Yellowstone cover and habitat types.

The PEM and PFO water regime classification trees are highly dependent on ancillary variables at upper levels. Flooded water regimes (PEMC or PFOA) were generally associated with lesser slopes or landforms likely to be flooded, e.g. alluvial (al), fluvial plateaus (fp), glaciated plateaus (gp), glaciofluvial terraces and plateaus (gtp), or hydrothermal landforms (hl). Saturated water regimes (PEMB or PFOB) were generally associated with greater slope and finer textured soils (figure 4.8 and figure 4.9). Relative unimportance of spectral variables in these trees may reflect the fact that the TM image of Yellowstone National Park was acquired on the 1st of August, perhaps too late in the growing season for hydrologic differences to be resolved by spectral data at a high level.

Failures to predict palustrine wetland were concentrated among pixels falling within polygons currently mapped as palustrine wetland by the Yellowstone NWI (table

4.4). However, the estimated total number of failures to identify wetland within NWI polygons, 27,579 pixels, was very small relative to the estimated total number of correctly identified not wetland pixels across the sampling frame, 1,483,344 pixels, or less than 2% (table 4.5). Also, nearly 30% of the predicted not palustrine pixels inside NWI polygons actually were not wetland, indicating that the classification tree method is detecting areas where wetland has reverted to upland or the Yellowstone NWI erroneously delineated wetland to begin with.

In general, National Wetland Inventory maps appear to err more by omission than by commission (Kuzila et al. 1991; Stolt and Baker 1995; Tiner 1997). Out of the 248 predicted wetland pixels that were visited in the field, 35 pixels that were not identified as wetland by the NWI actually were wetland, or approximately 14% of the total. Thus the classification tree method appears capable of identifying wetland missed by the NWI at a relatively high rate.

Some notable failures to detect palustrine wetlands were observed in the field. In one case, the wetland/upland model failed to detect a substantial portion of a large PEMC sedge meadow (figure 4.18) in the Bechler Meadows area in the southwest corner of the park, where extensive sedge marshes that flood in spring are typically dry by mid- to late-summer (Despain 1990). While an island of PEM wetland is predicted in figure 4.18, wetland likelihoods were just under 0.5 in surrounding pixels. When visited on 21 September, 2003 the site was dry and sedges appeared to be heavily browsed (see photographs in figure 4.18).

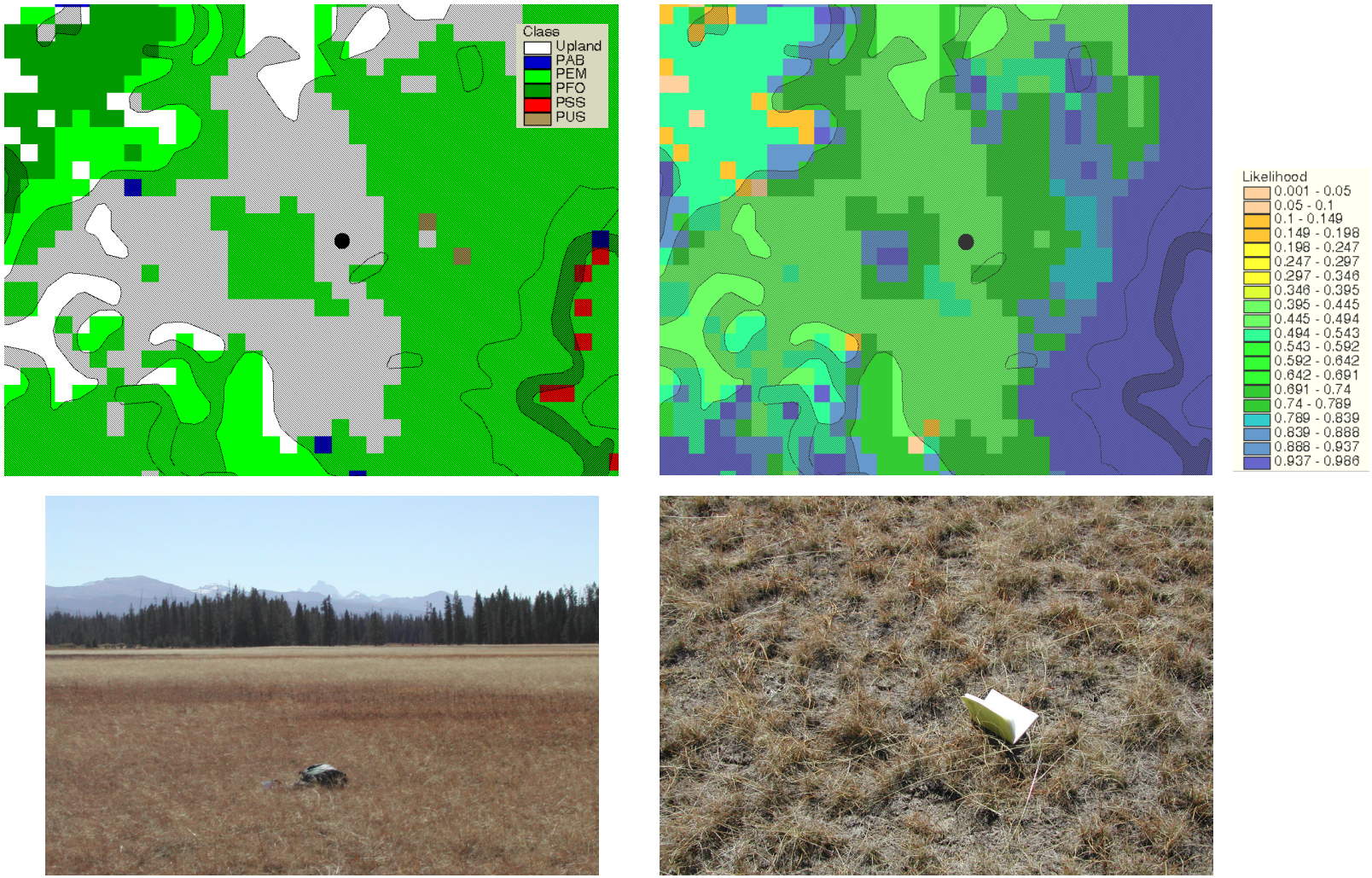

Figure 4.18. Palustrine wetland classes and likelihood in the Bechler Meadows area. Diagonal lines indicate NWI polygons. Black dot in the center of figures marks location of photographs.

Given a reasonably good ability to detect palustrine wetland in Yellowstone in general, failure to detect a large extent of drying sedge wetland suggests that not only is the classification tree methodology responding to attributes unique to palustrine wetlands, but is also sensitive to wetland condition. Definitionally, dry sedge meadows are wetland given the presence of hydrophytic vegetation (Cowardin et al. 1979), but functionally they lack the paramount feature of wetlands, i.e. that of being wet. From an amphibian perspective, wetland condition is obviously important. And while information regarding wetland condition cannot be obtained from a static NWI map, wetland likelihood maps derived from satellite remote sensing should tell us something about the state of wetlands over a very large geographic extent at a specific point in time.

Conversely, wetland likelihood mapping may indicate upland habitats that are similar to palustrine wetland, i.e. in the sense that they occupy or are close to the multivariate attribute space occupied by wetland. Though some patch of upland habitat might not be wetland by definition, one could imagine a scenario where that habitat plays a role functionally similar to definitional wetland, e.g. during unusually severe spring flooding. Higher wetland likelihood in presumed upland might also indicate an increased likelihood of finding smaller wetlands eluding direct detection given the innate spatial resolution of the TM instrument.

In terms of amphibian requirements, pixels classified as upland but similar to wetland in multivariate space (as quantified by wetland likelihoods close to 0.5) may represent preferable upland habitat or act as important corridors between wetlands. Along this line of reasoning, Spear (2004) used wetland likelihood values to estimate

least-cost paths between tiger salamander (*Ambystoma tigrinum*) breeding sites on the Northern Range of Yellowstone. Higher wetland likelihoods were assumed to incur less physiological costs-of-movement on tiger salamander adults. A regression model including least-cost paths computed from a wetland likelihood map accounted for 68% of the variability in gene flow between tiger salamander breeding sites (Spear 2004).

The classification tree methodology described in this paper has been used to generate palustrine wetland likelihood maps over the Yellowstone landscape for a number of years between 1988 and 2004 (Wright, unpublished data). One intriguing comparison that can be made from these maps is between 1988 and 1997. 1997 was an unusually wet year, with approximately 43 cm of precipitation recorded at Mammoth Hot Springs, Wyoming. 1988, the year of the catastrophic Yellowstone wildfires, was unusually dry with approximately 28 cm of precipitation recorded at Mammoth Hot Springs.

In the upper Lamar Valley, 1988 palustrine wetland likelihoods are subtracted from 1997 wetland likelihoods on a pixel-by-pixel basis (figure 4.19). Values from approximately 0.7 to 1.0 indicate areas where wetland likelihood was low in 1988 and relatively high in 1997, and are colored red. Moderate positive differences in wetland likelihood between 1997 and 1988 are shaded yellow. Turquoise and light blue shading indicate pixels where wetland likelihoods are similar in both years. Blue and violet tones indicate moderately negative differences in wetland likelihood over the two years. Pink and white indicate pixels where the likelihood of palustrine wetland was very small in 1997 and very high in 1988.

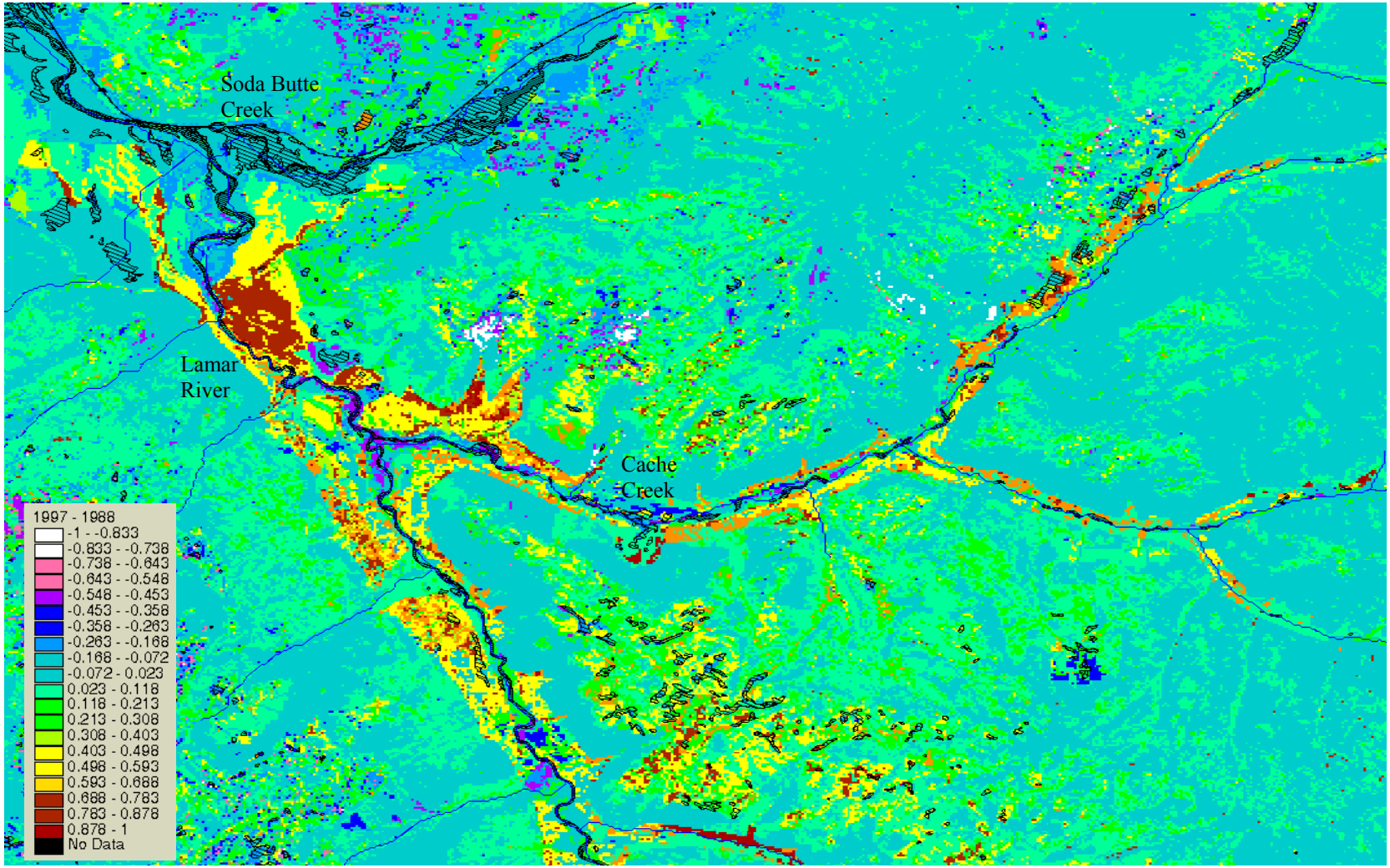

Figure 4.19. 1997 palustrine wetland likelihood minus 1988 palustrine wetland likelihood in the upper Lamar Valley. Diagonal lines indicate NWI polygons.

The overall tone of figure 4.19 is turquoise and light green; indicating that in most pixels, wetland likelihoods were similar in both years. Importantly, most pixels falling within NWI palustrine polygons exhibit little change in wetland likelihood between years. This suggests that training models using NWI data successfully identifies what definitional wetlands look like in different years. In other words, one might expect Yellowstone wetlands to have very different spectral signatures in wet and dry years, but training classification trees for each individual year calibrates models in a consistent fashion.

Yellow and red pixels tend to be adjacent to stream channels, though set back a bit, or on the periphery of palustrine wetland polygons away from stream channels (figure 4.19). Higher wetland likelihoods in these pixels in 1997 suggests that in a very wet year, these presumably upland pixels may be functionally similar to palustrine wetland, e.g. perhaps their soils are saturated or flooded, or they are very green. Also, smaller palustrine wetlands might be more likely in these areas, but only in a very wet year generate a signal detectable by the TM instrument.

In mountainous landscapes like Yellowstone, wetlands are nearly entirely dependent on precipitation as their source of water, and their presence and extent can be expected to vary as the amount of precipitation varies (Winter 2000). Given an expectation that Yellowstone wetlands should exhibit climate-driven variability, the ability to generate yearly wetland maps should allow amphibian researchers to relate amphibian population dynamics to wetland variability on a landscape scale.

Water regime prediction, especially within the palustrine emergent class, is relevant to ongoing Yellowstone amphibian surveys. Within randomly watersheds, survey crews limit their search for amphibians to all NWI polygons that are not in the saturated or temporary flooded regime, given a low expectation of finding suitable amphibian habitat in PEMB, PFOA, or PFOB polygons. Survey effort is typically focused in the seasonally flooded emergent (PEMC) class. In the summer of 2003, a number of spotted frog (*Rana luteiventris*) and tiger salamander breeding sites were discovered in the Hayden Valley and the Rocky Creek drainage at sites where either NWI polygons were not identified or the Yellowstone NWI classified emergent wetlands as saturated, but the classification tree method predicted PEMC pixels (Patla, unpublished data).

Bartelt et al. (unpublished data) used wetland likelihood maps in conjunction with amphibian survey data to map amphibian habitat suitability in Yellowstone. Finer grained habitat complexity predicted by the palustrine wetland types classification tree, generally in the form of smaller, isolated patches of scrub-shrub wetland, was more useful for predicting amphibian occurrence than the Yellowstone NWI (Bartelt et al., unpublished data). Though NWI polygons are delineated from higher-resolution aerial photography, human interpretation results in a coarser grained mosaic of palustrine wetland types that appear to omit finer grained habitat features important to amphibians.

Digital availability of NWI maps in the Greater Yellowstone area outside of Yellowstone National Park is limited, especially in Idaho and Montana. Classification

tree models developed for Yellowstone National Park might be effectively applied to evaluation of wetland habitat over the Greater Yellowstone Region.

Preliminary application of wetland remote sensing to Amphibian Research and Monitoring Initiative activities in Yellowstone National Park is encouraging. The classification tree methodology appears to be relatively accurate, sensitive to wetland condition, capable of detecting climate-driven wetland variability, and able to detect wetlands missed by the Yellowstone NWI. Importantly, the developed methodology might more generally be applied to wetland mapping in other physiographic settings. Ultimately, wetland remote sensing could prove to be a critical tool in large-scale efforts to conserve amphibians.

CHAPTER 5

SUMMARY DISCUSSION

Two issues related to both journal manuscripts that warrant further discussion are the role of fine-scale classification tree structure and the different way that image texture information is presented to the classification tree algorithm in each paper.

Fine-Scale Classification Tree Structure

In both manuscripts, simplified versions of classification trees tended to account for sizeable amounts of the deviance resolved by full classification trees and were useful for illustrative purposes. However, achieving reported classification accuracies required substantially more elaborate full trees. Additionally, the amount of tree pruning required to achieve high accuracy rates was generally limited. Taken together, these observations suggest that the fine scale structure in optimally pruned trees did not result from noise in the training data used to generate classification trees, but for lack of a better description, was “real” and reflected complicated conditional distributions of wetland pixels given the set of covariates. In this case, the choice of a classification tree methodology is appropriate given the ability of classification trees to accommodate non-homogeneity, or different relationships between variables in different parts of a multivariate measurement space (Breiman et al. 1984).

Image Texture

Image texture was used in different ways in the two manuscripts. In Chapter 3, a single moving-window size was selected for each model while in Chapter 4 the classification algorithm was presented with image textures from three different moving-windows. Individually, 2003 classification trees tended to use tasseled cap image textures from multiple window sizes. For example, the palustrine wetland/upland tree used greenness texture from 3-by-3, 5-by-5, and 7-by-7 moving windows while the palustrine wetland types tree used greenness and brightness textures from all three window sizes (table 4.2). While image textures from individual tasseled cap bands are positively correlated among the different window sizes, the fact that different window sizes were useful in terms of classification accuracy suggests that differences in image texture between wetland and upland, and between different palustrine wetland types, occur at different measurement scales.

Extension of Research in Yellowstone National Park

Results of this study suggest a number of directions for further research in Yellowstone, including examination of a more sophisticated topographic wetness index, the role of spatial dependence in wetland occurrence, spatio-temporal variability of palustrine wetlands, and coupled wetland-amphibian systems.

Topographic Wetness Index

The unimportance of the topographic wetness index as a predictor was disappointing, especially given the computational effort required to calculate the index

across the Yellowstone landscape. As noted in Chapter 3, the steady-state assumption of the index may not be appropriate in semi-arid areas of the park. Wilson and Gallant (2000b) present a more complicated topographic wetness index assuming non-steady-state subsurface flow and incorporating estimated solar insolation, soil hydraulic conductivity, evapotranspiration, and precipitation. An investigation of the utility of this index in selected lower elevation, low-precipitation watersheds might be warranted in order to establish whether or not landscape-scale hydrological analyses are useful for predicting wetland occurrence in Yellowstone.

Spatial Dependence

Results of this study demonstrate that improved detection of palustrine wetlands in Yellowstone National Park is achieved by combining spectral data with image texture measures, terrain data, and thematic ancillary GIS information. However, models developed in the course of this research rely solely on multivariate covariates of wetland occurrence to predict wetland likelihood across the Yellowstone landscape. While analyses are spatially explicit in terms of using data that is spatially organized, and predictions are generated on a regular 30 meter grid, the potential spatial influence of unmeasured environmental variables associated with wetland occurrence, or the potential role of hydrologic processes causing spatial clustering of wetlands were not considered.

Miller and Franklin (2002) used indicator kriging to add spatial dependence to both generalized additive models (GAM) and classification tree models of the probability of occurrence of four vegetation provinces in the Mohave Desert in California. An autologistic term (Besag 1972, Besag 1974) was computed as the sum of the kriged

probabilities of occurrence of a particular vegetation province occurring in the eight cell neighborhood of any arbitrary 30 meter cell, and generally improved the classification accuracy of both GAM and classification tree models (Miller and Franklin 2002).

Addition of spatial dependence to wetland models for Yellowstone National Park is complicated by consideration of datasets from which indicator kriging might be conducted. In an important sense, spatial sampling from the Yellowstone NWI would be redundant given that the NWI is already fully specified in space, i.e. you would be sampling something that is already known. Assuming that the Yellowstone NWI is generally accurate, indicator kriging would contribute additional evidence of wetland only along the margins of existing NWI polygons. If the NWI is not accurate, indicator kriging based on "known" wetland might lead to prediction of wetland in pixels where the vector of spectral and ancillary covariates suggests otherwise. Similarly, relying on the spatial structure of the Yellowstone NWI might limit sensitivity of classification trees to wetland condition.

Independent field sampling to estimate the spatial dependence of Yellowstone wetlands would seem impractical given the size of the park, the relative rareness of wetland on the Yellowstone landscape (with accompanying issues related to sample sizes required to ensure enough wetland sites in the sample), and difficulty in physically accessing large portions of the park.

Contextual classification methods that take into account the tendency of like land cover types to be near one another may be more appropriate for adding spatial dependence to wetland likelihood modeling. One contextual classifier, the iterative

conditional modes algorithm (ICM), is based on an assumption that the local prior probabilities of particular land cover classes vary spatially. Magnussen et al. (2004) used the ICM algorithm to improve classification of forest cover types. Following an initial land cover classification, local prior probabilities are calculated from the distribution of predicted land cover types within a specified neighborhood. Iteratively, a random sequence of all pixels within a land cover map is generated. For each pixel, the local prior probability distribution is determined and then the pixel is reclassified given its vector of multivariate covariates and the local prior. After all pixels in the random sequence have been reclassified, the process is repeated. The algorithm is halted when the proportion of pixels whose class label is changed falls below some threshold (Magnussen et al. 2004).

Wetland Spatio-Temporal Variability

Actual demonstration of wetland variability, both within and between growing seasons, was beyond the scope of this project. However, evidence that the developed methodology is sensitive to wetland condition, and by extension, functional wetland extent, suggests that a logical continuation of this work would be an examination of the spatio-temporal variability of Yellowstone wetlands. Given the ongoing drought in Yellowstone, it would be interesting to assess whether palustrine wetlands have contracted (either actually or functionally) from 1997 to present. Climate driven wetland variability is probably important with respect to the persistence of amphibian metapopulations. Wetland variability is likely to be apparent in terms of wetland extent but also, more subtly, may be manifest in changes in the spatial patterning of wetland

habitat (Turner et al. 2001). Field monitoring of selected wetlands would allow an examination of the relationship between remotely observed spectral variability and actual changes in wetland condition both within and between growing seasons.

Coupled Wetland-Amphibian Systems

Wetlands are arguably some of the most dynamic habitats in Yellowstone. On shorter time scales they respond to yearly variability in precipitation and evaporative demand. Over longer time scales, wetlands dependent on groundwater discharge experience lagged responses to precipitation variability. Similarly, amphibians rank among the most dynamic vertebrates in the park, with recruitment highly dependent on the vagaries of climate. Amphibian persistence on the landscape is likely an emergent property of metapopulation processes involving local extinction, dispersal, and recolonization.

Given this description of Yellowstone wetlands and amphibians, it seems reasonable to expect that coupled wetland/amphibian systems in Yellowstone would be extremely dynamic. One potential application of the methodology developed in this study would be an examination of coupled wetland/amphibian systems. Interactions between wetland dynamics and amphibian population dynamics may occur on time-scales short enough to explore deeper ecological questions concerning the relationship between variability of habitat condition and connectivity and species persistence at a landscape scale.

Summary

This study has demonstrated the feasibility of combining satellite imagery with ancillary spatial information to map palustrine wetland over Yellowstone National Park. The developed methodology is general enough that it could readily be extended to wetland mapping in other settings and over larger areas.

Outside of wetland mapping applications, the classification tree approach used in this research represents a more general case study in the integration of multi-source spatial information. Datasets compiled over the course of this project should prove to be useful for comparing different methods of multi-source data integration.

Preliminary application of wetland likelihood mapping in support of amphibian research in Yellowstone is encouraging. Ultimately, wetland mapping by satellite remote sensing should prove valuable to amphibian conservation efforts at a national scale.

LITERATURE CITED

Adams, M.J. 1999. Correlated factors in amphibian declines: exotic species and habitat change in western Washington. Journal of Wildlife Management. 63:1162-1171.

Alford, R.A., and S.J. Richards. 1999. Global amphibian declines: a problem in applied ecology. Annual Review of Ecology and Systematics. 30:133-65.

Arzandeh, S., and J. Wang. 2001. Texture evaluation of RADARSAT imagery for wetland mapping. Canadian Journal of Remote Sensing. 28:653-666.

Aspinall, R.J. 1991. Use of an inductive modeling procedure based on Bayes theorem for analysis of pattern in spatial data. *In* Computer Modeling in the Environmental Sciences, D.G. Farmer and M.J. Rycroft (editors). Institute of Mathematics and its Applications Conference Series No. 28. Oxford University Press, Oxford. 325-339.

Aspinall, R.J., and N. Veitch. 1993. Habitat modeling from satellite imagery and wildlife survey using a Bayesian modeling procedure in a GIS. Photogrammetric Engineering and Remote Sensing. 59:537-543.

Beebee, T.J.C. 1995. Amphibian breeding and climate. Nature. 374:219-220.

Besag, J. 1972. Nearest-neighbour systems and the autologistic model for binary data. J. Roy. Stat Soc. B. 34:75-83.

Besag, J. 1974. Spatial interaction and the statistical analysis of lattice systems. J. Roy. Stat Soc. B. 36:192-236.

Benediktsson, J.A., Swain, P.H., and O.K. Ersoy. 1990. Neural network approaches versus statistical methods in classification of multisource remote sensing data. IEEE Transactions on Geoscience and Remote Sensing. 28:540-552.

Bischof, H., Schneider, W., and A.J. Pinz. 1992. Multispectral classification of Landsat images using neural networks. IEEE Transactions on Geoscience and Remote Sensing. 30:482-490.

Bolstad, P.V. and T.M. Lillesand. 1992. Rule-based classification models: flexible integration of satellite imagery and thematic spatial data. Photogrammetric Engineering and Remote Sensing. 58:965-971.

Blaustein, A.R., Wake, D.B., and W.P. Sousa. 1994. Amphibian declines: judging stability, persistence, and susceptibility of populations to local and global extinctions. Conservation Biology. 8:60-71.

Blaustein, A.R., Hoffman, P.D., Hokit, D.G., Kiesecker, J.M., Walls, S.C., and J.B. Hays. 1994. UV repair and resistance to solar UV-B in amphibian eggs: a link to population declines. Proceedings of the National Academy of Science, USA. 91:1791-1795.

Breiman, L., Friedman, J.H., Olshen, R.A., and C.J. Stone. 1984. Classification and regression trees. Chapman and Hall. 358 pp.

Bruzzone, L., Conese, C., Maselli, F., and F. Roli. 1997. Multisource classification of complex rural areas by statistical and neural-network approaches. Photogrammetric Engineering and Remote Sensing. 523-533.

Butera, M.K. 1983. Remote sensing of wetlands. IEEE Transactions on Geoscience and Remote Sensing. 3:383-392.

Card, D.H. 1982. Using known map category marginal frequencies to improve estimates of thematic map accuracy. Photogrammetric Engineering and Remote Sensing. 48:431-439.

Carey, C. 1993. Hypothesis concerning the causes of the disappearance of boreal toads from the mountains of Colorado. Conservation Biology. 7:355-362.

Chan, J.C., Defries R.S., Zhan, X., Huang, C., and J.R.G. Townshend. 2000. Texture features for land cover change detection at 250 m resolution – an application of machine learning feature subset selection. *In* Proceedings of IEEE 2000 International Geoscience and Remote Sensing Symposium, IGARSS, Honolulu, Hawaii. 3060-3063.

Chen, K.S., Tzeng, Y.C., Chen, C.F., and W.L. Kao. 1995. Land-cover classification of multispectral imagery using a dynamic learning neural network. Photogrammetric Engingeering and Remote Sensing. 403-408.

Clark, L.A., and D. Pregibon. 1992. Tree-based models. *In* Statistical Models in S, J.M. Chambers and T.J. Hastie (eds.). Wadsworth and Brooks/Cole. Pacific Grove, CA. 377-419.

Cohen, W.B., and T.A. Spies. 1992. Estimating structural attributes of Douglas-Fir/Western Hemlock forest stands from Landsat and SPOT imagery. Remote Sensing Environment. 41:1-17.

Connors, R.W., and C.A. Harlow. 1980. A theoretical comparison of texture algorithms. IEEE Transactions on Pattern Analysis and Machine Intelligence. 2:204-222.

Corn, P.S. 1998. Effects of ultraviolet radiation on boreal toads in Colorado. Ecological Applications. 8:18-26.

Cowardin, L.M., Carter, V., Golet, F.C., and E.T. LaRoe. 1979. Classification of wetlands and deepwater habitats of the United States. U.S. Fish and Wildlife Service. Washington, DC.

Cowardin, L.M., and F.C. Golet. 1995. U.S. Fish and Wildlife Service 1979 wetland classification: a review. Vegetatio. 118:134-152.

Crist, E.P., and R.C. Cicone. 1984. A physically-based transformation of thematic mapper data – the TM tasseled cap. IEEE Transactions of Geoscience and Remote Sensing. GE-22:256-263.

Dahl, T.E. 1990. Wetlands losses in the United States: 1780s to 1980s. U.S. Department of the Interior, Fish and Wildlife Service, Washington, D.C. 13 pp.

Dechka, J.A., Franklin, S.E., Watmough, M.D., Bennett, R.P., and D.W. Ingstrup. 2002. Classification of wetland habitat and vegetation communities using multi-temporal Ikonos imagery in southern Saskatchewan. Canadian Journal of Remote Sensing. 28:679-685.

Despain, D. 1990. Yellowstone vegetation: consequences of environment and history in a natural setting. Roberts Rinehart, Inc. Boulder, CO. 239 pp.

Dodd, C.K., and B.S. Cade. 1998. Movement patterns and the conservation of amphibians breeding in small, temporary wetlands. Conservation Biology. 12:331-339.

Dottavio, C.L., and F.D. Dottavio. 1984. Potential benefits of new satellite sensors to wetland mapping. Photogrammetric Engineering and Remote Sensing. 50:599-606.

Elliot, C.R., and M.M. Hektner. 2000. Wetland resources of Yellowstone National Park. Yellowstone National Park, Wyoming. 32 pp.

Ernst-Dottavio, C.L., Hoffer, R.M., and R.P. Mrocynski. 1981. Spectral characteristics of wetland habitats. Photogrammetric Engineering and Remote Sensing. 47:223-227.

Federal Geographic Data Committee. 1992. Application of satellite data for mapping and monitoring wetlands: fact finding report. Wetlands Subcommittee, Technical Report 1. 32 pp.

Ferro, C.J.S., and T.A. Warner. 2002. Scale and texture in digital image classification. Photogrammetric Engineering and Remote Sensing. 68:51-63.

Findlay, C.S., and J. Houlahan. 1996. Anthropogenic correlates of species richness in southeastern Ontario wetlands. Conservation Biology. 11:1000-1009.

Fisher, R.N., and H.B. Shaffer. 1996. The decline of amphibians in California's Great Central Valley. Conservation Biology. 10:1387-1397.

Foody, G.M., McCulloch, and W.B. Yates. 1995. Classification of remotely sensed data by an artificial neural network: issues related to training data characteristics. 61:391-401.

Franklin, S.E., and D.R. Peddle. 1989. Spectral texture for improved class discrimination in complex terrain. International Journal of Remote Sensing. 8:1437-1443.

Franklin, S.E., Moskal, L.M., Lavigne, M.B., and K. Pugh. 2000. Interpretation and classification of partially harvested forest stands in the Fundy model forest using multitemporal Landsat TM digital data. Canadian Journal of Remote Sensing. 26:318-332.

Franklin, S.E., Lavigne, M.B., Moskal, L.M., Wulder, M.A., and T.M. McCaffrey. 2001a. Interpretation of forest harvest conditions in New Brunswick using Landsat TM enhanced wetness difference imagery (EWDI). Canadian Journal of Remote Sensing. 27:118-128.

Franklin, S.E., Maudie, A.J., and M.B. Lavigne. 2001b. Using spatial co-occurrence texture to increase forest structure and species composition classification accuracy. Photogrammetric Engineering and Remote Sensing. 67:849-855.

Friedl, M.A., and C.E. Brodley. 1997. Decision tree classification of land cover from remotely sensed data. Remote Sensing Environment. 61:399-409.

Gammon, P.T. and V.P. Carter. 1976. Comparison of vegetation classes in the Great Dismal Swamp using two individual Landsat images and a temporal composite. *In* Proceedings of Purdue Symposium on Machine Processing of Remotely Sensed Data. 3B-1.

Gary, M.R., McAfee, Jr., C., and R. Wolf, eds. 1974. Glossary of geology. American Geological Institute. Washington, D.C.

German, G.W.H, West, G., and M. Gahegan. 1999. Statistical and AI techniques in GIS classification: a comparison. *In* Proceedings of the Eleventh Annual Colloquium of the Spatial Information Research Centre, P.A. Whigham (ed.). University of Otago, Dunedin, New Zealand, 310 pp.

Gibbs, J.P. 1998. Distribution of woodland amphibians along a forest fragmentation gradient. Landscape Ecology. 13:263-268.

Gong, P. 1994. Integrated analysis of spatial data from multiple sources: an overview. Canadian Journal of Remote Sensing. 20:349-359.

Green, E.J., Strawderman, W.E., and T.M. Airola. 1993. Assessing classification probabilities for thematic maps. Photogrammetric Engineering and Remote Sensing. 59:635-639.

Halley, J. M., Oldham, R. S., and J. W. Arntzen. 1996. Predicting the persistence of amphibian populations with the help of a spatial model. Journal of Applied Ecology. 33:455-470.

Hand, D.J., and K. Yu. 2001. Idiot's Bayes – not so stupid after all? International Statistical Review. 69:385-398.

Hansen, M., Dubayah, R., and R. Defries. 1996. Classification trees: an alternative to traditional land cover classifiers. International Journal of Remote Sensing. 17:1075-1081.

Hansen, M.J., Franklin, S.E., Woudsma, C., and M. Peterson. 2001. Forest structure classification in the north Columbia mountains using the Landsat TM tasseled cap wetness component. Canadian Journal of Remote Sensing. 27:20-31.

Haralick, R.M. 1979. Statistical and structural approaches to texture. Proceedings of the IEEE. 5:786-804.

Hayes, T., Haston, K., Tsui, M., Hoang, A., Haeffele, C., and A. Vonk. 2003. Atrazine-induced hermaphroditism at 0.1 ppb in American leopard frogs (*Rana pipiens*): Laboratory and field evidence. Environmental Health Perspectives. 11:568-575.

Hecnar, S.J., and R.M. M'Closkey. 1996. Regional dynamics and the status of amphibians. Ecology. 77:2091-2097.

Hecnar, S.J., and R.M. M'Closkey. 1997. Spatial scale and determination of species status of the green frog. Conservation Biology. 11:670-682.

Hodgson, M.E., Jensen, J.R., and M.C. Coulter. 1987. Monitoring wood stork foraging habitat using remote sensing and geographic information systems. Photogrammetric Engingeering and Remote Sensing. 54:1601-1607.

Houlahan, J.E., Findlay, C.S., Schmidt, B.R., Meyer, A.H., and S.L. Kuzmin. 2000. Quantitative evidence for global amphibian population declines. Nature. 404:752-755.

Huang, X., and J.R. Jensen. 1997. A machine-learning approach to automated knowledge-base building for remote sensing image analysis with GIS data. Photogrammetric Engingeering and Remote Sensing. 63:1185-1194.

Huang, C., Wylie, B., Yang, L., Homer, C., and G. Zylstra. 2002. Derivation of a tasseled cap transformation based on the Landsat 7 at-satellite reflectance. International Journal of Remote Sensing. 23:1741-1748.

Hutchinson, C.F. 1982. Techniques for combining Landsat and ancillary data for digital classification improvement. Photogrammetric Engingeering and Remote Sensing. 48:123-130.

Jensen, S.K. and J.O. Domingue. 1988. Extracting topographic structure from digital elevation data for geographic information system analysis. Photogrammetric Engineering and Remote Sensing. 54:1593-1600.

Jensen, J.R., Hodgson, M.E., Christensen, E., Mackey, H.E., Tinney, L.R., and R. Sharitz. 1986. Remote sensing inland wetlands: a multispectral approach. Photogrammetric Engineering and Remote Sensing. 52:87-100.

Jensen, J.R., Narumalani, S., Weatherbee, O., Morris, K.S., and H.E. Mackey. 1993. Predictive modeling of cattail and waterlily distribution in a South Carolina reservoir using GIS. Photogrammetric Engingeering and Remote Sensing. 58:1561-1568.

Jensen, J.R., Rutchey, K., Koch, M.S., and S. Narumalani. 1995. Inland wetland change detection in the Everglades water conservation area 2A using a time series of normalized remotely sensed data. Photogrammetric Engineering and Remote Sensing. 61:199-209.

Jensen, J.R., Huang, X., and Mackey, H.E. 1997. Remote sensing of successional changes in wetland vegetation as monitored during a four-year drawdown of a forming cooling lake. Applied Geographic Studies. 1:31-44.

Johnston, R.M. and M.M. Barson. 1993. Remote sensing of Australian wetlands: an evaluation of Landsat TM data for inventory and classification. Australian Journal of Marine Freshwater Resources. 44:235-52.

Jones, N.L. and F. Shahrokhi. 1977. Application of Landsat data to wetland study and land use classification in west Tennesee. *In* Proceedings of the 11th International Symposium on Remote Sensing of Environment Volume I, Environmental Research Institute of Michigan, Ann Arbor, MI. 609-613.

Kiesecker, J.M., and A.R. Blaustein. 1997. Influences of egg laying behavior on pathogenic infection of amphibian eggs. Conservation Biology. 11:214-220.

Kiesecker, J.M., Blaustein, A.R., and L.K. Belden. 2001. Complex causes of amphibian population declines. Nature. 410:681-683.

Kindscher, K., Fraser, A., Jakubauskas, M.E., and D.M. Debinski. 1998. Identifying wetland meadows in Grand Teton National Park using remote sensing and average wetland values. Wetlands Ecology and Management. 5:265-273.

Knutson, M.G., Sauer, J.R., Olsen, D.A., Mossman, M.J., Hemesath, L.M., and M.J. Lanoo. 1999. Effects of landscape composition and wetland fragmentation on frog and toad abundance and species richness in Iowa and Wisconsin, U.S.A. Convservation Biology. 6:1437-1446.

Kolosarvy, M.B., and R.K. Swihart. 1999. Habitat fragmentation and the distribution of amphibians: patch and landscape correlates in farmland. Canadian Journal of Zoology. 77:1288-1299.

Kudray, G.M., and M.R. Gale. 2000. Evaluation of National Wetland Inventory maps in a heavily forested region in the upper Great Lakes. 20:581-587.

Kuzila, M.S., Rundquist, D.C., and J.A. Green. 1991. Methods for estimating wetland loss: the rainbasin region of Nebraska, 1927-1981. Journal of Soil and Water Conservation. 44:441-445.

Langley, P., and S. Sage. 1994. Induction of selective Bayesian classifiers. *From* Proceedings of the Tenth Conference on Uncertainty in Artificial Intelligence. Morgan Kaufmann. Seattle, WA.

Lawrence, R.L., and A. Wright. 2001. Rule-based classification systems using classification and regression tree (CART) analysis. Photogrammetric Engineering and Remote Sensing. 67:1137-1142.

Lee, T., Richards, J.A., and P.H. Swain. 1987. Probabilistic and evidential approaches for multisource data analysis. IEEE Transactions on Geoscience and Remote Sensing. 25:283-293.

Lehtinen, R.M., Galatowitsch, S.M., and J.R. Tester. 1999. Consequences of habitat loss and fragmentation for wetland amphibian assemblages. Wetlands. 19:1-12.

Ma, Z.M., Hart, M.M., and R.L. Redmond. 2001. Mapping vegetation across large geographic areas: integration of remote sensing and GIS to classify multisource data. Photogrammetric Engineering and Remote Sensing. 67:295-307.

Magnussen, S., Boudewyn, P., and M. Wulder. 2004. Contextual classification of Landsat TM images to forest inventory cover types. International Journal of Remote Sensing. 25:2421-2440.

Marceau, D.J., Howarth, P.J., Dubois, J.M., and D.J. Gratton. 1990. Evaluation of the grey-level co-occurrence method for landcover classification using SPOT imagery. IEEE Transactions on Geoscience and Remote Sensing. 28:513-519.

McKeown, D.M. 1987. The role of artificial intelligence in the integration of remotely sensed data with geographic information systems. IEEE Transactions on Geoscience and Remote Sensing. 25:330-348.

Middleton, E.M., Herman, J.R., Celarier, E.A., Wilkinson, J.W., Carey, C., and R.J. Rushin. 2001. Evaluating ultraviolet radiation exposure with satellite data at sites of amphibian declines in Central and South America. Conservation Biology. 15:914-929.

Miller, J., and J. Franklin. 2002. Modeling the distribution of four vegetation alliances using generalized linear models and classification trees with spatial dependence. Ecological Modelling. 157:227-247.

Moore, D.M., Lees, B.G., and S.M. Davey. 1991. A new method for predicting vegetation distributions using decision tree analysis in a geographic information system. Environmental Management. 15:59-71.

O'Loughlin, E.M. 1986. Prediction of surface saturation zones in natural catchments by topographic analysis. Water Resources Research. 22:794-804.

Pal, M., and P.M. Mather. 2001. Decision tree based classification of remotely sensed data. *In* Proceedings of the 22nd Asian Conference on Remote Sensing, Singapore.

Peddle, D.R. and S.E. Franklin. 1991. Image texture processing and data integration for surface pattern discrimination. 57:413-420.

Peddle, D.R. 1993. An empirical comparison of evidential reasoning, linear discriminant analysis, and maximum likelihood algorithms for alpine landcover classification. Canadian Journal of Remote Sensing. 19:31-44.

Peddle, D.R. and D.T. Ferguson. 2002. Optimisation of multisource data analyis: an example using evidential reasoning for GIS data classification. Computers and Geosciences. 28:45-52.

Peterson, C.D., Burton, S.R., and D.A. Patla. 2001. Using geographical information systems to design amphibian surveys. *In* Status and Conservation of U.S. Amphibians. M Lannoo (Ed.). University of California Press, Berkeley, CA.

Planchon, O., and F. Darboux. 2002. A fast, simple and versatile algorithm to fill the depressions of digital elevation models. Catena. 46:159-176.

Pounds, J.A., and M.L. Crump. 1994. Amphibian declines and climate disturbance: the case of the golden toad and the harlequin frog. Conservation Biology. 8:72-85.

Pounds, J.A., Fogden, M.P., Savage, J.M., and G.C. Gorman. 1997. Tests of null models for amphibian declines on a tropical mountain. Conservation Biology. 11:1307-1322.

Richards, J.A. 1993. Remote sensing digital image analysis: an introduction. 2nd edition. Springer-Verlag. Berlin, Germany.

Rodman, A., H.F. Shovic, and D. Thoma. 1996. Soils of Yellowstone National Park. Yellowstone National Park, Yellowstone Center for Resources. Mammoth, WY. 324 pp.

Ricchetti, E. 2000. Multispectral satellite image and ancillary data integration for geological classification. Photogrammetric Engineering and Remote Sensing. 66:429-435.

Rutchey, K., and L. Vilcheck. 1994. Development of an Everglades vegetation map using a SPOT image and the global positioning system. Photogrammetric Engineering and Remote Sensing. 60:767-775.

Sader, S.A., Ahl, D., and W-S Liou. 1995. Accuracy of Landsat-TM and GIS rule-based methods for forest wetland classification in Maine. Remote Sensing Environment. 53:133-144.

Semlitsch, R.D., and J.R. Bodie. 1998. Are small, isolated wetlands expendable? Conservation Biology. 12:1129-1133.

Shovic, H.F. 1996. Landforms and associated surficial materials of Yellowstone National Park. Yellowstone National Park, Center for Resources. Mammoth, WY. 230 pp.

Sjogren Gulve, P. 1994. Distribution and extinction patterns within a northern metapopulation of the pool frog, *Rana lessonae*. Ecology. 75:1357-1367.

Skelly, D.K., Werner, E.E., and S.A. Cortwright. 1999. Long-term distributional dynamics of a Michigan amphibian assemblage. Ecology. 80:2326-2337.

Spear, S. 2004. Landscape effects on genetic structure in tiger salamander (*Ambystoma tigrinum melanostictum*) populations across the northern range of Yellowstone National Park. Master's thesis, Idaho State University, Pocatello, ID.

Starnes, S.M., Kennedy, C.A., and J.W. Petranka. 2000. Sensitivity of embryos of southern Appalachian amphibians to ambient solar UV-B radiation. Conservation Biology. 14:277-282.

Stehman, S.V. 1995. Thematic map accuracy assessment from the perspective of finite population sampling. Int. J. Remote Sensing. 16:589-593.

Stolt, M.H., and J.C. Baker. 1995. Evaluation of National Wetland Inventory maps to inventory wetlands in the southern Blue Ridge of Virginia. Wetlands. 15:346-353.

Swarthout, D.J., MacConnell, and J.T. Finn. 1981. An evaluation of the National Inventories Workshop, University of Maine, Orono, ME. 685-691.

Tiner, R.W. 1990. Use of high-altitude aerial photography for inventorying forested wetlands in the United States. Forest Ecology and Management. 33/34:593-604.

Tiner, R.W. 1997. NWI maps: what they tell us. National Wetlands Newsletter. 19:7-12.

Treitz, P., and P. Howarth. 2000. Integrating spectral, spatial, and terrain variables for forest ecosystem classification. Photogrammetric Engineering and Remote Sensing. 66:305-317.

Turner, M.G., Gardner, R.H., and R.V. O'Neill. 2001. Landscape ecology in theory and practice: pattern and process. Springer-Verlag. 401 pp.

U.S. Fish and Wildlife Service. 2003. National wetlands inventory status. Retrieved April 1, 2003 from U.S. Fish and Wildlife Service National Wetlands Inventory website: http://wetlands.fws.gov.

Wake, D.B. 1991. Declining amphibian populations. Science. 253:860.

Wang, M., and P.J. Howarth. 1994. Multi-source spatial data integration: problems and some solutions. Canadian Journal of Remote Sensing. 20:360-367.

Wang, J., Shang, J., Brisco, B., and R.J. Brown. 1998. Evaluation of multidate ERS-1 and multispectral Landsat imagery for wetland detection in southern Ontario. Canadian Journal of Remote Sensing. 24:60-68.

Weszka, J.S., Dyer, C.R., and A. Rosenfeld. 1976. A comparative study of texture measures for terrain classification. IEEE Transactions on Systems, Man, and Cybernetics. 6:269-285.

Wilen, B.O. and M.K. Bates. 1995. The U.S. Fish and Wildlife Service's national wetlands inventory project. Vegetatio. 119:153-169.

Wilen, B.O. and G.S. Smith. 1996. Assessment of remote sensing/GIS technologies to improve national wetland inventory maps. *In* Remote sensing: people in partnership with technology; Proceedings of the Sixth Forest Service Remote Sensing Application Conference, April 29-May 3, Denver, CO. 50-64.

Wilson, J.P., and J.C. Gallant. 2000a. Primary topographic attributes. *In* Terrain Analysis: Principles and Applications, J.P. Wilson and J.C. Gallant (Eds.). Wiley. NY, NY.

Wilson, J.P., and J.C. Gallant. 2000b. Secondary topographic attributes. *In* Terrain Analysis: Principles and Applications. J.P. Wilson and J.C. Gallant (Eds.). Wiley. NY, NY.

Wilson, P.A. 1997. Rule-based classification of water in Landsat MSS images using the variance filter. Photogrammetric Engingeering and Remote Sensing. 63:485-491.

Winter, T.C. 2000. The vulnerability of wetlands to climate change: a hydrologic landscape perspective. Journal of the American Water Resources Association. 36:305-311.

Work. E.A., and D.S. Gilmer. 1976. Utilization of satellite data for inventorying prairie ponds and potholes. Photogrammetric Engineering and Remote Sensing. 5:685-694.

Wylie, B.K, Meyer, D.J., Choate, M.J., Vierling, L., and P.K. Kozak. 2001. Mapping woody vegetation and eastern red cedar in the Nebraska sand hills using AVIRIS. *In* Summaries of the 9th JPL Airborne Earth Science Workshop, R.O. Green, ed. NASA Jet Propulsion Laboratory, California Institute of Technology, Pasadena, CA.